UNIVERSITAT POLITÈCNICA DE VALÈNCIA

Escuela Técnica Superior de Ingeniería del Diseño

UNIVERSITAT POLITÈCNICA DE VALÈNCIA

Escuela Técnica Superior de Ingeniería del Diseño

BOUNDARY LAYER FLASHBACK SENSITIVITY FOR A PREMIXED METHANE/OXYGEN COMBUSTION

Master's thesis

Master's Degree in Aeronautical Engineering

AUTHOR: Marcos García Castelló

Tutor: Joaquín de la Morena Borja

Cotutor: Gabriela Cristina Bracho León

External cotutor: Pietro Paolo Ciottoli

ACADEMIC YEAR: 2021/2022

Boundary layer flashback sensitivity for a premixed methane/oxygen combustion

Laurea Magistrale in Ingegneria Aeronautica

Professor (Italy): Pietro Paolo Ciottoli

Professor (Spain): Gabriela Cristina Bracho León

Professor (Spain): Joaquín de la Morena Borja

Student:

Marcos García Castelló

July 12, 2022

SAPIENZA UNIVERSITÀ DI ROMA

Abstract

Recent studies have shown that the use of a premixed flame inside a combustion chamber may involve a certain operational instability, which appears when the premixed flame propagates against the main flow direction close to the wall boundary layers. This phenomenon is well-known as wall flashback, which has been studied both experimentally and numerically since the 1940's. In this study, it has been simulated a methane/oxygen premixed combustion for a constant values of $p = 1$ Pa and $u = 5$ m/s, through a backward-facing step with a height of $h = 0.0254$ m, for different operational parameters. Results have shown that equivalent ratios close to the stoichiometric or greater wall temperatures tend to propagate the flame upstream. In addition, two skeletal kinetic mechanisms obtained with the `PyCSP` toolkit have been compared. Finally, the importance of the transient phase after the change in the way the flame is ignited has been shown.

Key words: Combustion; flashback; equivalent ratio; boundary layer; boundary wall flashback; instability.

Resumen

Estudios recientes han demostrado que el uso de una llama premezclada en el interior de una cámara de combustión puede suponer la aparición de cierta inestabilidad a la hora del quemado, la cual aparece cuando la llama premezclada se propaga en dirección contraria a la del flujo principal, especialmente cerca de las zonas donde aparece la capa límite. Este fenómeno es conocido como "*flashback* cerca de la pared", el cual ha sido estudiado tanto experimental como numéricamente desde la década de 1940. En este proyecto se ha simulado una combustión premezclada de metano/oxígeno para unos valores constantes de $p = 1$ Pa y $u = 5$ m/s, además, el flujo pasa a través de un escalón (*backward-facing step*) con una altura de $h = 0{,}0254$ m para diferentes parámetros de operación. Los resultados han mostrado que para dosados cercanos a las condiciones estequiométricas o una refrigeración ineficiente de la pared de la cámara de combustión tienden a propagar la llama aguas arriba. Asimismo, se ha llevado a cabo una comparación entre dos mecanismos de reacción obtenidos con la herramienta denominada `PyCSP`. Por último, se ha mostrado la importancia de la fase transitoria sobre el fenómeno de textitflashback tras el cambio en la forma de ignición de la llama premezclada.

Palabras clave: Combustión; retroceso de llama; dosado; capa límite; inestabilidad.

Sommario

Studi recenti hanno dimostrato che l'uso di una fiamma premiscelata all'interno di una camera di combustione può comportare una certa instabilità operativa, che si manifesta quando la fiamma premiscelata si propaga contro la direzione principale del flusso in prossimità degli strati limite della parete. Questo fenomeno, noto come ritorno di fiamma in parete, è stato studiato sia sperimentalmente che numericamente fin dagli anni Quaranta. In questo studio è stata simulata una combustione premiscelata metano/ossigeno per valori costanti di $p = 1$ Pa e $u = 5$ m/s, con uno step backward-facing con un'altezza di $h = 0{,}0254$ m e per diversi parametri operativi. I risultati hanno mostrato che rapporti equivalenti vicini alla stechiometria o temperature di parete maggiori tendono a propagare la fiamma verso l'alto. Inoltre, sono stati confrontati due meccanismi cinetici scheletrici ottenuti con il toolkit `PyCSP`. Infine, è stata dimostrata l'importanza della fase transitoria dopo il cambiamento della modalità di accensione della fiamma.

Parole chiave: Combustione; ritorno di fiamma; rapporto di equivalenza; strato limite; instabilità.

Resum

Estudis recents han demostrat que l'ús d'una flama premesclada a l'interior d'una cambra de combustió pot suposar l'aparició d'una certa inestabilitat, esta apareix quan la flama premesclada es propaga en direcció contrària a la del flux principal, especialment prop de les regions on apareix la capa límit. Este fenomen és conegut com "*flashback* prop de la paret", el qual ha sigut estudiat tant experimentalment com numèricament des de la dècada de 1940. En este projecte s'ha simulat una combustió premesclada de metà/oxigen per a uns valors constants de $p = 1$ Pa i $u = 5$ m/s, a més, el flux passa a través d'un escaló (*backward-facing step*) amb una altura de $h = 0{,}0254$ m per a diferents paràmetres d'operació. Els resultats han mostrat que per a relacions equivalents pròxims a les condicions estequiomètriques o una refrigeració ineficient de la paret de la cambra de combustió impliquen una propagació de la flama aigües amunt. Així mateix, s'ha fet una comparació entre dos mecanismes de reacció obtinguts amb la ferramenta denominada *PyCSP*. Finalment, s'ha mostrat la importància de la fase transitòria sobre el fenomen de *flashback* després del canvi en la forma d'ignició de la flama premesclada.

Paraules clau: Combustió; retrocés de flama; relació equivalent; capa límit; inestabilitat

Contents

Nomenclature

Abbreviations

LOX/CH4	Liquid oxygen and methane
CFD	Computational Fluid Dynamics
DNS	Direct Numerical Simulation
RANS	Reynolds-averaged Navier–Stokes
LES	Large Eddy Simulation
FVM	Finite Volume Method
CV	Control Volume
UDS	Upwind Difference Scheme
CDS	Central Difference Scheme
QUICK	Quadratic Upstream Interpolation for Convective Kinematics
CFL	Courant-Friedrichs-Lewy
TDAC	Tabulation of Dynamic Adaptive Chemistry
ISAT	In situ Adaptive Tabulation technique
DAC	Dynamic Adaptive Chemistry
EDC	Eddy Dissipation Model

CSP	Computational Singular Perturbation
PISO	Pressure-Implicit Split-Operator
SIMPLE	Semi-Implicit Method for Pressure-Linked Equations
EBU	Eddy Break-Up

Parameters

ρ	Density	kg m^{-3}
x_i	Position in i direction	m
u_i	Velocity in i direction	m s^{-1}
t	time	s
p	Pressure	Pa
τ_{ij}	Viscous stress tensor	Pa
α	Chemical specie	[-]
Y_α	Mass fraction for specie α	[-]
m_α	Mass for specie α	[kg]
D_α	Diffusion coefficient for specie α	m^2 s^{-1}
λ	Thermal conductivity	W m^{-1} K^{-1}
c_p	Specific heat at constant pressure	J kg^{-1} K^{-1}
h_α	Absolute enthalpy for specie α	J kg^{-1}
h^o_α	Enthalpy of formation for specie α	J kg^{-1}
$\mathcal{M}$	Molar mixture ratio	kg $kmol^{-1}$
$\mathcal{R}$	Ideal constant gas	J mol^{-1} K^{-1}
u	Characteristic velocity	m s^{-1}
l	Characteristic length	m
u'	Fluctuating velocity	m s^{-1}
$\bar{u}$	Mean velocity	m s^{-1}
μ	Dynamic viscosity	kg s^{-1} m^{-1}
k	Characteristic velocity fluctuation	m^2 s^{-2}
ϵ	Energy transfer rate	m^2 s^{-3}

τ	Time scale	s
K	Wavenumber	m^{-1}
μ_t	Turbulent dynamic viscosity	kg m^{-1} s^{-1}
ν	Kinematic viscosity	m^2 s^{-1}
C_μ	Model constant	[-]
V	Volume	m^3
Δt	Time step	s
Δx	Mesh size	m
ϕ	Equivalence ratio	[-]
s_u^o	Laminar flame speed	m s^{-1}
M	Chemical symbol for an specie i	[-]
ν_i	Stoichiometric constant for an specie i	[-]
k_k	Proportionality factor of the reaction	[-]
ω_k	Reaction rate for reaction k	mol s^{-1}
c_α	Concentration for an specie α	[-]

Dimensionless numbers

δ_{ij}	Kronecker delta
Sc	Schmidt number
Da	Damköhler number
Ka	Karlovitz number
Le	Lewis number
Re	Reynolds number
Co	Courant number

List of Figures

List of Tables

Part I

REPORT

Chapter 1

Introduction

1.1 Context and Motivation

Combustion of fossil fuels, such as coal, oil and natural gas, Figure 1.1, will still be the primary global energy source in the coming decades [1][2]. Fossil fuels are constantly present in human life such as transport, house heating and even electricity generation [3][4]. Since the industrial revolution, many sectors have benefited from its driving force, being one of them the aerospace industry.

Over the last 20 years, the necessity of reducing the operational cost of launching has led to a focus on fuel propellants used for in-space and launcher rocket propulsion which could improve the performance and operation efficiency of the rockets [5]. For instance, despite the cost, hydrogen provides high values of specific impulse, while kerosene offers lower costs for the launch vehicle. However, methane presents properties between hydrogen and kerosene. Mixed with liquid oxygen, LOX/CH_4 has become a gripping propellant combination, which is present in a wide variety of space propulsion applications, such as liquid booster stages, upper stages, and in-orbit transfer stages [6]. With the growth of the aerospace sector, various Research & Technology programs have been initiated throughout the world in order to find out proper mechanisms of LOX/CH_4 propellants for their use in rocket engine systems [7].

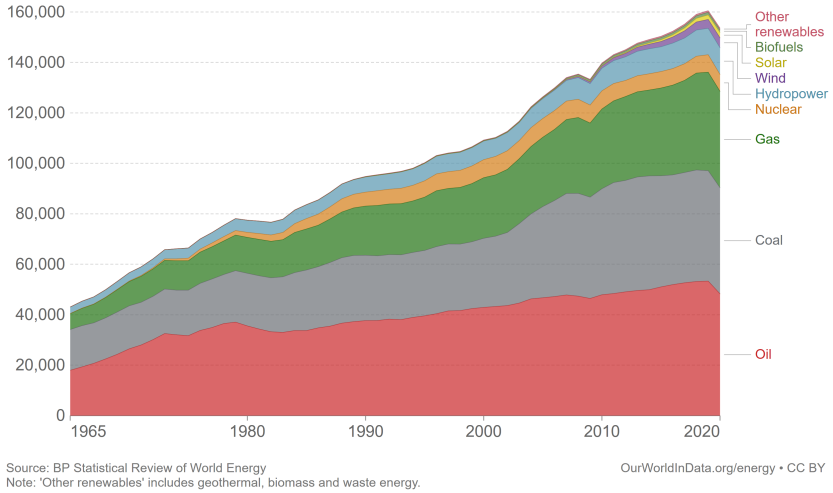

Figure 1.1: World energy consumption by source. Source: Our World in Data.

The use of methane in rocket engines, provides multiple advantages, such as reducing costs during its production and storage. In addition, methane has similar thermodynamic properties to liquid oxygen, allowing a better cooling performance than kerosene. Due to the high density of the methane concerning the hydrogen, the rocket's fuel tank could be reduced, thus providing more payload mass in return [8].

Despite the fact of the significant number of advantages provided by the methane, like all fuels known until now, emissions of pollutants play an essential role during the combustion processes. Some of the best well-known are unburned and partially burned hydrocarbons (UHC), carbon monoxide (CO), particulate matter (C), oxides of nitrogen (NO_x) and oxides of sulfur (SO_x), which are mainly toxic to human health, even precursor of chemical smog and depletion of ozone in the stratosphere. Furthermore, some contaminants such as carbon dioxide (CO_2) and water (H_2O) are generated. It is well-known that, through human activities, CO2 is the primary greenhouse gas emitted which threatens to change the world's climate significantly.

To accurately predict the combustion performance, reliable chemical kinetic schemes have been developed as numerical tools that describe chemical reactions. Methane chemistry has been selected as the main reaction scheme that is capable of describing the hierarchical structure of hydrocarbon oxidation reactions in such a way that several researches about methane chemical reactions have been carried on to highlight the crucial features of the CH4 combustion [9].

Nevertheless, combustion devices become much more complex in both design and operating conditions which means more complex flow dynamics, which could lead to instabilities, hence, noise pollution and in the worst case, a mechanical failure due to high temperatures. Thereby, premixed combustion is imposed as the best option to manage the temperature inside the combustor [10]. Despite the fact of that temperature and pollution emissions, the use of premixed combustion leads to operability issues such as auto-ignition or flashback.

Subsequently, experimental research or numerical modelling have the chance to effectively contribute to assess the performance of premixed combustion under various operating conditions. Therefore, a good understanding of combustion and its control are essential to improve its processes and enhance its efficiency and reduce the number of pollutants emitted into the atmosphere.

1.2 Objectives of the project

The project is focused on two fundamental objectives: on the one hand, modelling of a premixed combustion in a reference backward facing step for a LOX/CH_4 step and find the optimal parameters for the simulations. On the other hand, to carry out a sensitivity study on the modification of certain parameters that can have a direct impact on one of the operability issues present in premixed combustion, the flashback.

In order to achieve these objectives, it will first be necessary to fulfil a number of intermediate objectives, these being:

- Bibliographic study on the phenomenon of flashback and the most relevant parameters of the process.
- Obtaining an optimal mesh in OpenFOAM. For this, a mesh independence study is performed to obtain reliable results
- Selection of the chemical kinetic mechanisms with the `PyCSP` algorithm based on the established requirements.
- Designing a model capable to evaluate different chemical kinetic mechanisms in a simple and efficient way.

1.3 Thesis outline

In order to achieve all these objectives, it has been decided to divide this project into three main parts, the report, the scope statement and the budget. These, in turn, are subdivided into chapters, which are detailed as follows:

- Report: This first document is the largest of the three documents and details the process followed throughout the project. It is subdivided into the following chapters:
  - Introduction: a brief combustion background is presented to justify the motivation of the project. In addition, the main objectives are presented.
  - Characteristics and modelling of turbulent flows: along this chapter the fundamental governing equations of the fluids will be presented. In addition, the energy cascade concept will be defined, showing which methods exist to solve it. Finally, it will be explained how to solve numerically all presented equations.
  - Characteristics and modelling of combustion: in order to have a better understanding about the interaction between combustion and turbulence, all the types of flames will be explained, highlighting their main properties. Then, the different types of chemical kinetic mechanisms used will be presented and will be concluded with a brief introduction of the flashback phenomenon.
  - Methodology: in order to solve all the previous equations, is necessary a mathematical tool. Therefore, this chapter focuses on a brief explanation of the OpenFOAM software. Then, the problem to be solved during the project will be specified using the OpenFOAM software and it will be ended with a generation of the final mesh.
  - Results and discussion: this chapter will present all the obtained results throughout the project, where all the effects generated after the modification of the chosen parameters will be analysed in detail, paying particular attention to the flashback area.
  - Conclusions and future works: finally, this chapter will include all the conclusions achieved during the project. In addition, future ways of work, which may be of interest for the improvement of the results, will be proposed.
- *Pliego de condiciones*: all the general conditions that should be taken into account at the time to carry out this project are detailed in this document.

Furthermore, certain technical, health and safety conditions have been included in relation to the present project.

- Budget: the last of the three documents specifies the project costs, both human and material, where it breaks down the prices and hours for each element, for each stage of the project.

Chapter 2

Characteristics and modelling of turbulent flows

This chapter aims to provide a theoretical background to describe turbulent fluid flows. It will begin by giving a brief description of the main equations that govern the physics of turbulent flows, which are based on the law-conservation of transported equations. The second part will present the main characteristics of turbulent flows, paying attention to turbulent scales and the energy spectrum. Finally, the different mathematical approaches used to solve turbulence will be discussed by taking an interest in Reynolds-averaged Navier–Stokes (RANS), the selected approach to solve the turbulence during the project. Further information could be found in [11] [12].

2.1 Fundamental governing equations

Talking about the movement of a viscous Newtonian fluid and how variables, such as velocity or pressure are related, implies talking about the Navier-Stokes equations. To define these governing equations, it has been assumed that the fluid is a continuous substance and properties of interest such as pressure, flow velocity, density and temperature are not supposed as differentiable but only integrable, which means weakly differentiable.

Furthermore, there are two ways to describe Newtonian fluid flows. The first one is the Lagrangian description, in which each fluid particle is tracked, then their position, velocities, etc., are described as a function of time. However, a complete description of each property inside the flow may become very complex. However, the Eulerian description suggests a closed control volume, within which macro-

scopic fluid flow properties of interest are defined, thereby reducing complexity. Thus, the best option for solving the fundamental equations.

Next, each differential equation's explanation and mathematical formulation are described below. In order to simplify notation, the Einstein summation notation has been used.

2.1.1 Conservation of Mass

Based on the basic principle of continuity mass (also known as continuity equation), which states that the mass cannot be generated or destroyed, the conservation of mass can be derived. This equation declares that the rate of change of mass concerning time shall be equal to the difference between incoming and outgoing mass flux. Then, the following differential expression is obtained:

$$\frac{\partial \rho}{\partial t} + \frac{\partial}{\partial x_i}(\rho u_i) = 0 \tag{2.1}$$

where ρ represents the density, t the time, whereas the position x_i, and velocity vector u_i, are represented by a Cartesian coordinates system. Assuming a compressible fluid, the first term of Equation 2.1 represents the temporal rate of change of the mass flux, while the second one denotes the net mass inflow and outflow through the defined walls of the infinitesimal control volume.

2.1.2 Conservation of Momentum

Momentum is defined as the quantity of motion of a moving body, in other words, the product of the mass density and flow velocity (ρu_i). The conservation of momentum can be deduced by Newton's second law, which states that a body will remain at rest or in continuous motion if any external force is applied. These kinds of forces could be of two types, surface forces or body forces. Thus, by establishing a momentum balance within the defined control volume and using the same form as used in equation 2.1, it is possible to define the momentum conservation law:

$$\frac{\partial \rho u_i}{\partial t} + \frac{\partial (\rho u_i u_j)}{\partial x_j} = -\frac{\partial p}{\partial x_i} + \frac{\partial \tau_{ij}}{\partial x_j} \tag{2.2}$$

where p represents the pressure and τ_{ij} is the viscous stress tensor. Similarly to the continuity equation, the first and second terms represent the temporal change of momentum and the flux over the control volume, respectively. In this case, two main external surface forces are involved in this project, which are the force due to

a pressure gradient $\partial p/\partial x_i$ and viscous stress tensor τ_{ij}. According to the Stokes's hypothesis, the tensor could be defined as:

$$\tau_{ij} = \mu(\frac{\partial u_i}{\partial x_j} + \frac{\partial u_j}{\partial x_i}) - \delta_{ij}\lambda\frac{\partial u_k}{\partial x_k} \tag{2.3}$$

where δ_{ij} is the Kronecker delta, μ the dynamic viscosity, and λ, which produces a viscous effect associated with volume change. However, λ tends to approximate $\lambda = -2/3\mu$.

2.1.3 Transport of Species

During a chemical process, such as combustion, the knowledge of the concentration of each species involved is essential. These chemical species may not only be transported due to the fluid flow, otherwise may also be generated or even consumed during the combustion process. A new concept needs to be defined, the mass fraction Y_α.

$$Y_\alpha = \frac{m_\alpha}{m} \tag{2.4}$$

where m_α represents the mass of specie α and m the total mass within the control volume. Considering a mixture, the summation of all the mass fractions must be equal to one.

Then, the general form of the transport of the species of the mixture is governed by the following equation:

$$\frac{\partial(\rho Y_\alpha)}{\partial t} + \frac{\partial(\rho u_j Y_\alpha)}{\partial x_j} = -\frac{\partial J_{j\alpha}}{\partial x_j} + \dot{\omega}_\alpha \tag{2.5}$$

where, $J_{j\alpha}$ represents the diffusive flux of chemical kinetics, and $\dot{\omega_\alpha}$ is the source term due to the chemical reactions. In comparison to Equation 2.1, two new terms have appeared beside the temporal and convection terms. The first term at the right of Equation 2.5 represents the diffusive flux due to the interaction between chemical species, while the second term $\dot{\omega_\alpha}$ appears due to the change of the mass fractions as a result of the various chemical reactions that may occur in the control volume. Using the kinetic reaction mechanism, this source term can be calculated.

By using Fick's law for diffusive flux, $\dot{\omega}_\alpha$ could be defined as:

$$J_{j\alpha} = -\rho D_\alpha \frac{\partial Y_\alpha}{\partial x_i} \tag{2.6}$$

where D_α refers to the diffusion coefficient for species α. In addition, it could be described as a function of the Schmidt number Sc_α, which is the ratio of momentum diffusivity (kinematic viscosity μ) and mass diffusivity:

$$D_\alpha = \frac{\mu}{\rho Sc_\alpha} \tag{2.7}$$

or the Lewis number Le_α, which is the ratio of thermal diffusivity to mass diffusivity:

$$D_\alpha = \frac{\lambda/\rho}{c_p Le_\alpha} \tag{2.8}$$

where λ is the thermal conductivity and c_p represents the isobaric specific heat of the mixture.

2.1.4 Transport of Enthalpy

According to the first law of thermodynamics, within an isolated system, energy can be neither created nor destroyed, only transformed. There are usually two ways of expressing energy, first is internal energy e, which refers to the amount of energy stored in a body for a constant volume, while the second, the enthalpy h, is based on constant pressure. Although both represent the same quantity, enthalpy is most commonly used to quantify gaseous systems. The enthalpy of a mixture could be defined as:

$$h = \sum_\alpha Y_\alpha h_\alpha \tag{2.9}$$

$$h_\alpha = h_\alpha^o + \int_{T^o}^{T} c_{p_\alpha}(T) dT \tag{2.10}$$

where h_α represents the specific enthalpy of the specie α, h_α^o is the enthalpy of formation of the specie α at reference values of temperature ($T^o = 298.15K$) and pressure ($p^o = 1atm$). Both the enthalpy of formation and isobaric thermal capacity properties for different species are obtained from libraries, JANAF and CHEMKIN, respectively.

Thus, by establishing an enthalpy balance, the general form of the enthalpy of the mixture is governed by the following equation:

$$\frac{\partial(\rho h)}{\partial t} + \frac{\partial(\rho h u_i)}{\partial x_i} = \tau_{ij}\frac{\partial u_i}{\partial x_j} + \frac{Dp}{Dt} - \frac{\partial q_i}{\partial x_i} + \dot{\omega}_h \tag{2.11}$$

where $\dot{\omega}_h$ is the source term for enthalpy, such as radiation or chemical reactions. On the left side, remains the variation of enthalpy with time and the convection term, respectively. Whereas, on the right hand, appears the variation of enthalpy due to the viscous heating and the pressure forces variations. Due to the fact that the internal velocity inside the control volume is low, both terms can be neglected. Then, the third term refers to the heat flux conduction due to a temperature gradient, described by Fourier's law as:

$$q_i = -\lambda\frac{\partial T}{\partial x_i} - \sum_{\alpha=1}^{N_\alpha} \rho h_\alpha D_\alpha \frac{\partial Y_\alpha}{\partial x_i} \tag{2.12}$$

2.1.5 Equation of State

Finally, an equation relating the different state variables is needed to describe the thermodynamic state. In this work, the equation of state for ideal compressible gases is assumed:

$$p\rho = \frac{\mathcal{M}}{T\mathcal{R}} \tag{2.13}$$

where $\mathcal{M}$ represents the mixture molar mass and $\mathcal{R}$ is the ideal gas constant, being $\mathcal{R} = 8.314 J/molK$.

2.2 Turbulence

In most practical combustion processes, the flow velocity is characterised by rapid and random fluctuations, as well as different scalar properties at a given region in the space. Thus, it is said to have a turbulent flow in this case. In addition, these fluctuations spread out over time due to convection or diffusion processes. The knowledge and modelling of turbulence remains a challenge in physics due to its incredible complexity.

Laminar flows can become turbulent by placing a small disturbance of infinitesimal intensity inside the flow. However, the growth of the disturbance is strongly dependent on the finite viscosity of the fluid, which is responsible for damping the disturbance and thereby stabilising the flow. At this point, appears a clear relation between inertial forces and viscous forces. These two important forces are related by an essential nondimensional parameter, which is the Reynolds number.

$$Re = \frac{\rho u l}{\mu} \tag{2.14}$$

where u and l refer to the characteristic velocity and length, respectively. Furthermore, it is possible to define three main regimes:

- Laminar: Re tends to be small due to viscous forces being greater than the inertial forces. Laminar flows are characterised by being smooth and streamlined.
- Turbulent: Re increases to the point where inertial forces are larger than viscous forces. Turbulent flow is characterised by being irregular and chaotic, mainly by the presence of vortexes.
- Transitional: This regime is defined as one in which the Re is neither low enough to be considered laminar nor high enough to be turbulent.

In addition, high values of Re mean that the turbulent flow has a substantial amount of kinetic energy, which is essential to sustain the generation of turbulent eddies. Therefore, a mathematical description, its properties and main modelling techniques are required in order to understand this phenomenon.

2.2.1 Turbulent flow properties

According to [9], for appropriately initial and boundary conditions, as the Navier-Stokes equation and the conservation equations for energy and species are deterministic, a unique solution obtaining a single solution is quite challenging for turbulent flow (large Reynolds number), mainly due to the flow conditions at remote points are continuously changing. In order to describe turbulent flows as well as possible, a statistical viewpoint is required, yielding solutions that are probabilistic. More details on the numerical description of turbulent flows that would go beyond the scope of this work can be found in these books [9] [13].

For a probabilistic description of an instantaneous variable u (pressure, velocity, temperature, ...), by using the Reynolds decomposition, is possible to distinguish two parts: mean value and a fluctuating value. That values will be denoted as $\bar{u}$ and u', respectively

Mean value is defined as:

$$\bar{u} = \frac{1}{\Delta t} \int_0^{\Delta t} u(t) dt \tag{2.15}$$

where $\bar{u}$ represents the mean value of the instantaneous variable over a sufficiently large period Δt.

Whereas the fluctuating value refers to:

$$u' = u - \bar{u} \tag{2.16}$$

such that $\bar{u'} \equiv 0$.

Usually, a turbulent flow presents a spectrum of eddy sizes. An eddy is a counter-rotating vortex riding on the mean flow, for which the velocity and length scales are determined by the average rotational velocity and diameter of the eddy. In addition, the intensity of the turbulent fluctuation can be derived from the measurement of the eddy's vortical velocity. Thereby, it can be summarised that a turbulent flow consists of a set of eddies that subtract energy from the main flow. In turn, these large eddies will divide into smaller eddies, up to a range in which the dissipative effects of viscosity are more significant and will disappear (Kolmogorov scale). This process is called energy cascade process, where three main zones can be distinguished.

- Integral scale. (characteristic variables are defined with the sub-index $[_o]$).
- Inertial subrange.
- Kolmogorov scale. (characteristic variables are defined with the sub-index $[_K]$).

At the integral scale, the length at which it is found the largest eddies with the highest amount of turbulent kinetic energy is called the characteristic length l_o. It is often associated with the large scale instabilities of the flow to the integral scale eddies.

Thus, the turbulent kinetic energy can be expressed as a function of the characteristic velocity fluctuation at the integral scale as $u_o^{'} = \overline{(u'^2)}^{1/2}$ and assuming isotropy, yields to:

$$k \approx \frac{3u_o^{'\,2}}{2} \tag{2.17}$$

In addition, from the definition of Reynolds number, equation 2.14, a turbulent Reynolds number can be expressed as:

$$Re_o = \frac{u_o^{'} l_o}{\nu} \tag{2.18}$$

where $\nu = \mu/\rho$ is the kinematic viscosity of the fluid.

Clearly, not all eddies are the same size, and not all eddies have the same amount of kinetic energy, which is outlined by the intensity of the velocity fluctuations at each scale. as it was said before, these large eddies break up into small eddies, transferring all its energy to the small ones without losing energy. This universal range, which is the second zone of the energy cascade, is well-known as the inertial subrange. This range is characterised by the energy transfer rate:

$$\varepsilon \approx \frac{u_o^{'3}}{l_o} \approx \frac{k^{3/2}}{l_o} \tag{2.19}$$

During the inertial subrange, the energy transfer rate is completely independent of the molecular viscosity.

In addition, the turbulent time or rotation time of the integral eddies can be identified as the integral time scale, which corresponds to:

$$\tau_o \approx \frac{l_o}{u_o^{'}} \approx \frac{k}{\varepsilon} \tag{2.20}$$

So that, through the inertial subrange, at a rate of ε, the turbulent kinetic energy in eddies of the integral moves from larger eddies to the small scale of eddies, where the viscous dissipation is greater. This minimum scale of eddies is the third and final zone of the energy cascade, defined by the Kolmogorov scale l_K. On the basis of the energy conservation, the energy transfer rate at the end of the inertial subrange must be equal to the initial energy dissipation rate in Kolmogorov's scale. Consequently, using ε and ν, it is possible to derive Kolmogorov parameters, such as the time scale, length scale and velocity as:

$$\tau_K \approx (\frac{\nu}{\varepsilon})^{1/2} \qquad l_K \approx (\frac{\nu^3}{\varepsilon})^{1/4} \qquad u_K^{'} \approx (\nu\varepsilon)^{1/4} \tag{2.21}$$

Subsequently, by using the definition of the turbulent Reynolds number leads to the relation between length and time scales between the integral and Kolmogorov scale as:

$$\frac{l_o}{l_K} \approx Re_o^{3/4} \qquad \frac{\tau_o}{\tau_K} \approx Re_o^{1/2} \tag{2.22}$$

On the whole, turbulent kinetic energy is related to the eddy's size, and, in turn, this is inversely related to the wavenumber K. In Figure 2.1 appears the turbulent kinetic energy spectrum $E(K) \sim dk/dK$ for different defined turbulent subranges.

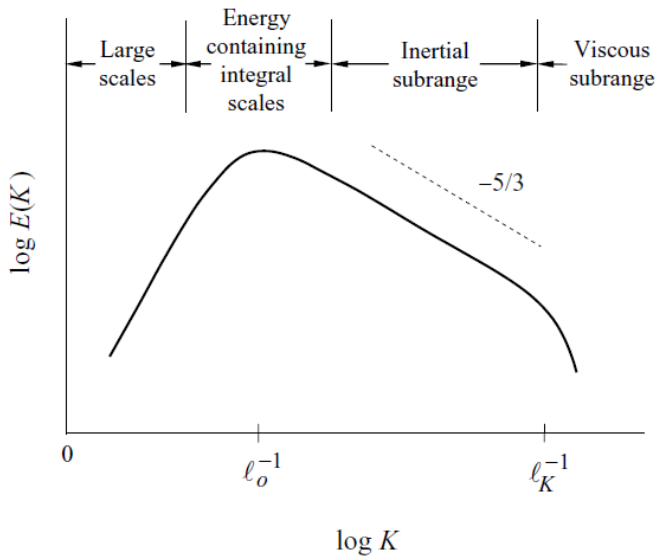

Figure 2.1: Schematic representation of the turbulent kinetic energy spectrum as a function of the wavenumber K. Source: [9].

2.3 Modelling approaches

As it was presented in Chapter 2, Navier-Stokes equations are employed to calculate the motion of fluid flows. Nevertheless, for turbulent cases and, primarily in the presence of chemical reactions, the complexity is substantially increased. Thus, in order to solve turbulent reacting flows a properly modelling turbulence is essential in Computational Fluid Dynamics (CFD).

Next, several numerical approaches that are commonly used for modelling the turbulence are presented. Figure 2.2 shows a brief overview of the three mathematical approaches.

- Direct Numerical Simulation (DNS): This approach solves directly the conservation equations of fluid flows, without the need to model the turbulence. Due to the fact that it is required unless to solve the Kolmogorov length scale, Equation 2.22, involves extremely small time steps and fine meshes. Thus, solving without modelling makes the DNS approach practically impossible for engineering applications.

- Large Eddy Simulation (LES): In this approach, it is possible to filter the Navier-Stokes equations to discard smaller wavelengths, whereas the most energy containing scales are solved directly. The most significant advantage

over DNS is that the computational cost of LES is a great deal lower than DNS, since the size of the mesh can be greater.

- Reynolds Averaged Navier-Stokes (RANS): Finally, by modelling all scales of turbulence without scales of turbulence without resolving them, RANS reduces the computational cost with respect to LES.

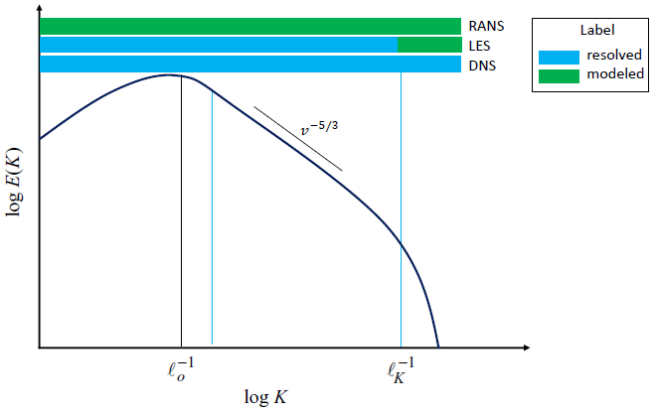

Figure 2.2: Schematic representation of the turbulent kinetic energy spectrum showing the main difference between the three numerical approaches. Source: [12]

On the whole, both LES and RANS are widely employed in modelling turbulent combustion processes. Consequently, due to the reduction of computational cost, it has been decided to use a RANS approach. Then, a larger description of this mathematical model is presented.

2.3.1 Reynolds Averaged Navier-Stokes (RANS)

In the RANS approach, an averaging operation is applied to all of the unsteadiness in the flow in order to model the turbulent flow. Navier-Stokes equations can be averaged according to the Reynolds decomposition as already defined for the velocity in Equation 2.15 and Equation 2.16. Thus, a physical quantity Φ within the turbulent flow can be split into an averaged over time part $\overline{\Phi}$ and the stochastic fluctuating part $\Phi^{'}$, thereby a general quantity Φ inside the turbulent flow could be expressed as

$$\Phi(x_i, t) = \overline{\Phi}(x_i) + \Phi^{'}(x_i, t) \tag{2.23}$$

Then, as a result of an averaging operation to the transported equations, it gives place to a new term, $\overline{\Phi^{'} u^{'}}$. If the momentum equation is considered, this term

becomes $\overline{u_i' u_j'}$, which is called Reynolds stress tensor R_{ij}. There are several approaches to calculate R_{ij}, which could be split into two main categories: the eddy viscosity hypothesis and the Reynolds stress equation models.

The most common approach is the 'Boussinesq's eddy viscosity hypothesis, it assumes that:

$$R_{ij} = \frac{2}{3}k\delta_{ij} - \mu_T \left(\frac{\partial u_i}{\partial x_j} + \frac{\partial u_j}{\partial x_i} - \frac{2}{3}\frac{\partial u_k}{\partial x_k}\delta_{ij} \right) \tag{2.24}$$

where the scalar field μ_T is known as turbulent viscosity. In addition, this μ_T increases the initial molecular viscosity μ. Then, this turbulent viscosity needs to be calculated in order to close the equations. Generally, μ_T is proportional to $\sqrt{k}$ and the mixing length l_m. However, there is the possibility of removing the necessity to define the mixing length l_m by modelling these both parameters and using the energy cascade concept. Several of the most widespread models are, the $k-\epsilon$ model, $k-\omega$ model and Spalart-allmaras. However, in this project, the selected model will be the $k-\epsilon$ model.

The $k-\epsilon$ model

This method is also known as the two-equation model. In turn, it could be broken down into the standard, RNG, and realizable $k-\epsilon$ models, but for this project, the standard model will be further detailed.

Besides the Navier-Stokes equations presented in chapter 2, two more equations are introduced. One of them is to solve the turbulent kinetic energy k, for which a rigorous development of these equations has made so as to obtain the equation. While the second one is used for the energy dissipation rate ϵ, however, for ϵ an empirical approximation is used due to the exact equation being derived from the dissipative range. A piece of further information about these equations can be found in [14]. According to section 2.2, an excellent approximation to model ϵ could be:

$$\epsilon = \frac{C_\mu^{0,75} k^{1,5}}{l_m} \tag{2.25}$$

where C_μ is a model constant and l_m is the length scale of turbulence which will be approximated. Thereby, the turbulent viscosity can be expressed as a function of k and ϵ as:

$$\mu_T = \frac{C_\mu k^2}{\epsilon} \tag{2.26}$$

Therefore, with the specification of the turbulent viscosity and the two transported equations for k and ϵ, the $k-\epsilon$ model is completed.

As it can be seen from references, these transported equations introduce constant models, which in this case, the following values are considered:

$$C_\mu = 0,09; C_1 = 1,44; C_2 = 1,92; \alpha_k = 1; \alpha_\epsilon = 0,76923; \tag{2.27}$$

2.4 General solution procedure

Starting from simple geometries and under ideal conditions, it is possible to derive analytical solutions from the Navier-Stokes equations. However, as time passes, geometries becomes more complex and, in turn, its analytical resolution. Consequently, the use of numerical methods has become essential. The Finite Volume Method (FVM) provides the required tools to solve Navier-Stokes equations by discretising the domain into small control volumes (CV).

2.4.1 Spatial discretisation

The first step in FVM, being one of the most important, is the space discretisation of the transport equations implemented in the CFD software, being, in this case, OpenFOAM. An accurate discretisation will suppose a closer approximation to reality.

As said before, FVM lies in splitting the whole domain into small volumes, which have been called control volumes. In its integral form, the conservation equations, are applied and solved within each CV. Moreover, the main advantage of using FV is that it is capable of adapting to complex geometries, creating a suitable grid for each region.

Thus, a grid or mesh of cells, such as the CVs, are generated. In Figure 2.3, a generic control volume is represented, where P and N refer to the centroid of the cell and its neighbour, respectively, being d_i the distance between each centroid. This centroid stores the value of the property of interest. Moreover, both cells are connected by an internal face, denoted as S_{fi}.

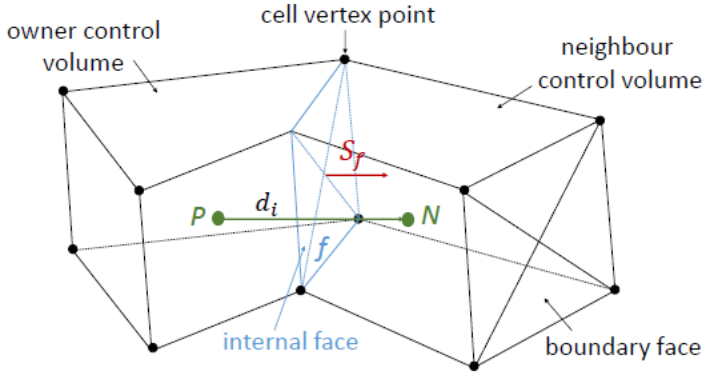

Figure 2.3: Basic representation of two control volumes used in FVM. Source: [12].

According to [12], in order to explain the discretisation and interpolation within each CV, a generic equation of a scalar Φ that represents a typical governing equation is used. This equation is composed as follows:

$$\underbrace{\frac{\partial}{\partial t}(\rho\Phi)}_{time\ derivative} + \underbrace{\frac{\partial}{\partial x_i}(\rho u_i \Phi)}_{convection\ term} = \underbrace{\frac{\partial}{\partial x_i}\left(\frac{\partial \Phi}{\partial x_i}(\rho D_\Phi)\right)}_{diffusion\ term} + \underbrace{\dot{\omega}_\Phi}_{source\ term} \tag{2.28}$$

With Equation 2.28, different generic terms are included, starting from the time derivative part, passing by the convection (or advection) and diffusion part and finishing with the source term. Nevertheless, Equation 2.28 must be expressed in the integral form for each CV with a generic volume V, yielding to:

$$\int_V \frac{\partial}{\partial t}(\rho\Phi)dV + \int_V \frac{\partial}{\partial x_i}(\rho u_i \Phi)dV = \int_V \frac{\partial}{\partial x_i}\left(\frac{\partial \Phi}{\partial x_i}(\rho D_\Phi)\right)dV + \int_V \dot{\omega}_\Phi dV \tag{2.29}$$

In order to simplify the Equation 2.29, by using the Gauss's theorem for the convective and diffusive terms, it is possible to change the volume integrals into surface integrals, being the S the surface of the CV and n_i it's a normal vector. Therefore, the following equation is obtained

$$\int_V \frac{\partial}{\partial t}(\rho\Phi)dV + \int_S \frac{\partial}{\partial x_i}(\rho u_i \Phi n_i)dS = \int_S \frac{\partial}{\partial x_i}\left(\frac{\partial \Phi}{\partial x_i}(\rho D_\Phi)\right)n_i dS + \int_V \dot{\omega}_\Phi dV \tag{2.30}$$

Furthermore, the gradient term, which remains with a volume integral, can be approximated by replacing the volume with the mean value of the general quantity Φ at the cell centre P. This is known as the midpoint rule, which is a second-order approximation. Then, the volume integrals are left as:

$$\int_V (\rho\Phi)dV \approx \rho_P\Phi_P \int_V dV = \rho_P\Phi_P V \tag{2.31}$$

Where Φ_P refers to the mean value of the field Φ at the centre of the cell P. Although the Simpsons' rule is another option to approximate the surface integral, the straightforward way is using the midpoint rule for each of the internal faces f of the CV, Figure 2.3. Hence, the surface integrals of the convective and diffusive terms are transformed as:

$$\int_S \rho u_i \Phi dS \approx \rho_f u_i \Phi_f \int_{S_f} dS_f = \rho_f u_i \Phi_f S_f \tag{2.32}$$

Subsequently, all the faces of the CV must be taken into account. Hence, the sum of all the faces from the CV must be introduced for the convective and diffusive part. Hence, the Equation 2.29 remains as:

$$\left(\frac{\partial(\rho_P\Phi_P)}{\partial t}\right)_P V + \sum_f \rho_f \Phi_f u_i S_f = \sum_f \left(\frac{\partial\Phi}{\partial x_i}\right)(\rho D_\Phi)_f S_f + \int_V \dot{\omega}_\Phi dV \tag{2.33}$$

As is observed in Equation 2.33, time derivative, convection and diffusion terms have been approximated. Although the mean value of Φ_P is known, the value of Φ at the cell faces and its corresponding derivatives must be estimated by interpolation in order to evaluate the convective and diffusive terms. In addition, a discretisation of the source term is needed.

2.4.2 Convection term

Following the discretisation and linearization procedure followed up until now, the convective term yields to:

$$\int_V \frac{\partial}{\partial x_i}(\rho u_i \Phi)dV = \int_S \frac{\partial}{\partial x_i}(\rho u_i \Phi n_i)dS \approx \sum_f \Phi_f \underbrace{(\rho_f u_i)S_f}_{F} \tag{2.34}$$

where F denotes the net flux of mass through the cell surface f of the CV. As it has been noted before, values of the quantity Φ in different points Φ_f of the CV (except in the centre P) are required to solve the approximation of the integral. Assuming that Φ_P and its gradient normal to the cell face in different locations of the CV are known, values at other locations can be derived by interpolation, then, the convective part can be solved. Although there are many forms of interpolation, some of the most commonly used today are presented below [12]:

- Upwind Difference Scheme (UDS): As the convective fluxes tend to have a clear direction, this first approximation assumes that the value of the field Φ in each cell is uniform and equal to its mean value. UDS is a first order method, and it is characterised by being very diffusive, and the error decreases linearly as the cell size decreases.
- Central Difference Scheme (CDS): This scheme interpolates linearly the solution between the centroid P and the centroid of the neighbour cell N. CDS is a second order method, and it is less diffusive than UDS and the error its error is lower for the same mesh size.
- Quadratic Upstream Interpolation for Convective Kinematics (QUICK): The solution at the face is obtained by using a second order interpolation that passes through three centroids, including the downstream one.

2.4.3 Diffusion term

The equivalent procedure used for the convective term was applied to the diffusion term, yielding to:

$$\int_V \frac{\partial}{\partial x_i}\left(\frac{\partial \Phi}{\partial x_i}(\rho D_\Phi)\right) dV = \int_S \frac{\partial \Phi}{\partial x_i}(\rho D_\Phi) dS \approx \sum_f \underbrace{(\rho D_\Phi)_f}_{term\ 1} \underbrace{\left(\frac{\partial \Phi}{\partial x_i}\right)_f S_f}_{term\ 2} \tag{2.35}$$

Regarding the last form of Equation 2.35, diffusion term can be split into two terms in order to derive its solution. The first term, $term1$, is interpolated with the schemes presented in subsection 2.4.2. While for the second term, $term2$, is strongly dependent on the type of mesh, Figure 2.4. When the vector that links the centroids P and N is parallel to the normal vector n_i of the surface S_f, the mesh is considered orthogonal. In this case, the face gradients can be approximated as:

$$\left(\frac{\partial \Phi}{\partial x_i}\right)_f S_f = |S_f| \frac{(\Phi_N - \Phi_P)}{|d_i|} \tag{2.36}$$

where d_i refers to the length between nodes P and N. Nevertheless, if the mesh is non-orthogonal, a correction term must be taken into account to compensate the non-orthogonality.

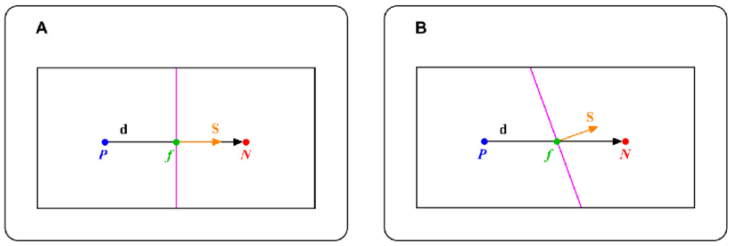

Figure 2.4: Basis representation of an orthogonal mesh (A) and a non-orthogonal mesh (B). Source: [15].

2.4.4 Source term discretisation

Last but not least, the source term refers to the chemical source term, however, does not depend linearly with the field Φ [12], after that, a linearisation is required, yielding to:

$$\dot{\omega}_P(\Phi) = \dot{\omega}_P^c + \dot{\omega}_P^p \Phi_P \tag{2.37}$$

where $\dot{\omega}_P^c$ denotes the constant part of the source term, c refers to constant, while $\dot{\omega}_P^p$ represents the coefficient of change of the source term when as the changing of the field Φ in the centroid P. According to this linearization, the integral of volume of the source terms yields to:

$$\int_V \dot{\omega}_P(\Phi) dV = (\dot{\omega}_P^c + \dot{\omega}_P^p \Phi_P) V \tag{2.38}$$

2.4.5 Time discretisation

Once the spatial discretisation has been approximated for the convection, diffusion and source terms, regarding Equation 2.28, is still missing the temporal discretisation of the time derivative part. This discretisation consists of dividing the time into time steps Δt. Discretizing the time derivative can be carried out by two methods:

- Implicit-time integration: for each time step, in order to solve coupled system of equations it is required the current and future values of the field Φ.

- Explicit-time integration: for each time step, future values are computed as an explicit function of the current ones.

Moreover, it is important to denote that the dependency domain of the numerical scheme must contain the domain of dependence on the physical problem. Otherwise, problems, errors, and divergence may be generated. So it is necessary to introduce the convergence condition by Courant–Friedrichs–Lewy (CFL), which denotes that the Courant number Co, defined in Equation 2.39 used to be lower than the unity.

$$Co = \frac{U}{\Delta x / \Delta t} \tag{2.39}$$

where U is the characteristic velocity, Δx denotes the mesh size and Δt the time step. A visual representation of the Courant number's role is shown in Figure 2.5.

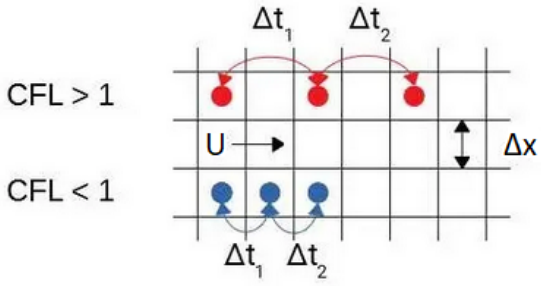

Figure 2.5: Representation of the Courant number and the Courant–Friedrichs–Lewy condition on a generic grid.

Thus, explicit schemes considerably reduce the computational cost, but require that Co is lower than 1. While, for implicit schemes, although solving coupling equations increases the computational cost, being this scheme unconditionally stable. The most widely used implicit methods are Euler (first order) and Crank-Nicolson (second order).

Chapter 3

Characteristics and modelling of combustion

According to Lefebvre [16], combustion may be defined as: "most simply as an exothermic reaction of a fuel and an oxidant". These exothermic reactions appear as results of recombination of chemical bonds that lead to heat and light by the presence of a flame. On the whole, in the aeronautical industry, fuel tends to be gaseous or liquid, while the oxidant is always present in gaseous form.

Along this chapter the different flames and their main properties that differentiate them will be discussed. In turn, the chemical kinetics will be analysed theoretically, differentiating the main types of chemical kinetic mechanisms. Furthermore a brief description of the interaction between turbulence and combustion in premixed flame is presented. Finally, a theoretical basis and a classification of the type of flashbacks present in references will be given.

3.1 Classification of flames

As previously mentioned, a combustion process leads to a flame's appearance, that tends to stabilise under given oxidant and fuel mixture conditions. Thus, depending on how the oxidant and fuel have been mixed before, flames can be divided into two main groups:

- Non-premixed flames: When the oxidant flow is clearly separated from the fuel flow, and later, both are mixed within the reaction zone of the flame. These kinds of flames are also known as diffusion flames.

- Premixed flames: When the oxidant and fuel flow are perfectly mixed before entering to the reaction zone.

The intensity of the combustion is strongly dependent on the concentration of fuel and oxidant present during the reaction process. For practical reasons, it has been decided to represent the main reaction of the whole work in the simplest way. This reaction is the methane oxidation without considering air, only oxygen. And it reads as:

$$CH_4 + 2O_2 \rightarrow 2H_2O + CO_2 \, . \tag{3.1}$$

Thus, according to Equation 3.1, the reaction between of the reactants, methane (fuel) CH_4 and oxygen (oxidant) O_2 gives as a result some products, water, H_2O and carbon dioxide CO_2. Thereby, when all the reactants present in the reaction have been totally consumed and transformed into products, this reaction is said to be stoichiometrically balanced. To assess whether or not a reaction is stoichiometrically balanced, an important property is defined below, the equivalence ratio ϕ:

$$\phi = \left(\frac{Y_{fuel}}{Y_{oxi}}\right) / \left(\frac{Y_{fuel}}{Y_{oxi}}\right)_{st} \, , \tag{3.2}$$

where Y_{fuel}/Y_{oxi} denotes the mass ratio of fuel and oxidizer and the subscript $_{st}$ refers to the stoichiometric state. Thus, ϕ measures the concentration of fuel and oxidizer in a mixture with respect to the stoichiometric concentration of the same mixture. Therefore, if $\phi = 1$ correspond to the stoichiometric condition, if $\phi < 1$, known as fuel-lean, refers to the concentration of fuel is lower than the stoichiometric or that there is an excess of oxidizer in the reaction, whereas, if $\phi > 1$, known as fuel-rich, is the complete opposite situation, there is an excess of fuel or lack of oxidizer.

Hereafter, the main qualitative characteristics between the two types of flames will be reported.

3.1.1 Laminar non-premixed flames

In a laminar non-premixed flame, reactants (fuel and oxidizer) initially are separated, and before, are mainly brought together through the molecular process of diffusion, thence, these sort of flames are called diffusion flames, even, by the possible convective motion of the flow. This flame is characterised due to the fact that both, the mixing and reaction process, happen within the reaction zone. In Figure 3.1 a one-dimensional structure of a non-premixed flame has been represented.

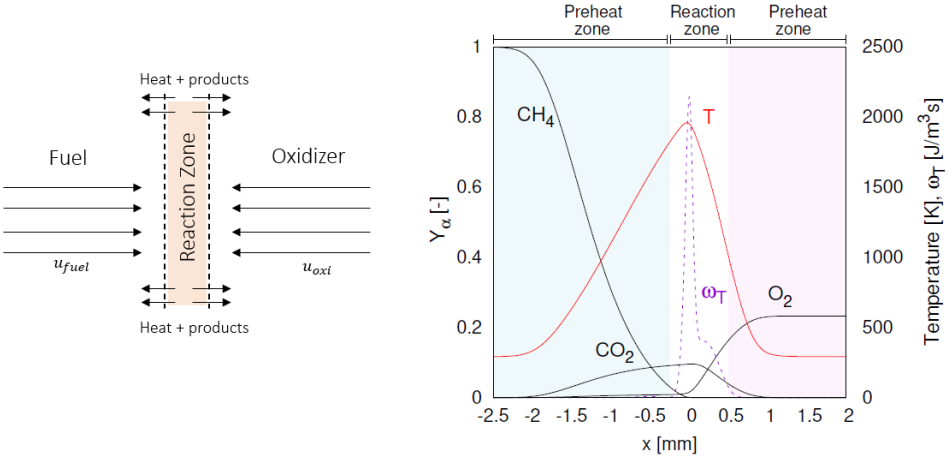

Figure 3.1: Basic one-dimensional physical structure of the non-premixed flame (left) and example of temperature and concentrations profiles for a generic non-premixed reaction CH_4/air [12] (right).

In Figure 3.1 (left) is represented a typical counterflow flame burner, where two opposing nozzles, one feed by fuel and other by oxidizer, which sustain the combustion process, being the convection and diffusion, responsible of the transport of the reactants, resulting in heat and products, which are moved away from the reaction zone. While in Figure 3.1 (right), the structure of the non-premixed flame is divided in two zones, the preheat zone, and this, in turn, a fuel-rich zone and oxidizer-rich zone and the reaction zone. It can be identified how the concentration of reactants starts to decrease as they move closer to the reaction zone, giving way to the reactants, such as CO_2, which go in the opposite direction to the reactants.

However, considering the reaction zone's finite thickness and the reaction's finite rate, acquiring a complete reaction becomes complicated. Consequently, a small quantity of fuel and oxidant does not react, and goes through the reaction zone. This effect is called leakage, and along with a reduction of the flame temperature, the flame may extinct.

3.1.2 Laminar premixed flames

Unlike non-premixed flames, in a laminar premixed flame, all the reactants are already perfectly mixed before the reaction. In addition, this sort of flame is a wave phenomenon, in other words, the flame tends to propagate in the direction of the unburned mixture. Similar to non-premixed flames, a diffusion flux is present as a consequence of a temperature gradient because a local high temperature increases kinetic energy of particles, which means more collisions among the particles of

fuel and oxidizer, resulting in new reactions and hence, the propagation of the flame. In order to reach a local high temperature and start the reactions, a spark is necessary. In Figure 3.2 a one-dimensional structure of a premixed flame has been represented.

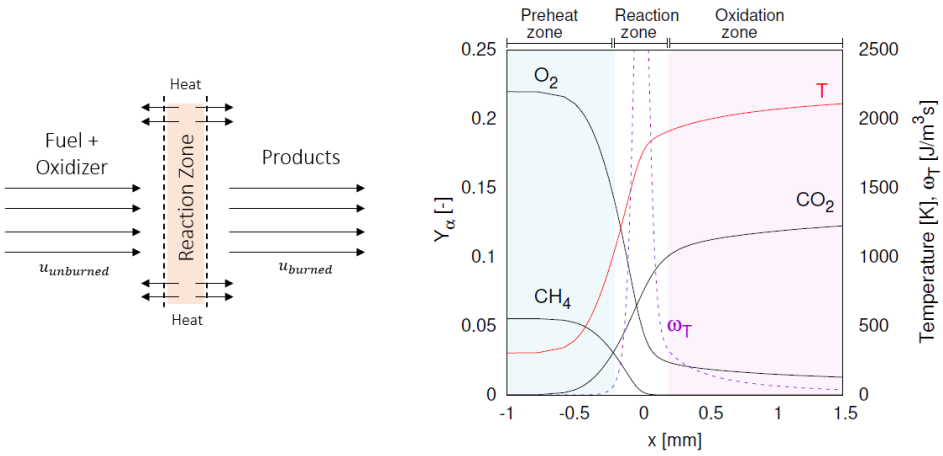

Figure 3.2: Basic one-dimensional physical structure of the premixed flame (left) and example of temperature and concentrations profiles for a generic lean premixed reaction CH_4/air [12] (right).

In Figure 3.2 (left) mixture, fuel/oxidizer is consumed by the propagation of the flame, contrary to the movement of the unburned mixture, being $u_{unburned}$ and u_{burned} the velocity of the unburned and burned mixture respectively. The laminar flame speed s_u^o depends on the diffusivity coefficients of the fuel and oxidizer, equivalence ratio. For instance, in Figure 3.3 the effect of the equivalence ratio can be appreciated for methane, ethane and propane, reaching their peak value at the correct position of the stoichiometric condition.

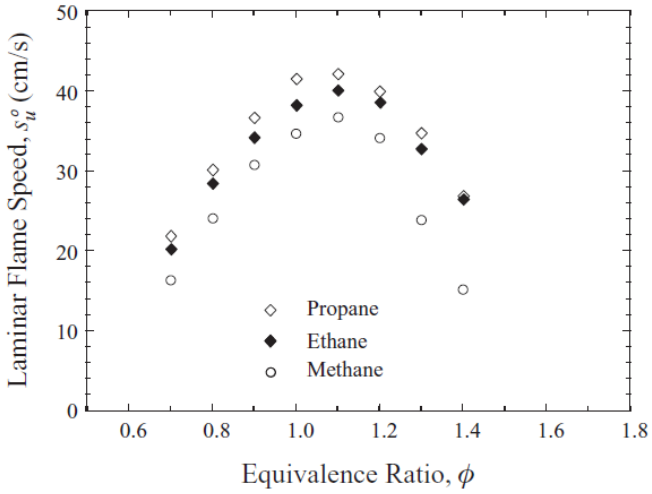

Figure 3.3: Measured laminar flame speed for different n-alkanes in air. Source: [9].

Whereas, in Figure 3.2 (right), three zones can be identified, preheat zone, reaction zone (both represent the diffusion zone) and the oxidation zone. In the preheat zone, the diffusion flux propagates the flame, and it could be identified an initial consumption of the reactants and some reactions due to the appearance of a small amount of CO_2. After the uninterrupted heating of the mixture fuel/air, ignition of the mixture tends to appear (and subsequent reactions). This process occurs within the reaction zone, which may be considered as a heat source or a sink for the reactants. Finally, in the oxidation zone the products of combustion appear, plus any unreacted excess fuel or air.

3.2 Theoretical basis of chemical kinetics

Chemical thermodynamics focuses on the study and description of the equilibrium states of reactions that lead to physical and chemical changes. Then, after reaching chemical equilibrium, from the initial state of a reactive mixture, it is possible to know the final state of the products, both their concentration and their thermodynamic state. However, there are not only two states, otherwise, a large amount of middle species are generated and depleted during the chemical reactions, which means more reactions. And these have different reaction rates and major or minor influence on the global reaction. For these reasons, a good comprehension of the chemical kinetics, which is concerned with understanding the different reaction rates, is essential to explain the combustion process.

With respect to Equation 3.1, reactants transform into products in one single step, but this is only a simplification. In fact, before the formation of the final products of the reaction, several intermediate reactions take place, with their respective intermediate species involved. Apart from CO_2 and H_2O, more species will be generated as a product of the global reaction. Thus, let's suppose that there are K intermediate reactions and N_α species involved:

$$\sum_{i=1}^{N_\alpha} \nu_{i,k}^{'} \mathrm{M}_i \underset{k_{k,b}}{\overset{k_{k,f}}{\rightleftharpoons}} \sum_{i=1}^{N_\alpha} \nu_{i,k}^{''} \mathrm{M}_i, \quad k = 1, 2, ..., K, \tag{3.3}$$

where M_i refers to the chemical symbol for the ith species and ν_i is the molar concentration coefficient of the reaction and $k_{k,f}$ and $k_{k,b}$ are the proportionality factor of the reaction in the forward or backward direction, respectively, also known as chemical rate coefficients. These coefficients are approximated by the Arrhenius law, yielding to:

$$k_{k,f/b} = C_{(f/b)} exp\left(-\frac{E^a_{(f/b)}}{\mathcal{R}T}\right) \tag{3.4}$$

where $C_{(f/b)}$ refers to a pre-exponential factor and $E^a_{(f/b)}$ states the activation energy, which is different for forward or backward direction.

In addition, using the definition of the law of mass action, which states that the chemical rate of any chemical reaction is proportional to the product of the concentration of each reacting substance c_α raised to a power equal to ν_i [16]. Thus, the reaction rate for each reaction ω_k reads:

$$\omega_k = k_{k,f} \prod_{\alpha=1}^{N_\alpha} c_i^{\nu_{i,k}^{'}} - k_{k,b} \prod_{\alpha=1}^{N_\alpha} c_i^{\nu_{i,k}^{''}}, \qquad k = 1, 2, ..., K, \tag{3.5}$$

The concentration of each specie c_α can be defined as:

$$c_\alpha = \rho \frac{Y_\alpha}{\mathcal{M}_\alpha} \tag{3.6}$$

finally, in such a way that:

$$\hat{\omega}_\alpha = \sum_{\alpha=1}^{N_\alpha} \left(\nu_{i,k}^{''} - \nu_{i,k}^{'}\right) \omega_k \tag{3.7}$$

where the subscript $\hat{\omega}_\alpha$ is employed for species α, while ω_k for the reaction k.

Along these lines, according to the initial system of equations, as well as the two transport equations that model the turbulence, being in this case a RANS ($k-\epsilon$ model), must be added N_α transport equations, including its respective chemical reaction rates. One only global reaction may be decomposed into hundred of intermediate reactions, with several intermediate species, which implies resolving thousands of equations.

Obviously, considering a larger number of reactions and species entails a higher accuracy of the resulting products of the combustion. Nevertheless, not all the species are present with the same concentration and importance along with the successive reactions. Based on the concept of major and minor species, both some reactions and species can be assumed to be negligible, hence, reducing the complexity of the reaction mechanism.

3.2.1 Chemical Kinetic Mechanisms

It has been remarked that chemical kinetic mechanisms have an important role in the combustion process, specially for methane combustion, and in turn, its modelling with CFD. However, CFD calculation becomes difficult as the complexity of the geometry or the case is greater, which means an increase in computational time and memory capacity. Thus, making use of very detailed kinetic mechanisms may involve extremely long times or the necessity of huge computational requirements (a lot of processors). Consequently, different mechanisms have been developed in these decades, from the simplest one to thousands of reactions.

Nowadays, as a function of its complexity, chemical kinetic mechanisms have been divided into four categories, being: *detailed*, *skeletal*, *reduced* and *global* mechanism [17] [18].

- *Detailed* mechanisms: These are the most "complete" mechanisms that replicate all the possible intermediate reactions and species involved in one *global* reaction. Obviously, these mechanisms are very accurate for the main combustion process, such as the methane combustion, but some simplifications are applied, thereby, it is possible that they are not fully accurate for the combustion prediction of a few small fuels such as CO or H_2. Some examples of *detailed* mechanisms for methane combustion are GRI 3.0 with 53 species and 325 reactions [19] or San Diego with 56 species and 235 reactions [20].
- *Skeletal* mechanisms: these mechanisms are based on elementary reactions that start from the fuel oxidation until they reach the final products of the combustion. The main difference between the *detailed* mechanisms is that *skeletal* mechanisms are obtained from the detailed ones by removing reac-

tions and species that do not contribute significant changes to the combustion process. An example could be GRI 1.2 with 32 species and 177 reactions [21].

- *Reduced* mechanisms: In the case of a further simplification, a reduction method described by Wang and Frenklach [22] is used to lump certain intermediate reactions in the reaction path. In Figure 3.4 a representative comparison between a *reduced* mechanism and a *detailed* mechanisms has been presented. Some examples of *reduced* mechanism are DRM22 with 22 species and 104 reactions or DRM19 with 19 species and 84 reactions [23].

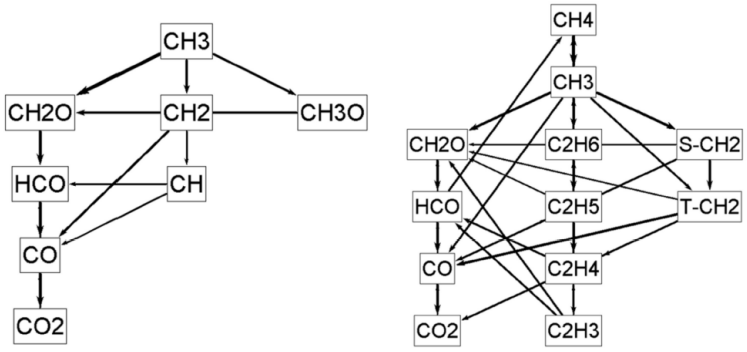

Figure 3.4: Example of reaction paths for a *reduced* mechanism (a) and a *detailed* mechanisms (b). Source: [24].

- *Global* mechanisms: these mechanisms are based on a few reactions, from 1 to a maximum of about 4 reactions for the basic fuels. This sort of mechanisms focus on describing global flame properties such as the flame velocity or temperature. While, further information about the chemical composition of the flame, such as pollutants, are out of range. A basic *global* mechanism was presented in Equation 3.1.

In the present work, two different *Skeletal* mechanism will be used for the simulations. For further insight, in [24] there is a whole evaluation and bibliographic study about several chemical kinetic mechanisms for methane combustion.

3.3 Turbulence and combustion interaction in premixed flames

Along the project, turbulence and combustion have been described separately, focusing on the main properties and categories. Furthermore, a few numerical approaches for turbulence have been presented, such as RANS, and different chemical kinetic mechanisms in order to describe the reactions involved during the combustion process, such as *skeletal* mechanisms. Nevertheless, combining both, analysing turbulent flows becomes more demanding due to the appearance of chemical reactions.

The presence of eddies facilitates the combustion process, as it promotes the mixing and diffusion process, while, at the same time, the surface area of the flame increases due to the wrinkling of the flame, which implies an increase in the total burning rate. However, it also may have unfavourable effects because, if the intensity of the turbulent eddies is greater, it may entail a local extinction of the flame, that can spread and quench the flame. As a result, different regimes of combustion have been identified for premixed and non-premixed flames. As a premixed mixture is used in this work, only the premixed combustion diagram has been presented, while for further information about non-premixed combustion can be given by Law [9].

In order to describe completely the different regimes present in a premixed turbulent flame, some parameters and its ratios should be defined. Denoting s_L as the laminar flame speed, the characteristic length l_L and time scales $\tau_L$of the laminar flame reads:

$$l_L = \frac{\nu}{s_L}, \quad \tau_L = \frac{\nu}{(s_L)^2} \tag{3.8}$$

and thus, according to integral scales defined in section 2.2, integral turbulent Reynolds can be defined as a ratio of the parameters defined in Equation 3.8:

$$Re_o = \frac{u_o^{'} l_o}{\nu} = \frac{u_o^{'}}{s_L} \frac{l_o}{l_L} \tag{3.9}$$

Furthermore, it is necessary to define a relevant parameter that relates whether it is possible to get a laminar flame within a fully turbulent flow. This parameter is called Karlovitz number (Ka), which represents the ratio between the characteristic time scale of the laminar flame and the smallest turbulence time scale, which is the Kolmogorov scale, and it reads as:

$$Ka_L = \frac{\tau_L}{\tau_K} = \left(\frac{l_L}{k_K}\right)^2 \tag{3.10}$$

In addition, Ka_R may be defined, which is the Karlovitz number for the reaction, hence, the ratio is referred to the reaction zone thickness l_R and it reads as:

$$Ka_R = \frac{\tau_R}{\tau_K} = \left(\frac{l_R}{k_K}\right)^2 \tag{3.11}$$

Thus, looking at Figure 3.5, different regimes can be identified as a function of the previous parameters.

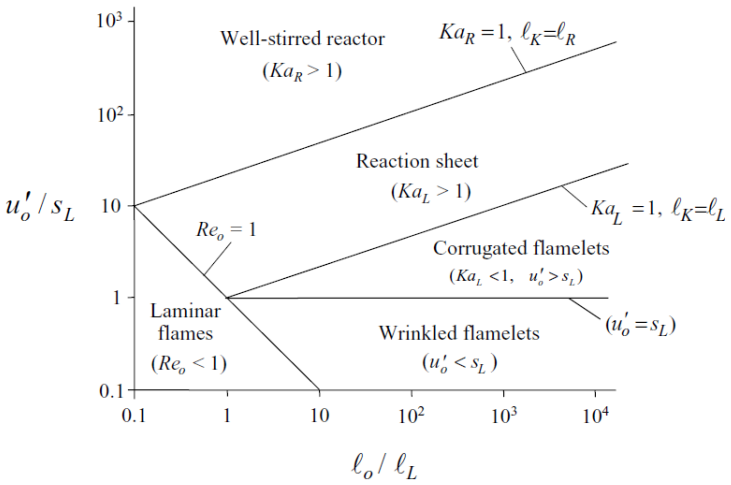

Figure 3.5: Premixed turbulent combustion diagram. Source: [9].

- Laminar Flame Regime ($Re_o < 1$): This regime is characterised by presenting a laminar flow, a slight flame wrinkling can be noticed as a consequence of the low turbulence intensity.
- Wrinkled Flamelet Regime ($Re_o > 1$, $Ka_L < 1$, $u_o^{'}/s_L < 1$): As the $Ka_L < 1$, the flame structure keeps laminar despite the presence of the turbulent flow, which means large eddies, that are greater than flame thickness, hence, only change the flamelet surface.
- Corrugated Flamelet Regime ($Re_o > 1$, $Ka_L < 1$, $u_o^{'}/s_L > 1$): While $Ka_L < 1$, the flame structure remains laminar. However, eddies generated by the turbulent flow start reducing its scale, therefore, a higher deformation of the

flame structure may be noticed. Even it is possible to expect a flame folding locally.

- Reaction-Sheet Regime ($Re_o > 1$, $Ka_L > 1$, $Ka_R < 1$): As $Ka_L > 1$ implies that a few eddies scales are smaller than the flame thickness, thus, eddies can penetrate within it. Large eddies carry on wrinkling the flame structure, whereas smaller eddies inside the preheat zone enhance the diffusion process, as a consequence, flame thickness becomes broader. While $Ka_R < 1$, Kolmogorov scales can not penetrate the reaction zone.
- Well-Stirred Reactor Regime ($Re_o > 1$, $Ka_R > 1$): In this last regime, $Ka_R > 1$, which means that Kolmogorov scales has a smaller size than the reaction zone. Consequently, smaller eddies within the preheat and reaction zone enhance highly diffusion and heat transfer, whereby flame temperatures decreases rapidly, ending with the extinction of the flame.

3.4 Boundary wall flashback

Using a premixed combustor carries with it several operability issues, such as blowout, autoignition, flashback or dynamic stability [25]. Characterise this kind of phenomena requires time and development. Since 1940, very few studies about flashback have been carried out. In Figure 3.6 can be observed the number of published reports addressing boundary layer flashback from 1934 to 2017.

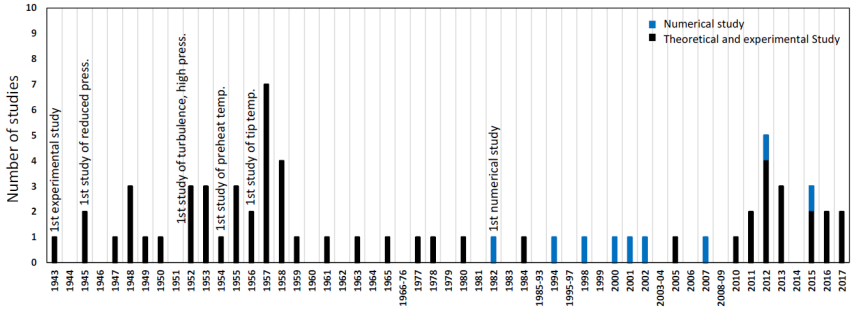

Figure 3.6: Number of studies carried out per year related to boundary layer flashback. Source: [26].

As it can be observed, few articles have been published about flashback, which reduces the insight about this phenomenon, in particular, studies addressed with the turbulent boundary layer flashback.

3.4.1 Flashback mechanisms

Flashback appears when the flame travels from the combustion region towards the premixing section of the combustor. This propagation arises when the flame speed reaches the flow velocity at some point of the premixing section [16]. Such cases tend to emerge mostly near the combustor walls, which may entail regions of undesired high temperatures that can seriously damage the engine.

Four types of flashback has been recognised in gas turbine combustor: (1) flashback in the core flow, (2) combustion induced vortex breakdown (CIVB) (3) flashback as a consequence of combustion instabilities and flashback in the wall boundary layer. Next, a briefly introduction to each of them. For further information and examples of each of them is recommended to read [26] and [27].

Core Flow Flashback

When the core flow velocity drops below the turbulent burning velocity, the flame tends to propagate in the core flow. In addition, if some swirl motion appears inside the flow motion, local axial velocity component decreases, even the turbulent burning velocity is increased due to the flame stretching as a consequence of the interaction between vortex and flame, making easier the flashback generation. Nevertheless, during gas turbine operations, high axial velocities are commonly reached inside the combustor, hence, this type of flashback tends to be neglected.

Combustion Induced Vortex Breakdown

In the aircraft industry, swirl-stabilised burners are used to retain the flame within the combustor. The swirl motion applied to the flow generates a vortex breakdown, that is strongly dependent of the swirl number, which indicates the relative amount of swirl strength. This value should be greater than a critical swirl number in order to generate a vortex breakdown.

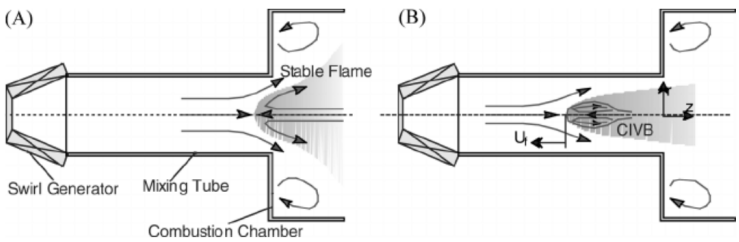

Figure 3.7: Core Flow Flashback due to a vortex breakdown inside a combustor (A) stable flame (B) flame propagation through premixed region. Source: [28].

In Figure 3.7 is presented an schematic example of a vortex breakdown flashback with the presence of the backward-facing step in the geometry. Furthermore, a closed bubble takes place at the tip of the recirculation zone. Due to the fact of the volumetric expansion, a positive vorticity is generated, moving of the bubble downstream and stabilising the flame. But as a result of non-aligned pressure and density gradients, a baroclinic torque is generated, producing negative vorticity, bringing on an upstream propagation of the bubble within the premixed region.

Combustion Instability Induced Flashback

Large oscillations inside the flow can lead to combustion instability, resulting in flashback. These instabilities appear as a result of the interaction between the heat release, acoustic modes, and flow structure. In Figure 3.8 it can be clearly appreciated that the backward-facing step generates large vortices, which at each acoustic cycle, results in the upstream flame propagation within the premixed region.

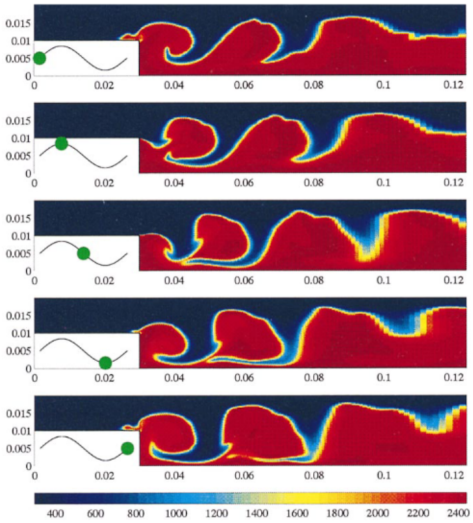

Figure 3.8: Temperature field in a backward-facing step for a premixed flames with LES. Source: [29].

In addition, in Figure 3.9 another case of premixed combustion with a backward-facing step is presented. This experiment was carried out with the following conditions, a premixed propane/air combustion with an equivalent ratio $\Phi = 0.65$, with an inlet velocity of $U = 6$ m/s and Re = 8475, being values close to those that will be used during the project. In Figure 3.9 (a) it has been observed the CH*

emissions, that are generated as a consequence of the high-temperature reactions which occur in the flame front of the combustion. Furthermore, Figure 3.9 (b) shows the volume fraction of the products and reactants during the combustion process. Looking at both figures, on the one hand, it can be clearly seen that due to the flow reversal generated by the large fluctuations, the flames propagates upstream the step. On the other hand, it can be noticed that, due to the large vortices generated after the step, the flame front collides on the top wall and the leading edge folds. Looking carefully at the third frame, Figure 3.9 (b)(3), some products seems to be trapped to the top wall during the combustion evolution. This effect is due to the last mechanism, the boundary layer flashback, which this project will focus on.

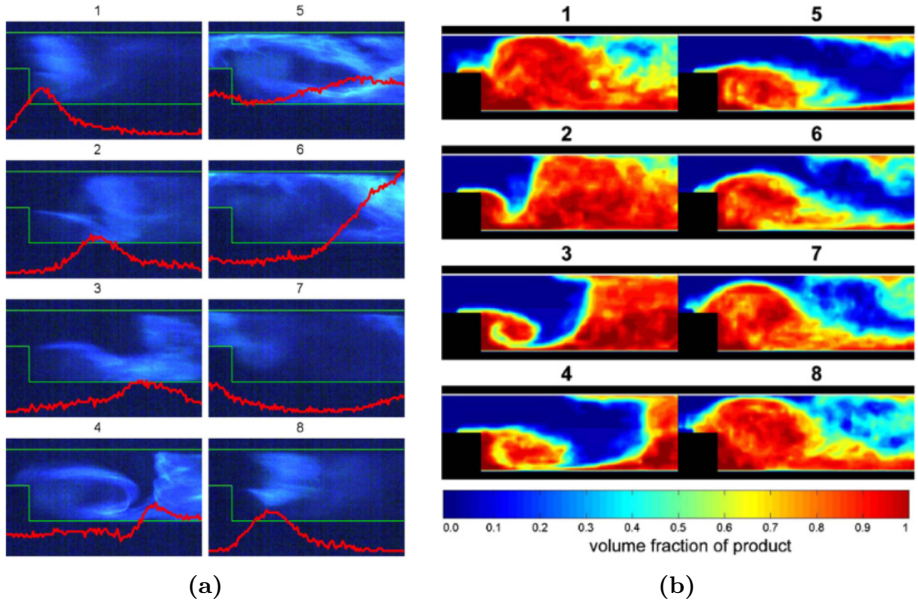

(a) **(b)**

Figure 3.9: (a) CH* chemiluminescent emissions in premixed combustion experiment with a backward-facing step (b) local products concentration, being products and reactants depicted as red and blue, respectively. Source: [30].

Boundary Layer Flashback

Boundary layer flashback or boundary wall flashback tends to be the most common mechanism of flashback in gas turbine combustors. As it was mentioned earlier, high axial velocities are reached in the combustion chamber, greater than the turbulent flame speed. However, the flow velocity tends to decrease close to the wall due to the no-slip condition. Moreover, the burning velocity decreases as it approximates to the wall as a consequence of the heat loss or flame stretch as well, this region is also known as "quenching distance". Thus, flashback will take place where the burning velocity is greater than the flow velocity near the wall.

In Figure 3.10 has been presented four usual flashback scenarios in gas turbine combustors. The most representative and the object of study will be the case (a), as this will be the situation that will arise along the future simulations.

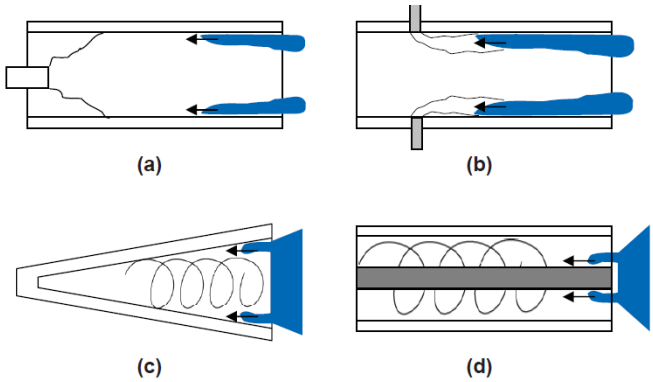

Figure 3.10: Different types of wall flashback in gas turbine combustors. Source: [27]

In order to characterise the boundary wall flashback, references have defined the critical velocity gradient, which states the bulk flow velocity when the flashback occurs, which serves to predict the behaviour of the flashback for a given condition and helps to explain the phenomenon of boundary layer flashback.

3.4.2 Simple model for wall flashback prediction in laminar flows

In order to predict the boundary wall flashback the critical velocity gradient model of Lewis and von Elbe is presented. This model disregards the interaction between the flame and the local flow and assumes a constant laminar velocity profile. In Figure 3.11 an schematic representation of the critical velocity gradient prediction model is illustrated, where the velocity profile of the unburned mixture $u(y)$ and

the stabilised flame front near the wall, characterised by the flame speed $S_f(y)$ can be identified.

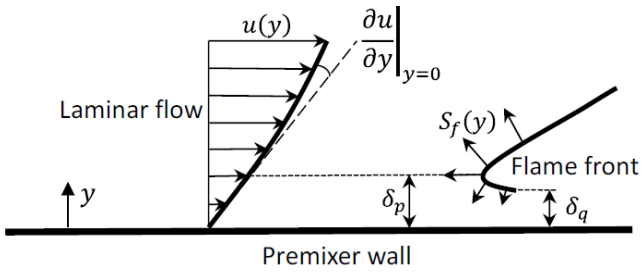

Figure 3.11: Schematic model for wall flashback prediction in laminar flows. Source: [26].

Approaching the wall intensifies heat losses and quenching of radicals begetting a decrease of the flame speed. Distance at which the flame is quenched is denoted by δ_q. The streamwise velocity gradient close to the wall reads:

$$g = \left.\frac{\partial u}{\partial y}\right|_{y=0} = \frac{|\tau_\omega|}{\mu_u} \tag{3.12}$$

where τ_ω is the wall shear stress and μ_u the dynamic viscosity of the unburned mixture for a given condition. According to this theory, flashback is located at a certain distance δ_b from the wall, also called penetration distance, where flow velocity is equal to the burning velocity. Thus, the value of the flow velocity at this δ_b refers to the critical velocity gradient g_c and it is satisfied that:

$$S_f(\delta_b) = g_c \delta_b \tag{3.13}$$

Therefore, the flame remains stationary as long as the velocity gradient is not greater than the critical value. In order to have a better understanding of the model, Figure 3.12 illustrates a burning velocity profile against three different flow velocity profiles. Along the quenching distance δ_q, the burning velocity is zero. At the penetration distance δ_p the critical velocity gradient condition is reached (line 2) being possible the emergence of the flashback. If the free stream velocity decreases (line 1) the flame arises back and then propagates upstream until reaches a balancing condition. Nevertheless, if free stream velocity is increased (line 3), no flashback is possible.

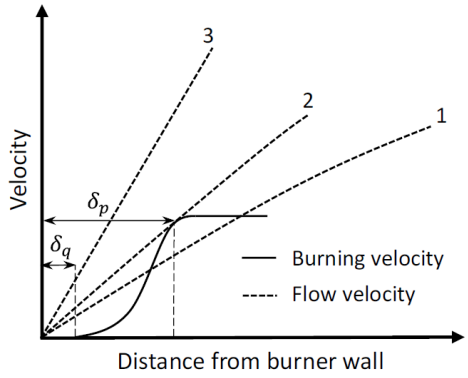

Figure 3.12: Burning velocity profile with respect to there different flow velocity profiles at flashback condition. Source: [26]

However, both laminar and turbulent regimes, when a flame confined between two walls is considered, the interaction wall-flow and the wall-flame cannot be neglected. Subsequently, several parameters have an important influence on flashback propensity, which can be divided into:

- Flow and combustion characteristics
- Operating conditions
- Flame configuration and boundary layer heating

It will be in the results section where each of the groups is briefly described, as they are the object of study of this project.

Chapter 4

Methodology

As time goes by, the perception and insights about fluid dynamics have been growing exponentially, and its complexity with it. Consequently, it surges the necessity of using mathematical tools capable of solving, or rather, simulate the fluid motion and heat transfer. This part of the fluid mechanics is well-known as Computational Fluid Dynamics (CFD) and can be simulated by data structures and numerical calculations implemented in commercial CFD software. Nowadays, the CFD market is expanding and developing, providing high-quality mathematical tools, Autodesk CFD, SimScale, Ansys and OpenFOAM are just some of the most widely used commercial CFD software in the engineering industry.

Subsequently, this chapter focuses on the OpenFOAM software environment, which will be briefly explained. Next, the problem to be covered during the project will be defined, specifying both the physical parameters and the parameters selected for each file in the OpenFOAM software. Lastly, it will finish with the generation of the mesh and a mesh independence based in a simple case of methane/air.

4.1 OpenFOAM Software

OpenFOAM is characterised by being a free and open source CFD software by OpenCFD Ltd. in 2004. This software is structured in a set of modules (in C++ language) capable of simulating turbulence, heat transfer, and even chemical reactions within a fluid field. Many companies and institutional academies take advantage of this free software. For these reasons, it has been decided to use OpenFOAM along this project.

As it has been mentioned before, each OpenFOAM case has a set of files that describes the whole case and are required to run the simulation. These files are

organised in three principal directories as can be shown in Figure 4.1 and described as follows.

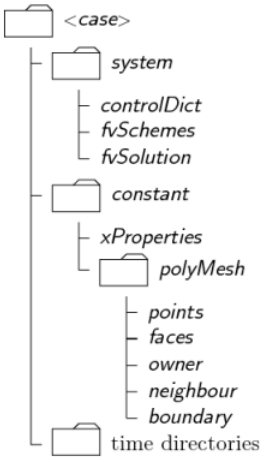

Figure 4.1: OpenFOAM Basic directory structure.

- A `constant` directory: Inside this folder, it can be found the updated files generated by the user, that describe the physical properties of the case to be simulated, such as $transportProperties$. Furthermore, a full description of the generated mesh for the study case (points, faces, etc.), which is located in the $polyMesh$ folder.

- A `system` directory: In this folder is carried out the configuration of the main parameters that define the procedure to be followed in order to solve the case. Three are the main files: $controlDict$ file specifies the run control parameters, such as the start/end time, time step and data output settings; $fvSchemes$ file defines the spatial and time discretization for each time step; $fvSolution$ file controls the equation solvers, tolerances and algorithms set. At least, these three files must be present during the simulation, in fact, extra files may be added to locally modify the initial case or decompose it to run it in parallel.

- A '`time`' directory: This folder is composed of different files that define the fields to be solved in the case, such as pressure, temperature or chemical species. As these parameter must be defined in an initial time or iteration, this folder is stated as 0, for example, the pressure field is initialised at $t = 0$ in the file located $0/p$. As the iterations progress, initial defined fields are stored in new '$time$' folders with the name of the users specified time step or iteration.

Following, the case to be simulated will be presented, focusing on the essential parameters that describe the model, starting from the initial and boundary conditions going through the chemical properties and ending by indicating the selected parameters in the *system* folder.

4.2 Problem specification

In 1983, an experiment was carried out by Robert W. Pitz and John W. Daily and its purpose was to evaluate the premixed combustion of propane and air in the presence of a turbulent mixing layer [31]. This experiment used the Pitz-Daily geometry (to honour its researchers), which generates a recirculation zone that enhances the turbulence after a backward facing step, as it can be seen in Figure 4.2. One of the main objectives of the project is to replicate a premixed combustion of methane and oxygen within a turbulent mixing layer, subsequently, it has been decided to use the same Pitz-Daily geometry due to the fact of the presence of a backward facing step, as well as its effectiveness and simplicity.

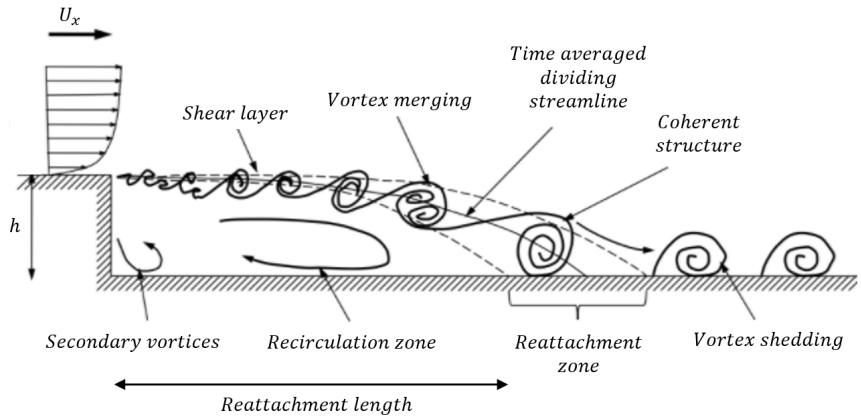

Figure 4.2: Flow over a backward-facing step.

4.2.1 Solution domain

In Figure 4.3 the Pitz-Daily geometry has been represented. This two dimensional domain is composed by a short inlet, a backward-facing step that is the responsible of the flow separation and developed recirculation area inside the domain, while for the flow outlet, the geometry features a convergent nozzle. Dimensions are presented in millimetres.

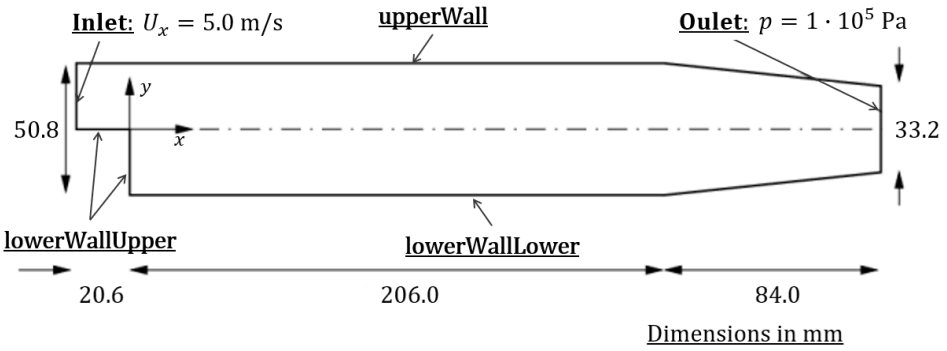

Figure 4.3: Geometry 2D of Pitz-Daily.

Moreover, from the Figure 4.3, it can be identified that the shape of the geometry has been divided into different patches. The types of each patch are: both `inlet` and `outlet` are defined as `patch`; `upperWall`, `lowerWallLower` and `lowerWallUpper` are `wall`; while `frontAndBack` is `empty`, this patch is used as a consequence of the two dimensional domain. Next, it has been represented in Table 4.1 the corresponding boundary conditions at each patch for the most relevant fields of the model, which will be explained in the following paragraphs.

	`inlet`	`oulet`	`walls`
epsilon	turbulentMixingLength--DissipationRateInlet	zeroGradient	epsilonWallFunction
k	turbulentIntensity--KineticEnergyInlet	zeroGradient	kqRWallFunction
p	waveTransmissive	waveTransmissive	zeroGradient
T	fixedValue	inletOutlet	fixedValue
U	fixedValue	inletOutlet	noSlip
Ydefault	fixedValue	zeroGradient	zeroGradient

Table 4.1: Boundary conditions of the patches `inlet`, `outlet` and `walls` for the relevant properties.

Initial and boundary conditions: the 0 directory

Initial and boundary conditions are specified in the `0 directory`. First, an inlet velocity of $u = 5$ m/s has been chosen. Thereby, by using the Equation 2.14, considering a kinematic viscosity of air as $\nu = 10^{-5}$ m^2/s and the height of the step $h = 0.0254$ m, the Reynolds number of the flow is $Re = 12700$. In addition, no slip boundary conditions have been selected for the `walls`. Then, the turbulence has been modelled by RANS, using the $k - \epsilon$ model. Both physical boundary conditions, turbulent kinetic energy k and dissipation rate ϵ, must be specified according to the problem specification. Therefore, assuming an isotropic flow and estimating a 5% of fluctuations of U, the characteristic velocity fluctuation $u_o^{'} = 0.25$ m/s, then, by Equation 2.17, $k = 0.094$ m^2 s^{-2}. Furthermore, by the initial approximation of Equation 2.25, and considering as initial turbulent length scale the 10% of the height of the inlet, $\epsilon = 1.857$ m^2 s^{-3}. Whereas, properly wall functions have been chosen for the different `walls`, Table 4.1.

Regarding to the pressure field p, while `walls` a condition of `zeroGradient` is used, both `inlet` and `outlet` are not supposed to reflect waves, hence a `waveTransmissive` boundary condition has been selected, which by basic thermodynamic calculations removes the possible reflected waves that could modify the simulation.

A standard temperature has been chosen for the `inlet`, $T = 293$ K. However, a good approximation of the `walls` is complex considering that any laboratory experiments has been carried out. Therefore, owing to the high temperatures reached at the combustion process and an efficient cooling system, temperature at `lowerWallLower` will be approximated with a $T = 800$ K, while a standard temperature has been selected for the rest of `walls`. In order to ignite the mixture, a value of $T = 1700$ K is imposed within the domain (auto-ignition by preheating the domain). Furthermore, for the `outlet`, a `inletOulet` boundary condition has been chosen, which is similar to `zeroGradient`, but it substitutes to `fixedValue` if a backward flow is involved. This boundary condition is also applied to the outlet velocity.

Finally, a representative field `Ydefault` symbolises the mass fractions of each specie. Files, such as CH_4 or O_2, which have the same boundary conditions, assign initial mass fractions to each specie, both at the `inlet` and inside the domain. However, as an initial condition, the domain is only filled with an inert gas, nitrogen (N_2). Moreover, adding the file `Ydefault` allows OpenFOAM to create files of initial species that had not been specified.

Mathematical model and numerical techniques: the Constant directory

In this directory, the first file is the `chemistryProperties`, where reaction rates are obtained from the kinetic data. Inside this file, the `chemistryType` solver is defined, such as `EulerImplicit` or `ode` (Ordinary Differential Equations), and in turn, a global approach called Tabulation of Dynamic Adaptive Chemistry (TDAC) could be implemented [32]. This approach is based on a coupling of two simplification methods introduced between the resolution of the CFD and the chemistry. This approach gets together an in situ adaptive tabulation technique (ISAT) [13] with the dynamic adaptive chemistry (DAC) method [33]. Furthermore, the coefficients of the solvers are also specified, and if the `ode` solver has been selected, there are different types of solvers with different orders, among them, `Euler` (order (0)1), `seulex` (order (0)1) or `Rosenbrock34` (order (3)4).

The second file is the `combustionProperties` which specifies the mechanism that models how species mix in each control volume when a reactive mechanism is considered. The mixing rate of reactants takes an important role within the combustion process, hence, an accurate model has to be chosen. These include: `laminar`, `none`, `PaSR`, `EDC`, `zoneCombustion` and `infinitelyFastChemistry`. In this work, the eddy dissipation concept (`EDC`) model has been selected, which is based on Eddy Dissipation Model, that is a turbulent-chemistry reaction model [34]. It is based on splitting the fluid into the reacting zone ("fine structures") and non-reacting zone ("surroundings"). This model has been validated and tested on a wide variety of combustion models with a high degree of success, and is even used in commercial software [35]. In Figure 4.4 shows a schematic representation of the EDC model.

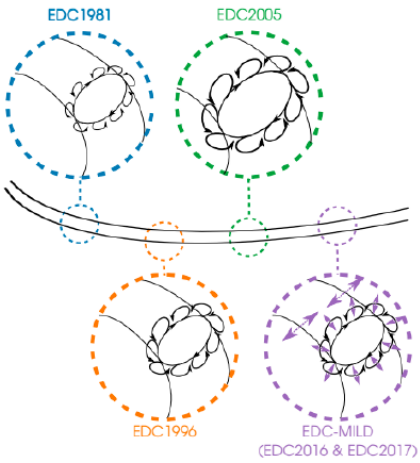

Figure 4.4: Schematic representation of the EDC combustion model. Source: [34]

The third file is the `momentumTransport`, where the turbulence properties are specified. As a RANS approach has been selected, the `chemistryType` should be written as `RAS` and model `kEpsilon`.

The last file required by OpenFOAM is the `thermophysicalProperties`, where all the thermodynamic settings can be modified and adjusted according to the problem to be simulated. Below has been presented the chosen parameters.

```
type                hePsiThermo
mixture             multiComponentMixture
transport           sutherland
thermo              janaf
energy              sensibleEnthalpy
equationOfState     perfectGas
specie              specie
```

Finally, it is required to provide the CHEMKIN information, which is divided into `reactions` and `thermo.compressibleGas`, in other words, the chemical kinetic mechanisms. For this project, two skeletal mechanisms have been generated via the `PyCSP` algorithm [36]. Based on an iterative method proposed by Lam and Goussis which reduces the number of ordinary differential equations with multiple time scales, called the computational singular perturbation (CSP) [37], `PyCSP` algorithm proposes a strategy that analyses and reduces the uncertainty of chemical kinetic models. From a combination of chemical states and the original detailed mechanism proposed by the user, `PyCSP` sequentially applies a series of thresholds to provide a family of skeletal mechanism that preserve the most important species and reactions. In [38] further information about how the algorithm works is described. An schematic representation of the `PyCSP` is presented in Figure 4.5.

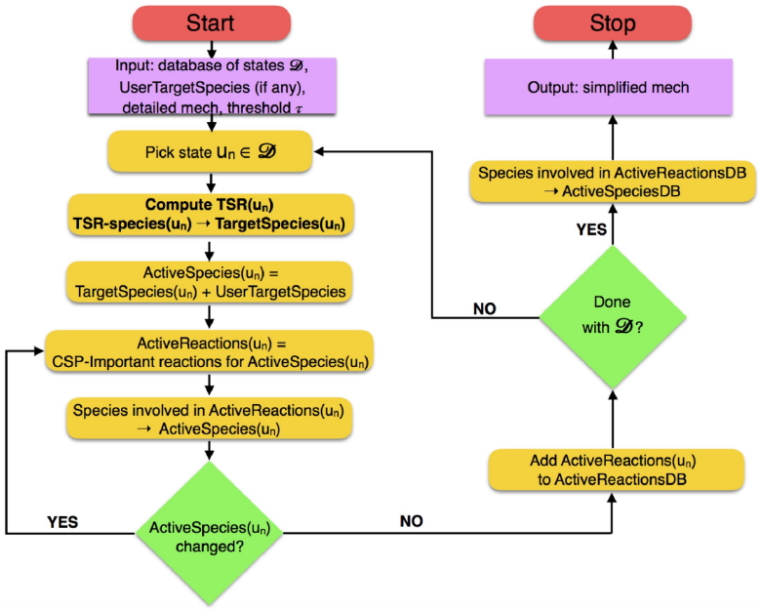

Figure 4.5: Simplified `PyCSP` algorithm. Source: [38]

Therefore, two skeletal mechanism have been generated with the `PyCSP` algorithm.

- `N13-R42`: This skeletal mechanism is composed by 13 species and 42 reactions. It is generated by a training data set of thermochemical states driven from the resolution of 1D counterflow diffusion flame.
- `N19-R68`: This skeletal mechanism is composed by 19 species and 68 reactions. It is generated by a training data set of thermochemical states driven from the resolution of 1D premixed flame.

Numerical discretization and integration: the System directory

Last directory is composed by five files. The first one is the `blockMeshDict` and it is responsible of the mesh generation based on the provided data by the user, such as the vertices or boundary conditions. This file generates the mesh and creates `points`, `faces`, `cells` and `boundary` files located in `constant/polyMesh`. Any modification of the mesh has to be done on the file `blockMeshDict`. As previously mentioned, the PitzDaily case will be used, in consequence, it has been decided to use the mesh provided by OpenFOAM.

By default, OpenFOAM runs in serial, using only a single processor. Nevertheless, the second file `decomposeParDict` allows the user to run each simulation on distributed processors. In this case, as it has worked with a virtual machine and a commercial computer, a maximum of 6 processors have been employed.

Then, for the next files, only the most important parameters within the file itself will be highlighted. The third file is the `controlDict`, where the application or solver, time control, data writing and other settings are defined. The most important inputs from this file are:

```
application             reactingFoam
stopAt                  endTime
writeControl            adjustableRunTime
runTimeModifiable       true
adjustTimeStep          yes
maxCo                   0.4
```

The transient solver `reactingFoam` has been chosen for simulations, which is capable to resolve the turbulent chemical reactions. This solver is based on the stoichiometric reactions and chemical kinetic mechanisms provided by the user to evaluate the production and consumption rate of species. Furthermore, combining, the solver and some thermophysical models, it is possible to acquire required properties of the fluid mixture phase. A simplified structure of the solver is shown in Figure 4.6:

```
...
#include "rhoEqn.H"             //calculate density
while (pimple.loop())
{
    #include "UEqn.H"           //calculate the U/p field
    #include "YEqn.H"           //species transport equation with reaction source term
    #include "EEqn.H"           //determine T from chemical reaction enthalpy lookup
    while (pimple.correct())
    {
        #include "pEqn.H"       //PISO loop to calculate p
    }
    turbulence->correct();      //turbulence modelling
}
rho = thermo.rho();             //update rho from T
...
```

Figure 4.6: Basic structure of the `reactingFoam` solver. Source: [39]

Other essential parameter is the `adjustTimeStep`, which allows `reactingFoam` to adjust the time step along the simulation, in agreement with `maxCo`, which in this case, a value of `0.4` has been selected based of references [40].

The fourth file is the `fvSchemes`, where the numerical schemes are established for each of the terms, such as derivatives in equations. These terms can be divided into different categories as follows:

- `timeScheme or ddtSchemes`: first and second time derivatives, e.g. $\partial/\partial t$. According to the order or accuracy and the steadiness or unsteadiness of the problem different discretisation schemes can be selected. In this case, an `Euler` scheme has been selected, which is a transient, first order implicit and bounded scheme.

```
default         Euler
```

- `gradSchemes`: gradient ∇. This sub-dictionary is composed of gradient terms. Selecting `Gauss` refers to the finite volume discretisation of Gaussian integration, and for the interpolation of values from cell centres to face centres a `linear` interpolation (or central differencing) has been selected.

```
default         Gauss linear
```

- `divSchemes`: divergence $\nabla\cdot$. Excluding Laplacian terms, this sub-dictionary is composed of divregence terms. This includes advection and diffusive terms. Based on several tutorials of `reactingFoam` in OpenFOAM, it has been concluded that the schemes to be used are:

```
div(phi,U)                                  Gauss limitedLinearV 1
div(phi,Yi)                                 Gauss limitedLinear01 1
div(phi,h)                                  Gauss limitedLinear 1
div(phi,K)                                  Gauss limitedLinear 1
div(phid,p)                                 Gauss limitedLinear 1
div(phi,epsilon)                            Gauss limitedLinear 1
div(phi,Yi_h)                               Gauss limitedLinear01 1
div(phi,k)                                  Gauss limitedLinear 1
div(((rho*nuEff)*dev2(T(grad(U)))))         Gauss linear
```

  where `limitedLinear` refers to a `linear` scheme that becomes `upwind` in zones where a quickly changing gradient is present. The required coefficient varies between 1 and 0, `upwind` and `linear`, respectively. Adding a `01` means a stronger bounding between 0 and 1, commonly used for the specie mass transport equations Y_i. Besides, 'V'-schemes are used for vector fields, such as the velocity U.

- `laplacianSchemes`: Laplacian ∇^2. This sub-dictionary is composed of Laplacian terms, which corresponds to the diffusion term in the momen-

tum equations. `Gauss` scheme is the only scheme available, with a `linear` interpolation, and according our mesh, due to the low non-orthogonality of the mesh, an `orthogonal` scheme is selected.

```
default         Gauss linear orthogonal
```

- `interpolationSchemes`: cell to face interpolations of values. A `linear` interpolation for values from cell centres to face centres.

```
default         linear
```

- `snGradSchemes`: component of gradient normal to a cell face. According to the low non-orthogonality of the mesh, an `orthogonal` scheme is selected.

```
default         orthogonal
```

Finally, it remains to define the equation solvers, their tolerances and algorithms, these parameters are specified in the last file, `fvSolution`. Two main sub-directories are implemented in `fvSolution`.

- `solvers`: For each discretised equation, a `linear`-solver has to be defined, which is different from the solver specified in `application` solver (this case: `reactingFoam`) which refers to the complete set of equations and algorithms to solve as specific problem. A `linear`-solver describes how to solve a matrix equation. For instance, for the pressure equation p reads:

```
solver                PCG
preconditioner        DIC
tolerance             1e-6
relTol                0.1
```

where `PCG` or `PBiCGStab` are iterative methods known as the biconjugate gradient stabilized method, which is used for solving numerical, both symmetric and asymmetric linear systems. For the preconditioners, a `DIC` or `DILU` is specified, which refers to a simplified Diagonal-based Incomplete Cholesky preconditioner. In addition, a `tolerance`, value for which the residual is sufficiently small to be considered accurate and `relTol` (relative tolerance), which restricts the relative improvement from the initial to the final solution, are specified. These parameters have been selected on the basis of the OpenFOAM tutorials.

The initial residual is calculated based on the current parameters, then the equation is solved for each field and, for each solver iteration, the residual is recalculated. The solver stops if any of the following conditions occurs:

- The residual reaches the solver `tolerance`.
- The difference between current to initial residuals is lower than `relTol`.
- The number of iterations overcomes the maximum iterations `maxIter`, by default is 1000.

Moreover, even if convergence has been achieved, some field may need to be re-solved again. For instance, if the PISO algorithm is used, the pressure equation has to be solved according to the `nCorrectors` and different settings may need to be specified. These new settings are specified in *pFinal*, such as:

```
$p
tolerance        1e-6
relTol           0
```

For transient simulations, a `relTol` value of 0 is usually employed in order to reach the convergence of the solver tolerance in each time step.

- `relaxationFactors`: In order to improve the stability of the simulation, it is possible to include some relaxation factors. For this case, it has not been considered necessary to include them.
- `PISO, SIMPLE and PIMPLE` algorithms: These algorithms are used to impose mass conservation by coupling equations for momentum and mass conservation. While the semi-implicit method for pressure-linked equations (`SIMPLE`) algorithm is used for steady-state, the pressure-implicit split-operator (`PISO`) and combined `PIMPLE` algorithms are employed in transient cases. For this work, it has been decided to use the `PIMPLE` algorithm.

```
momentumPredictor               yes
nOuterCorrectors                1
nCorrectors                     2
nNonOrthogonalCorrectors        0
```

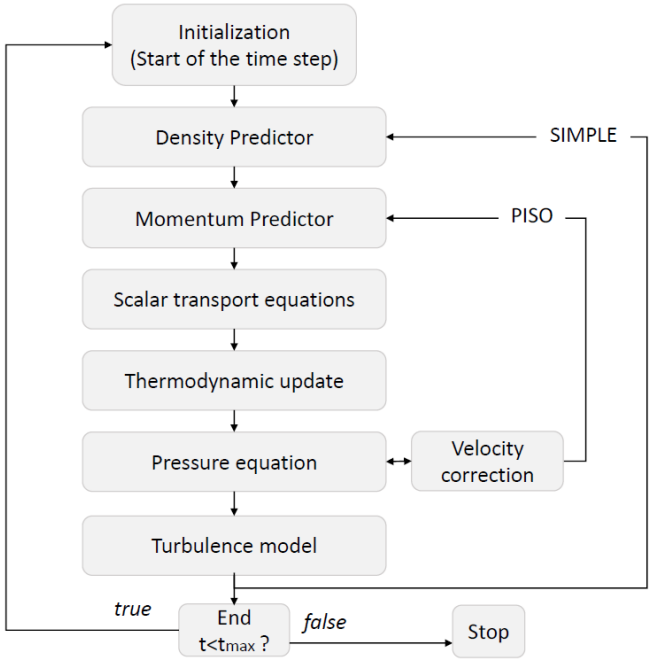

Figure 4.7: Schematic PIMPLE algorithm flowchart. Source: OpenFOAM.

4.3 Mesh generation

The meshing of the domain to be studied is presented next. Due to the presence of a backward-facing step in the domain makes the flow motion much more complex in certain regions of the domain, it is required a grading of the mesh. These regions require a finer mesh because of the highest shear, while a coarse mesh can be applied in the rest of the domain. At the inlet, the flow is completely uniform in the `x` direction, however, when it goes through the step, it induces an intense shear on the fluid below, resulting in a recirculation region (vortex) in the bottom half of the domain, as it can be observed in Figure 4.2. Thereby, a finer mesh is required to be generated close to the corner of the step and stretched out the grading of the mesh along the `x` direction.

In OpenFOAM, the mesh needs to be three dimensional, even though the domain is two dimensional. Then, in `z` direction, the domain is divided only in one cell, with a width of $z = 1$ mm. Subsequently, the computational domain is discretised in 12225 cells in the `x-y` plane, as it shown in Figure 4.8. In turn, the 2D grid is divided into 6 sub-domains, according to the number of processors, each one with approximately 2037 cells. The smallest cell is located near the step and its

corresponding dimensions are $\Delta x = 0.5$ mm and $\Delta y = 0.25$ mm. In Figure 4.8 (a) it is possible to observe a much finer mesh near the step and elongating in the `x` direction. Furthermore, the mesh at the top wall of the domain has been refined, as it can be noticed in Figure 4.8 (b), which allows a suitable range of y^+ (approximately varies from 0.7 up to 22), which has been compared to reference values of y^+ in [14]. Finally, the rest of the domain has been meshed with coarser cells to reduce computational cost.

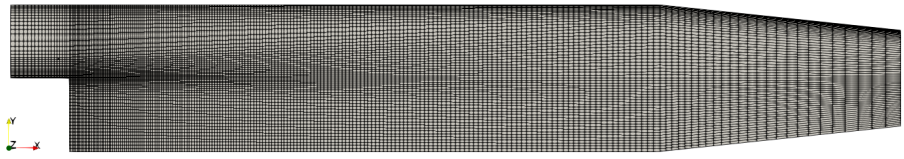

(a)

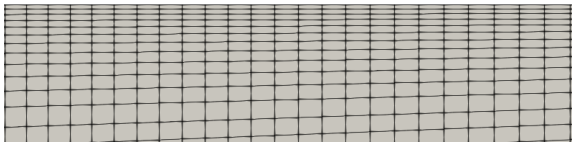

(b)

Figure 4.8: (a) Final mesh of the PitzDaily case. (b) Zoom at the top wall of the domain.

4.3.1 Mesh independence

It is well-known that a numerical model converges if and only if, as the mesh of the entire domain is refined, the solution tends to an invariant solution. However, demonstrating analytically the stability and convergence of a method may be complex whether a non-linear problem is considered, such as the resolution of the Navier-Stokes equations.

Subsequently, before moving on to simulate the problem, a mesh independence study is required in order to be ensure that results are not influenced by the selected mesh. In order to carry out this study, it was decided to simulate a combustion of a mixture CH_4/air with an equivalence ratio of $\Phi = 0.8$ and initial conditions are the same that have been presented in Section 4.2.1, summarised in Table 4.2:

Φ	Y_{CH_4}	Y_{O_2}	Y_{N_2}	T_{N_2} [K]	p [Pa]	U_x [m/s]
0.8	0.0445	0.2228	0.7327	1700	$1{\cdot}10^5$	5.0

Table 4.2: Initial physical conditions for the mesh independence simulations with OpenFOAM.

In this case, only a single reaction has been considered in order to increase the computational velocity. Finally, it has been chosen `EulerImplicit` for the solver of the `chemistryType` without considering TDAC.

As a convergence criterion, it has been decided to simulate the case for 10 times the residence time, which implies a total of t_{res} =0.5 s. In Figure 4.9 a converged solution for 12225 cells is shown. As it is expected, it can be observed the recirculation zone and secondary vortices after the step, equal to Figure 4.2. In addition, this step allows to recirculate combustion hot gases around this region, in order to keep burning the incoming fresh mixture, and hence, the combustion process. Furthermore, it is noticeable that the recirculation zone is overestimated with respect to LES approach [41]. However, it is reasonable to continue using RANS with EDC model as it exhibits a similar behaviour to other references, such as [42], which uses a RANS with EBU (Eddy Break-Up) model.

Nevertheless, looking at the corresponding residuals, it has been proved that convergence is ensured for a $t = 0.3$ s. Because of this, simulations will only be calculated up to this time interval in order to reduce time and computational cost, since, as will be seen in the following sections, the calculation time will be considerably increased by including more species and reactions in the combustion process.

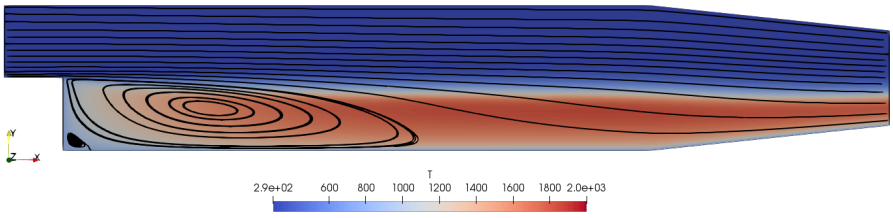

Figure 4.9: Representation of the streamlines and temperature field [in K], for 12225 cells after 0.5 s.

Next, axial values of velocity, temperature and mass fractions of CH_4 and CO_2 have been presented for different numbers of cells (N_i): N_1 = 48900 cells, N_2 = 12225 cells, N_3 = 10677 cells and N_4 = 9337 cells.

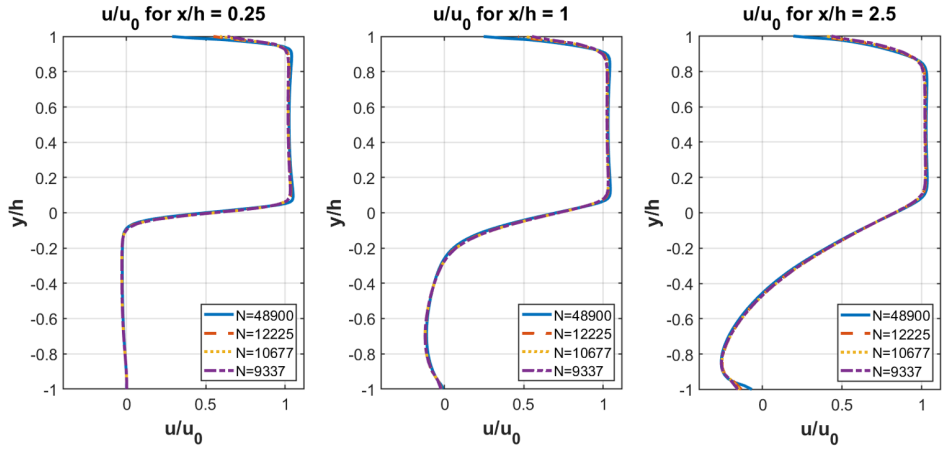

Figure 4.10: Comparison between different number of cells for the normalised average axial velocity at different normalised axial positions at $\Phi = 0.8$.

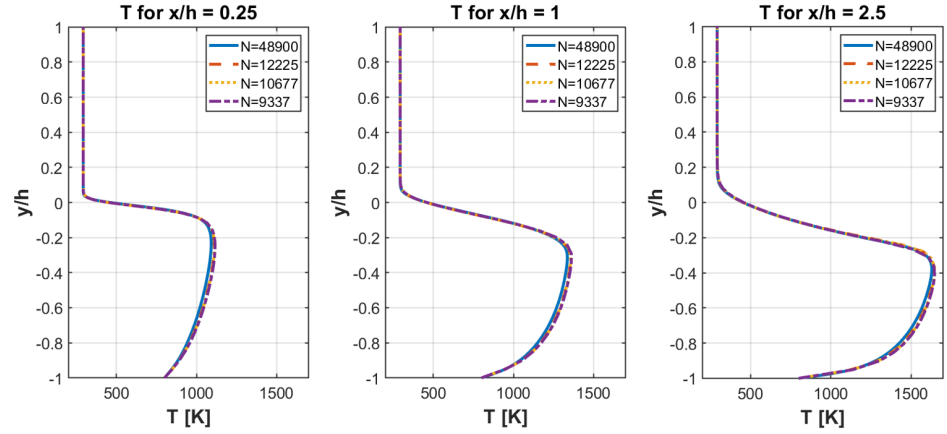

Figure 4.11: Comparison between different number of cells for the axial temperature at different normalised axial positions at $\Phi = 0.8$.

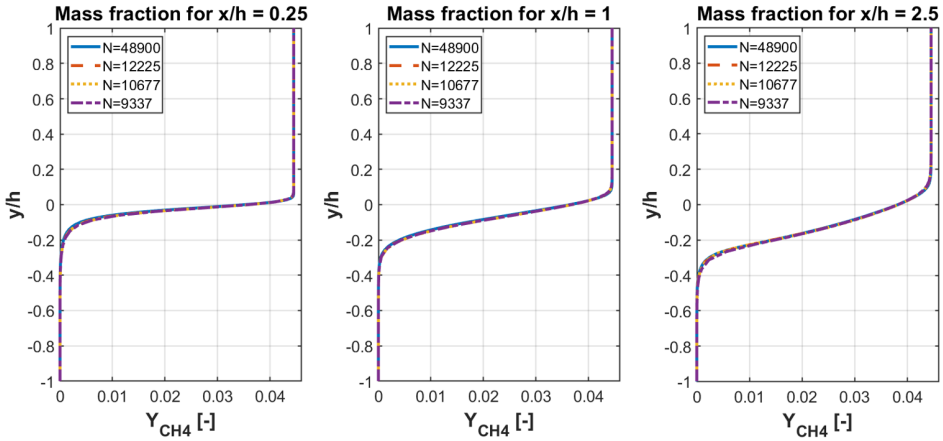

Figure 4.12: Comparison between different number of cells for the axial mass fraction of CH_4 at different normalised axial positions at $\Phi = 0.8$.

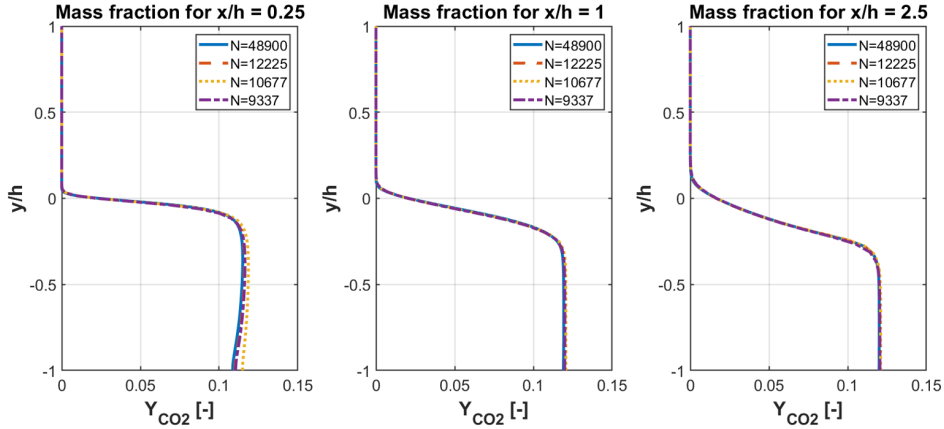

Figure 4.13: Comparison between different number of cells for the axial mass fraction of CO_2 at different normalised axial positions at $\Phi = 0.8$.

After analysing the obtained results for the different meshes, it is reasonable to assume that the effect of the mesh slightly affects the results, as the values of the curves for the different parameters and axial positions are almost identical. The recirculation region is considered the most critical zone, that is why remarkable differences between different meshes are located for $x/h = 0.25$. Then, the relative error for $N_2 = 12225$ with respect to $N_1 = 48900$ for each parameter has been calculated, being $\varepsilon_{u/u_o} = 2.47$ %, $\varepsilon_T = 0.74$ %, $\varepsilon_{CH_4} = 2.10$ % and $\varepsilon_{CO_2} = 1.23$ %.

Furthermore, in Table 4.3 computational time for each simulations is presented.

Number of cells	**Computational time [s]**
48900	9533
12225	1136
10677	1094
9337	767

Table 4.3: Comparison between different number of cells and computational time.

In conclusion, using a finer mesh results is more accurate results within the recirculation zone. However, the mesh with $N_1 = 48900$ entails almost an increasing of 10 times the computational time with respect to $N_2 = 12225$. Therefore, due to the significant reduction in computational time and assuming as acceptable the relative errors lower than 5%, a mesh with $N = 12225$ cells is selected to simulate the the PitzDaily case.

Chapter 5

Results and discussion

In the first part of the chapter, it has been decided to evaluate several `solvers` provided by OpenFOAM and observe whether they have some remarkable effects in the generation and consumption of each specie as well as analysing its effect on the flashback. Subsequently, after chosen the best and affordable solver, it will be continued by checking the effect of a geometry change in the solution. Afterwards, different values of equivalence ratio and wall temperature has been studied to evaluate their effect on the boundary layer flashback. In addition, using the `PyCSP` algorithm, the two different chemical kinetics mechanisms presented in Section 4.2 have been compared to see the influence of introducing new reactions and species on the flashback. Finally, two ways to initiate the combustion of the mixture have been considered in order to observe its effect on the transient regime.

5.1 Sensibility to OpenFOAM solvers

As it was highlighted in previous sections, focusing on obtaining the presence of each specie inside the domain with the utmost precision, taking into consideration the computational limitations is essential. Furthermore, it has been observed along the simulations, that using a premixed mixture of CH_4/O_2, with the same geometry, generates a boundary layer flashback at the upper wall, unlike in the Figure 4.9, this is why using different solvers can provide more or less accurate values of these values.

According to several references, the PitzDaily case is commonly simulated with OpenFOAM [43][44], however, they do not specify the corresponding solver that has been used for their simulation. Therefore, it is possible that huge differences could appear as a function of the selected solver. Then, the main objective is to

assess if they have a noteworthy effect in the results, and if it is worth for the computational cost.

For these simulations, it has been decided to study the combustion of a premixed mixture of CH_4/O_2 for four different solvers. The selected chemical kinetic mechanism is the `N13-R42`. The corresponding physical conditions are an equivalent ratio of $\Phi = 0.75$, and the corresponding mass fractions at the inlet are $Y_{CH_4} = 0.1579$ and $Y_{O_2} = 0.8421$. The whole domain is initially filled with N_2 at 1700 K in order to achieve the ignition.

Φ	Y_{CH_4}	Y_{O_2}	T_{N_2} [K]	p [Pa]	u_x [m/s]
0.75	0.1579	0.8421	1700	$1{\cdot}10^5$	5.0

Table 5.1: Initial physical conditions for the solvers simulations with OpenFOAM.

Furthermore, in Table 5.2 has been presented the chosen solvers, and its respective computational time.

`chemistryType`	**solver**	**Computational time [s]**	Co
`EulerImplicit`	-	Diverge	-
`ode`	`seulex`	91803	0.4
`ode`	`Rosenbrock34`	80629	0.5
`ode`	`seulex` + TDAC	4071	0.4

Table 5.2: Comparison between different solvers and their computational time.

It should be noted that, although an `EulerImplicit` solver has been used before for the mesh independence, if a combustion without the presence of nitrogen in the initial mixture is considered, the solver generates errors during the simulation, probably due to the fact of that reactions are not sufficiently stiff. Therefore, other higher-order ODE solvers have been analysed.

Subsequently, values for normalised velocity, temperature and mass fraction of some species, such as CH_4, CO_2 and OH for different normalised axial positions has been presented below.

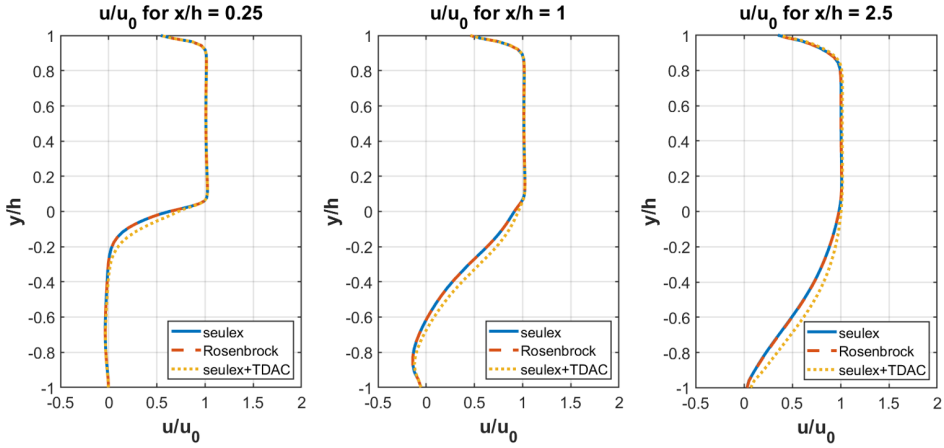

Figure 5.1: Comparison between different number of cells for the normalised average axial velocity at different normalised axial positions at $\Phi = 0.75$.

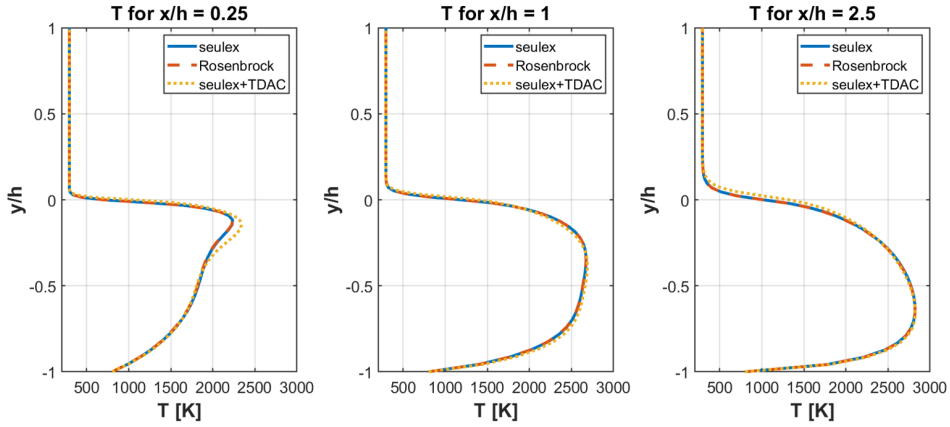

Figure 5.2: Comparison between different solvers for the axial temperature at different normalised axial positions at $\Phi = 0.75$.

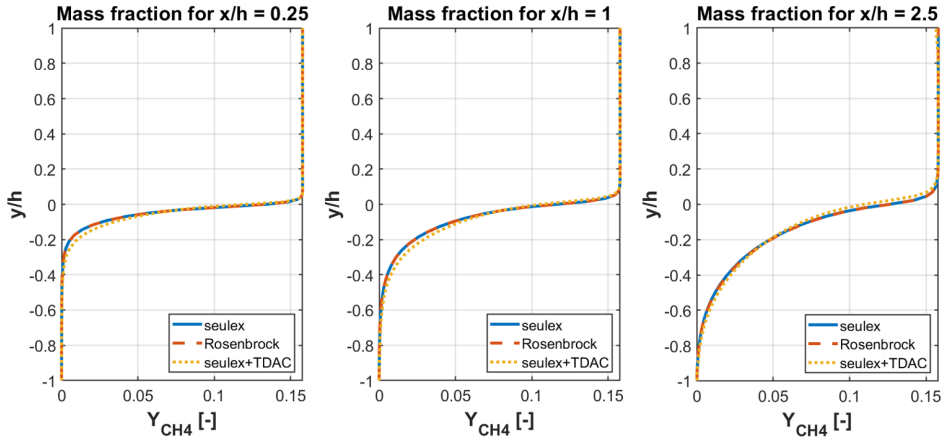

Figure 5.3: Comparison between different solvers for the axial mass fraction of CH_4 at different normalised axial positions at $\Phi = 0.75$.

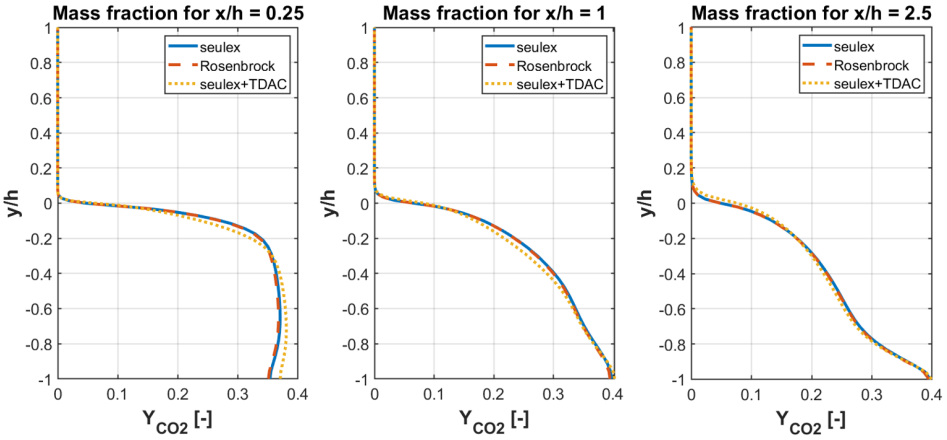

Figure 5.4: Comparison between different solvers for the axial mass fraction of CO_2 at different normalised axial positions at $\Phi = 0.75$.

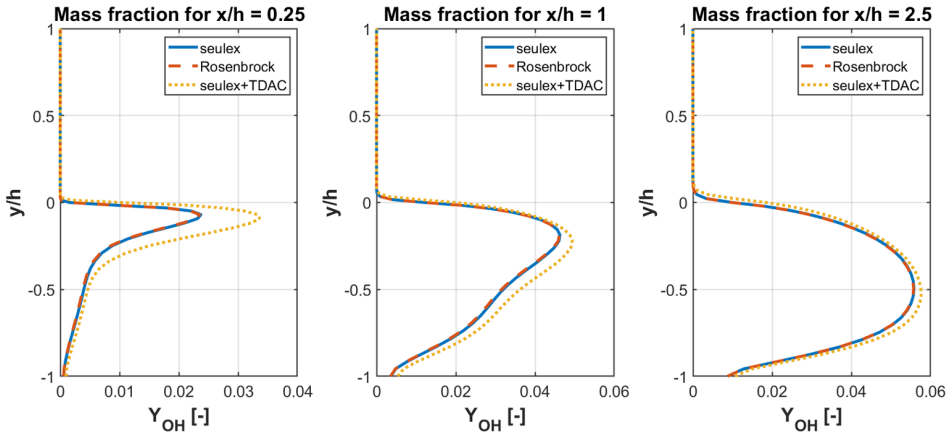

Figure 5.5: Comparison between different solvers for the axial mass fraction of OH at different normalised axial positions at $\Phi = 0.75$.

In Figure 5.1 can be seen that, both for `seulex` and `Rosenbrock34`, values of axial velocity are practically the same, regardless of the Courant number. However, if TDAC approach is considered, a slight increase in axial velocity in the streamwise direction is observed, which will have an effect on both the mass fractions of the species and the recirculation zone. In Figure 5.2 an small increase of temperature is present at the x/h = 0.25 for the `seulex+TDAC` solver, in spite of that, the three cases presented lead to practically identical values.

Regarding to the mass fractions of the species, it can be observed in Figure 5.3 that the consumption of CH_4 is very similar for all the cases, and may even be considered as acceptable the solution provided by the `seulex+TDAC` solver. However, this solver starts to become less accurate as it approaches the recirculation zone, as shown in Figure 5.4. But these differences are much more evident if intermediate species, such as OH is considered. In Figure 5.5 is noted that `seulex+TDAC` solver overestimates the mass fraction of OH above the values obtained with `seulex` and `Rosenbrock34`.

Furthermore, a representation of the corresponding streamlines over the temperature field for all the cases are illustrated in Figure 5.6.

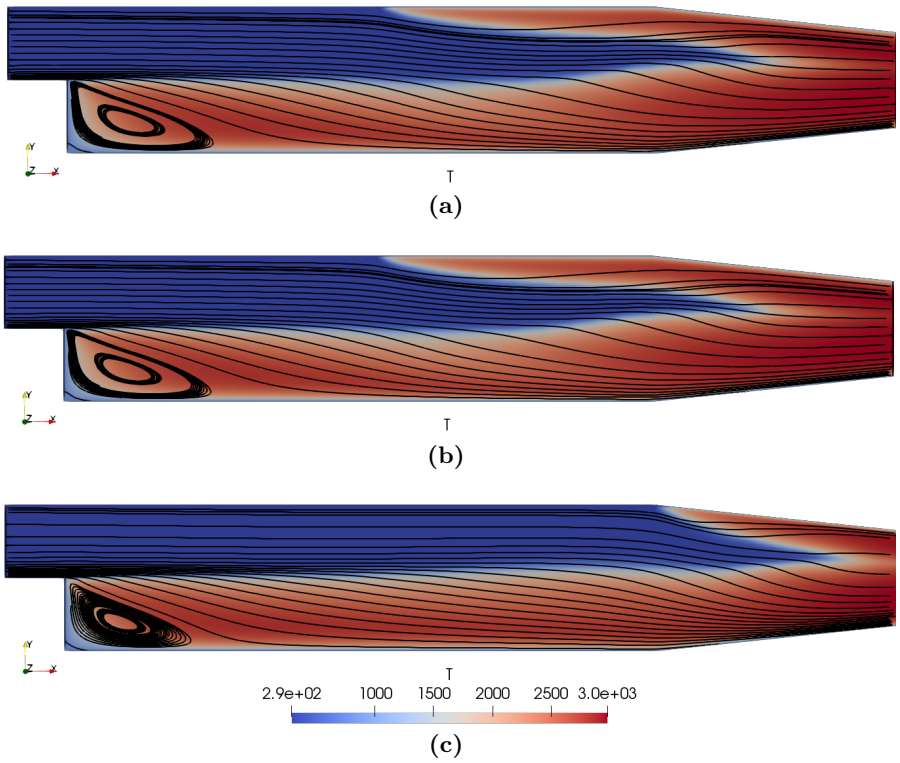

Figure 5.6: Representation of the streamlines and temperature [in K] for a combustion of a premixed mixture of CH_4/O_2, with $\Phi = 0.75$, after t = 0.3 s, for (a) `ode-seulex`, (b) `ode-Rosenbrock34`, (c) `ode-seulex+TDAC`.

After paying attention to the previous results and representations, the appearance of a burning region on the top wall has been noticed. This effect had not appeared during the mesh independence study, Figure 4.9, where a premixed combustion of methane and air had been simulated. However, when air, which is composed of oxygen and nitrogen, is replaced by pure oxygen, there is a considerably increment of the combustion temperature, and hence, the laminar flame speed increases as well. This effect is well-known as boundary layer flashback.

Before making a comparison between the results obtained with the different solvers, it should be emphasised the reduction of the recirculation zone after removing the nitrogen from the initial mixture, bringing the flame front closer to the step. Furthermore, this reduction carries with it a greatly mitigation of the secondary vortices.

Regarding to the employed solvers, `seulex` and `Rosenbrock34` provide same results, even having increased the Courant number, since both streamlines and temperature field are practically the same. However, even though the `seulex+TDAC` solver generates similar values for the studied parameters, remarkable differences have been noticed after observing Figure 5.6. The flashback on the top wall has been considerably reduced due to the chemistry reduction. In addition, the reticulation bubble has different dimensions whether TDAC is considered or not. While for `seulex` solver a reattachment length of 0.0562 m is obtained, a lower length is acquired with the TDAC approach, 0.0495 m.

It has been concluded that it is necessary to know precisely all the intermediate species that are generated during the combustion process, for that reason, the use of TDAC approach over the simulation should be rejected, despite the great computational advantage that it offers (a reduction of 20 times the computational time over the `Rosenbrock34`). Then, as the `Rosenbrock34` is a higher order solver, it has been decided to use it during the rest of the project.

Furthermore, it has been noticed that a high velocity field is present in the convergent zone, which implies a negative effect on the computational time. Moreover, this decrease of the area at the final region of the domain, may be the cause or incentive of the boundary flashback, as the flame front begins to rise as it goes through this region Figure 5.6, and may make contact at some point of the top wall, thus, initiating this undesirable effect in the combustor.

5.2 Sensitivity to geometry change

The simulations carried out so far have been performed in a subsonic regime, which implies that in the presence of an area change, the flow velocity is affected. As presented in Section 4.2, the PitzDaily geometry presents a convergence region at the end of the domain. This area change provides an increase in the local velocity, and hence, it may be an remarkable effect to influence the flashback region.

The geometry to be compared with the PitzDaily case has the same properties and characteristics as the initial one. However, the convergent part has been removed, setting up a constant area over the whole domain, being the height of the `oulet` of 50.8 mm. In Figure 5.7 the mesh of the new geometry has been presented.

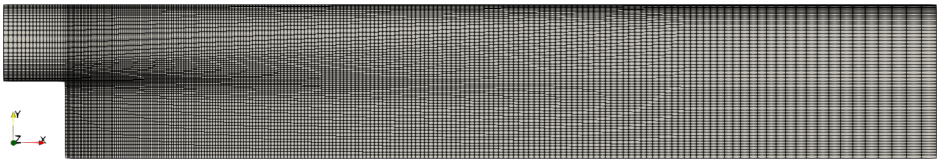

Figure 5.7: Final mesh of the PitzDaily case without the convergent region.

In addition, a suitable range of y^+ has been obtained, being similar to that obtained in the initial case, which approximately varies from 0.7 up to 22. Therefore, initiating with the same initial conditions presented in Table 5.1, the parameters of velocity, temperature fields and mass fraction values of CH_4, CO_2 and OH for the two geometries have been presented below.

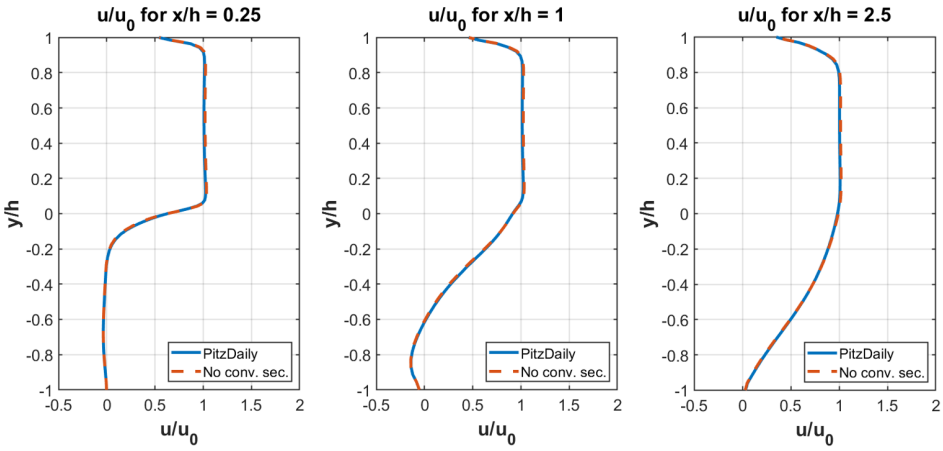

Figure 5.8: Comparison between including or not the convergence part for the normalised average axial velocity at different normalised axial positions at $\Phi = 0.75$.

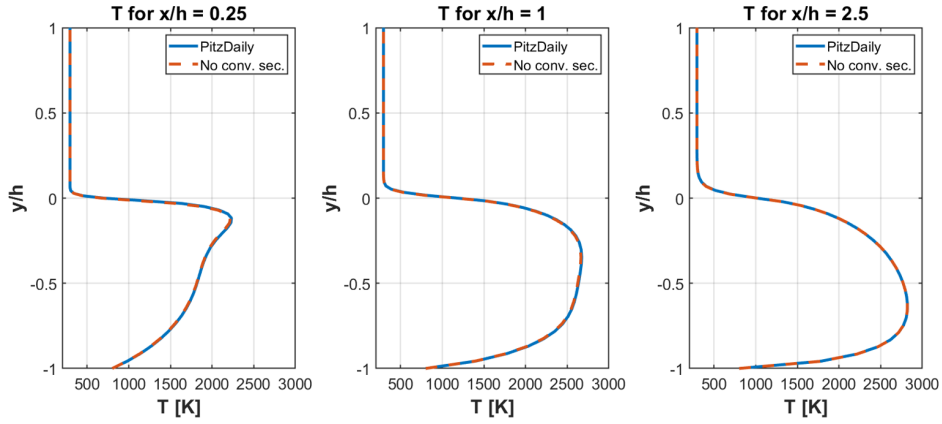

Figure 5.9: Comparison between including or not the convergence part for the axial temperature at different normalised axial positions at $\Phi = 0.75$.

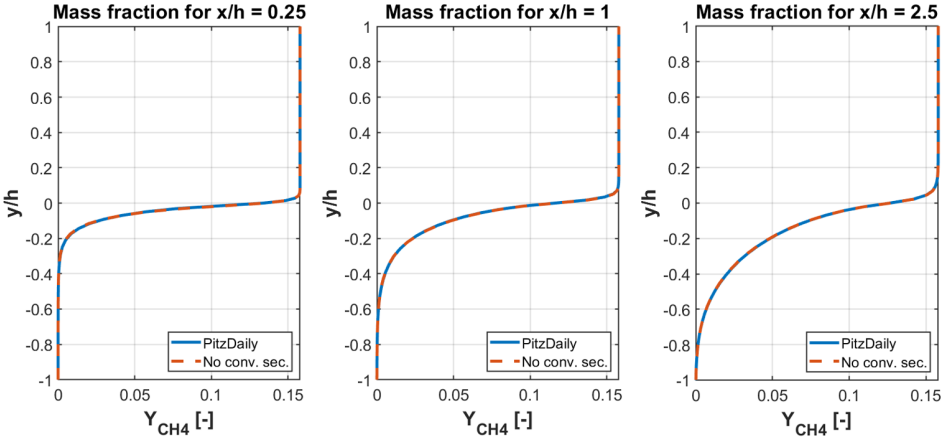

Figure 5.10: Comparison between including or not the convergence part for the axial mass fraction of CH_4 at different normalised axial positions at $\Phi = 0.75$.

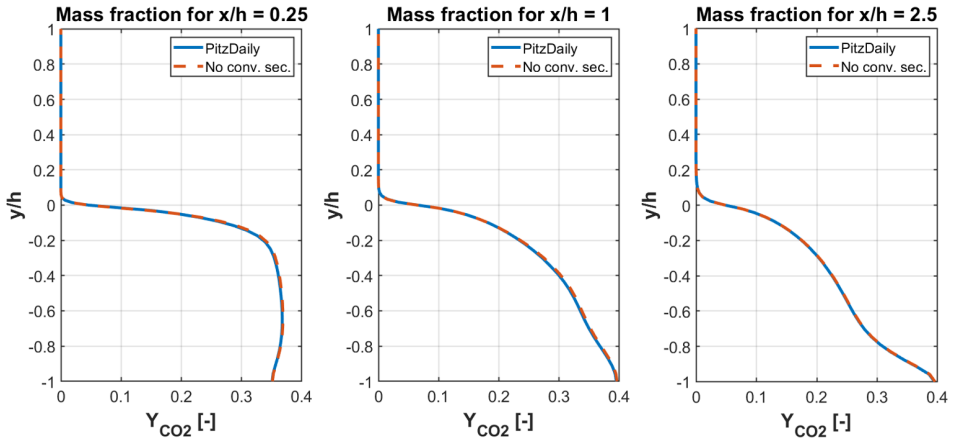

Figure 5.11: Comparison between including or not the convergence part for the axial mass fraction of CO_2 at different normalised axial positions at $\Phi = 0.75$.

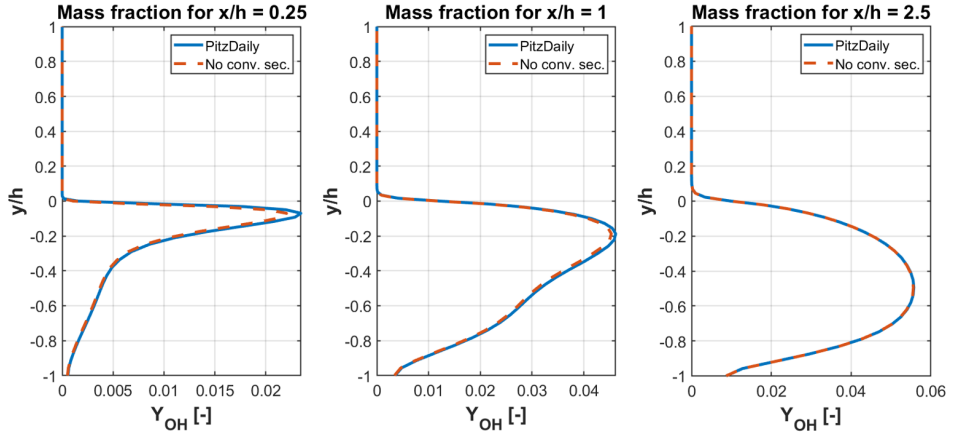

Figure 5.12: Comparison between including or not the convergence part for the axial mass fraction of OH at different normalised axial positions at $\Phi = 0.75$.

After removing the convergence section and comparing both results, it can be verified that slightly differences are appreciated for all the parameters, as can be seen in the upper region of the axial velocity component, (Figure 5.8), or in the mass fraction of OH, (Figure 5.12). However, as it moves away from the recirculation zone, the difference between the two results becomes almost imperceptible. As it is expected, these little differences appear due to the removal of the area change at the ending of the domain, and hence the small acceleration of the flow along the convergent part.

In addition, in Figure 5.13, the streamlines and temperature fields have been represented including or not the convergence part. From these figures, it is possible to see at first sight that both the recirculation zone and the flashback present in the upper zone of the domain still appear. Furthermore, despite having eliminated the convergent zone, these two zones have been slightly altered, obtaining practically identical results. It is also interesting to observe that the temperature of the recirculation gases of the products downstream of the flame is significantly higher than the gases near the step as a consequence of the high velocities. Besides, it is possible that the streamlines may appear to be different, but this is due to the automatic generation of streamlines of the `ParaVIEW` software.

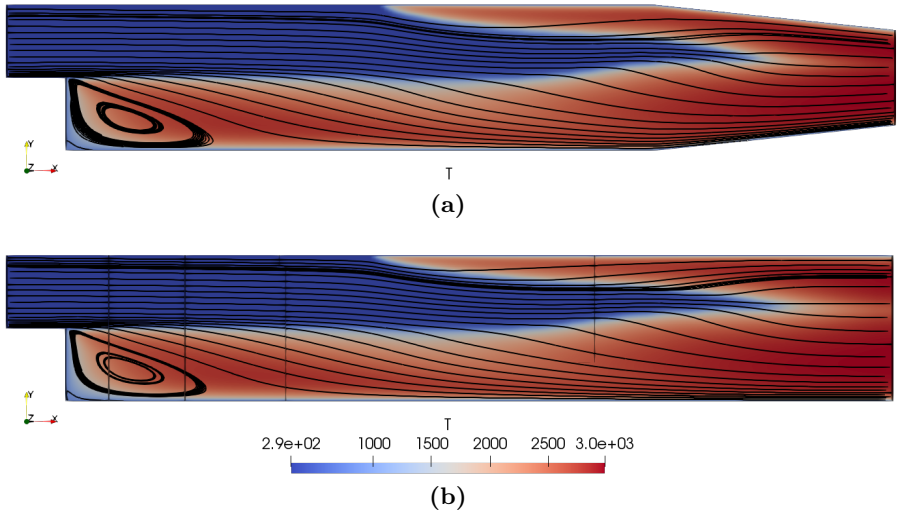

Figure 5.13: Representation of the streamlines and temperature [in K] for a combustion of a premixed mixture of CH_4/O_2, with $\Phi = 0.75$, after t = 0.3 s, for (a) with the convergence part, (b) without the convergence part.

Furthermore, the computational time for the case presented in Figure 5.7 was t = 70104 s, providing a temporary reduction of 13% from the computational time presented in Table 5.2.

It can be concluded that the slightly differences has been observed in some fields, in spite of this, its effect may be considered as negligible, because as it has been seen, both the appearance of the flashback and its location remain unchanged. Therefore, from now on, as the new geometry is practically identical to the initial one, it has been deemed convenient to use it for the subsequent simulations due to the great improvement in computational time.

5.3 Sensitivity to equivalence ratio

As it was illustrated in Figure 3.12, the flow bulk velocity has a key role at the onset of the flashback. Since the free stream velocity increases, in order to maintain the position of the flashback, the flame speed must increase as well. for that reason, the local flame speed acquired will have a noticeable effect on the flashback.

As was depicted in Figure 3.3, local flame speed increases for equivalent ratios close to the stoichiometric, mainly for slightly rich mixtures [27]. Moreover, turbulent regimes, are characterised by the turbulence intensity, which directly impacts on the turbulent flame speed, resulting in a greater flashback propensity.

In Figure 5.14 have been presented several results of critical velocity gradients for hydrogen-air flames, both for laminar and turbulent regimes.

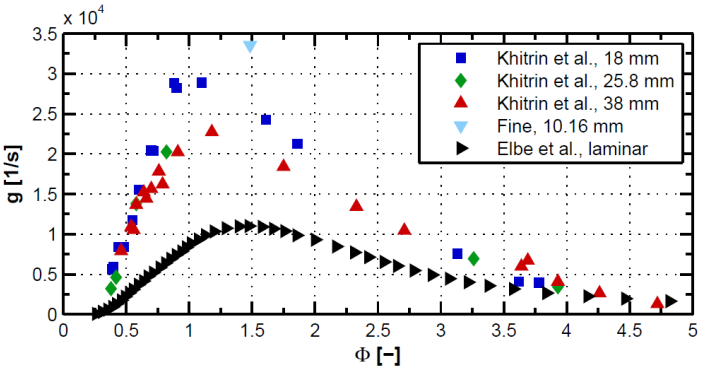

Figure 5.14: Critical velocity gradients at wall flashback for different equivalence ratios. Source: [27].

It can be observed that for rich and lean conditions, turbulence simulations provide trustworthy data. Nevertheless, relatively large scatter is present near the stoichiometric conditions. Thanks to these results, it is possible to select a better equivalence ratio study range in order to obtain reliable results. This is why it has been decided to simulate lean conditions and check if it is possible to remove the occurrence of the flashback. The cases to be studied are shown in the Table 5.3.

	Φ	Y_{CH_4}	Y_{O_2}	T_{N_2} [K]	p [Pa]	u_x [m/s]
case 1	0.5	0.1111	0.8889	1700	$1{\cdot}10^5$	5.0
case 2	0.6	0.1304	0.8696	1700	$1{\cdot}10^5$	5.0
case 3	0.75	0.1579	0.8421	1700	$1{\cdot}10^5$	5.0

Table 5.3: Initial physical conditions for the equivalence ratio simulations with OpenFOAM.

Next, in Figure 5.15 shows the the streamlines and temperature field for different equivalent ratios, $\Phi = 0.5$, $\Phi = 0.6$ and $\Phi = 0.75$.

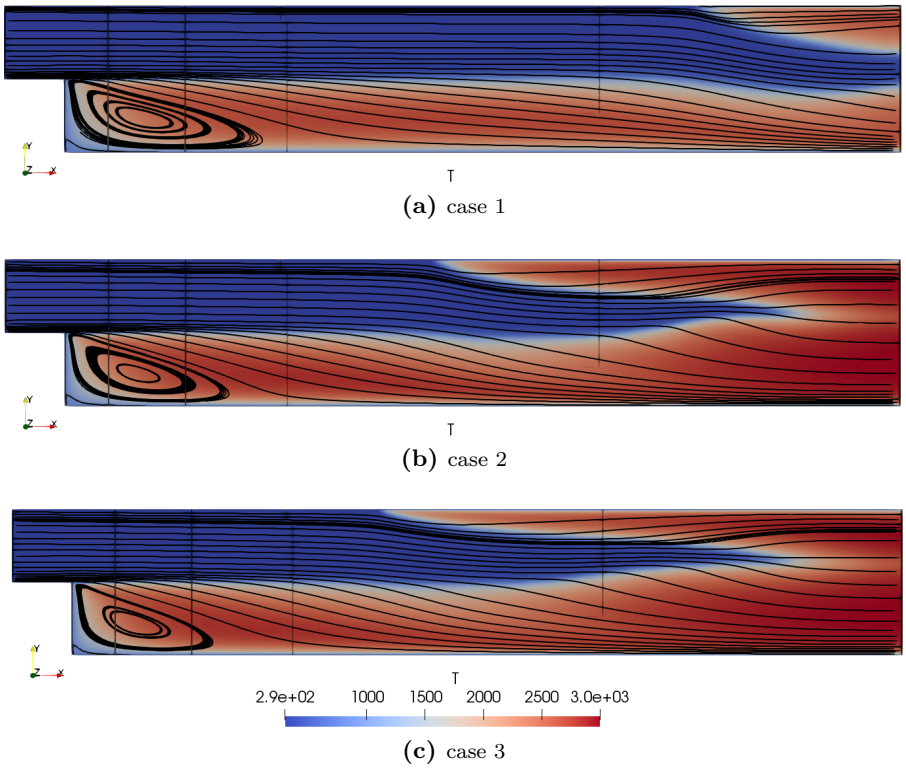

(a) case 1

(b) case 2

(c) case 3

Figure 5.15: Representation of the streamlines and temperature [in K] for a combustion of a premixed mixture of CH_4/O_2, for different values of equivalent ratio after t = 0.3 s, (a) $\Phi = 0.5$, (b) $\Phi = 0.6$, (c) $\Phi = 0.75$.

Looking at the figures for the different equivalence ratios, it can be seen that as the amount of CH_4 increases, local flame velocity increases, which implies a

movement of the flashback. It can be observed that for a $\Phi = 0.5$, Figure 5.15a, local flame speed reaches its lowest value, and the flame propagates downstream until it reaches a new balancing condition between the local flow velocity and flame speed. Then, for a $\Phi = 0.6$, Figure 5.15a, the speed of the flame is increased, causing the flashback to move upstream. In addition, it is worth noting that the new position of the flashback is much more evident after the transition from $\Phi = 0.5$ to $\Phi = 0.6$, than the $\Phi = 0.6$ to $\Phi = 0.75$, mainly because viscous effects and velocity reduction near the wall are more noticeable downstream the domain.

In addition, as the equivalence ratio increases, the leading edge or the flame tip is approaching the step. At lower equivalence ratios, the flame is stabilised shortly after the average recirculation zone. However, for higher equivalence ratios, the flame tip propagates upstream, being almost stuck to the step, where the primary eddy is generated. In turn, the recirculation region becomes smaller as the anchoring of the flame near the wall, and hence, the reattachment length becomes lower. Furthermore, an increasing in the equivalence ratio implies higher burning velocity, reflected in the angle of the flame (changes in the streamlines direction), which increases according to the laminar flame speed. These effects were also verified with a mixture of propane/air [41].

5.4 Sensitivity to chemical kinetic mechanisms

In the previous section the dependence of the flame speed on the equivalence ratio has been shown, which has a direct effect on the position of the flashback. In addition, the mixture burning velocity is mainly a function of chemical kinetic mechanisms, thereby, has a direct impact in triggering the flashback.

In this section, it has been decided to check what new effects and how the composition changes inside the recirculation zone changing the chemical kinetic mechanism and observe whether it has a effect on the position of the flashback. For this purpose, the initial skeletal mechanism (which has been used throughout the project) is composed by 13 species and 42 reactions, `N13-R42`, has been replaced by a mechanism composed by 19 species and 68 reactions `N19-R68`. The initial conditions for both cases are shown below:

	Φ	Y_{CH_4}	Y_{O_2}	T_{N_2} [K]	p [Pa]	u_x [m/s]	Mechanism
case 4	0.75	0.1579	0.8421	1700	$1{\cdot}10^5$	5.0	`N13-R42`
case 5	0.75	0.1579	0.8421	1700	$1{\cdot}10^5$	5.0	`N19-R68`

Table 5.4: Initial physical conditions for the chemical kinetic mechanisms simulations with OpenFOAM.

In order to test the effect of introducing a different mechanism with more reactions and intermediate species, a converged solution of `N13-R42` has been used to evaluate the transition from `N13-R42` to `N19-R68` to check how the flame propagates from the previous converged solution to the new equilibrium condition. The temperature field for various intermediate states when introducing the new mechanism and observing its behaviour over time is shown in Figure 5.16.

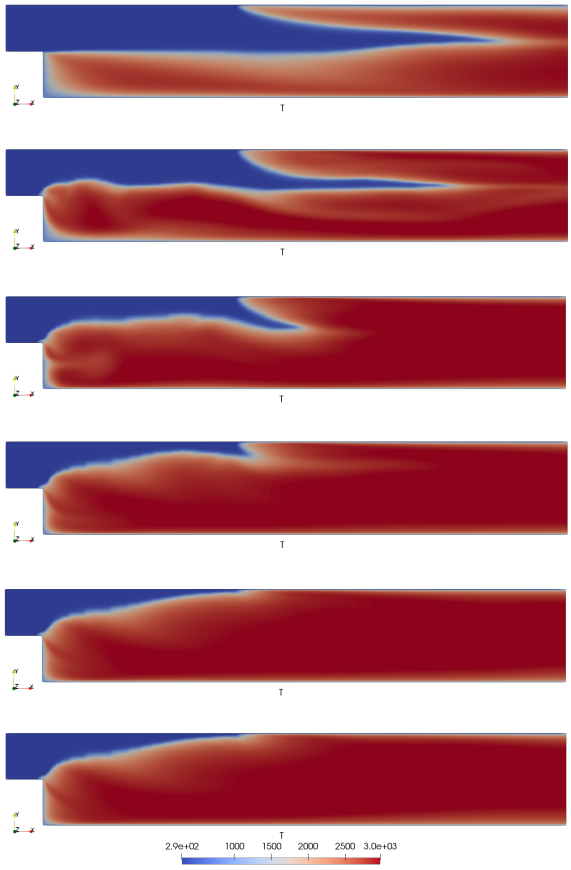

Figure 5.16: Transient regime of the temperature field [in K] during several time instants from the converged solution of `N13-R42` to a converged solution `N19-R68`, with a time step of 0.005 s.

Furthermore, in Figure 5.17 streamlines and temperature field is illustrated for both chemical kinetic mechanisms.

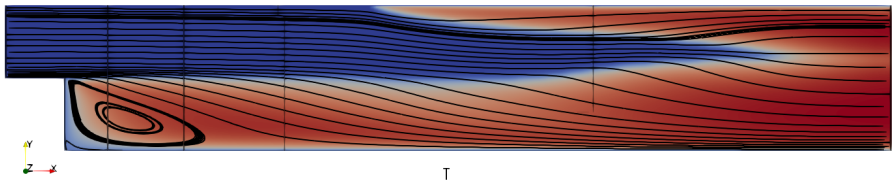

(a) case 4

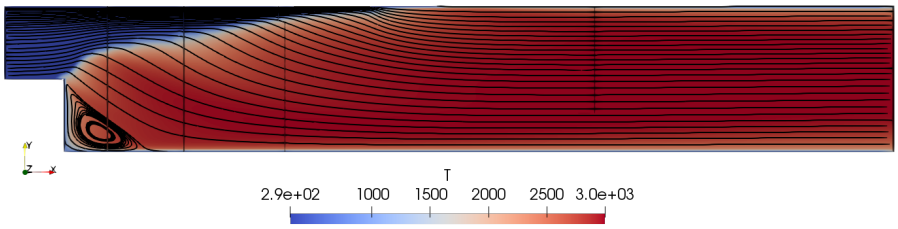

(b) case 5

Figure 5.17: Representation of the streamlines and temperature [in K] for a combustion of a premixed mixture of CH_4/O_2, with $\Phi = 0.75$, after t = 0.3 s, for the chemical kinetic mechanism (a) `N13-R42`, (b) `N19-R68`.

According to the flashback theory, is expected to have a change in the location of this phenomenon, due to a change in the mixture burning velocity, which implies a different spatial fuel composition. Nevertheless, looking at the Figure 5.16, it is noticeable that the position of the flashback has not experienced significant changes, but rather its surroundings. This effect is due to the fact that the velocity of the unburned mixture increases as a consequence of the convergent zone created by the flame front, as can be seen in the streamlines in Figure 5.17. This point will be explained in more detail in Section 5.5.

It is now interesting to know why, when the `N19-R68` mechanism has been introduced, the burning velocity has significantly changed, and hence the upstream flame propagation. Based on the two used mechanisms, new intermediate species are involved in the combustion process. These species are: CH_3O, CH_3O_2, C_3H_3, CH_2 $CH_2(S)$ and C_2H.

On the one hand, according to references [45], based on results of the sensitivity analysis, it has been verified that species such as CH_2 $CH_2(S)$ and C_2H have negligible influence and can even be eliminated from the kinetic mechanism. Furthermore, from results of the reaction path analysis, it can be concluded that C3 and heavier species are not essential to characterise a methane–oxygen combustion, thereby, C_3H_3 can also be ruled out as the cause of the mixture burning velocity increment.

On the other hand, from a sensitivity analysis, for a methane–oxygen mixture, its kinetics are sensitive to CH_3O_2 [45]. Moreover, CH_3O has been observed to be important to play a role on the flame speed.

The reaction path for a premixed stoichiometric methane–oxygen mixture in a range of temperatures from 1000 K up to 3000 K at high pressures reads:

$$CH_4 \rightarrow CH_3 \rightarrow CH_3O \rightarrow CH_2O \rightarrow HCO \rightarrow CO \rightarrow CO_2 \tag{5.1}$$

Highlight that, the `N19-R68` mechanism incorporates the path passing through CH_3O, whereas the `N13-R42` mechanism lacks such a specie.

Then, one of the most critical species within the combustion process is the formyl radical HCO. This radical is mainly a product from the highly exothermic reactions that involve the formaldehyde CH2O as follows:

$$H + CH_2O \rightarrow H_2 + HCO \quad (\Delta H_{0K} = -16.6 \text{ kcal/mol}) \tag{5.2}$$

$$OH + CH_2O \rightarrow H_2O + HCO \quad (\Delta H_{0K} = -30.9 \text{ kcal/mol}) \tag{5.3}$$

Furthermore, HCO ends up being destroyed in multiple reactions, the main 3 reactions being:

$$HCO(+M) \rightarrow H + CO(+M) \tag{5.4}$$

$$HCO + O_2 \rightarrow HO_2 + CO \tag{5.5}$$

$$H + HCO \rightarrow H_2 + CO \tag{5.6}$$

While the reaction 5.4 is a chain propagation reaction that determines the generation of reactive H-atoms, reactions 5.5 and 5.6 are terminating reactions, which reduce the amount of these reactive H-atoms. From reaction 5.5 more stable radicals are generated, such as HO_2 and in turn reaction 5.6 quenches the reactive H-atoms. Therefore, a high net rate of production of H-atoms, which are consumed in the chain branching reaction $H + O_2 \rightarrow OH + O$, has a direct impact with the laminar flame speed [46].

Next, in Figure 5.18 is illustrated the axial mass fraction of HCO, H and OH for x/h = 1 for both chemical kinetic mechanism.

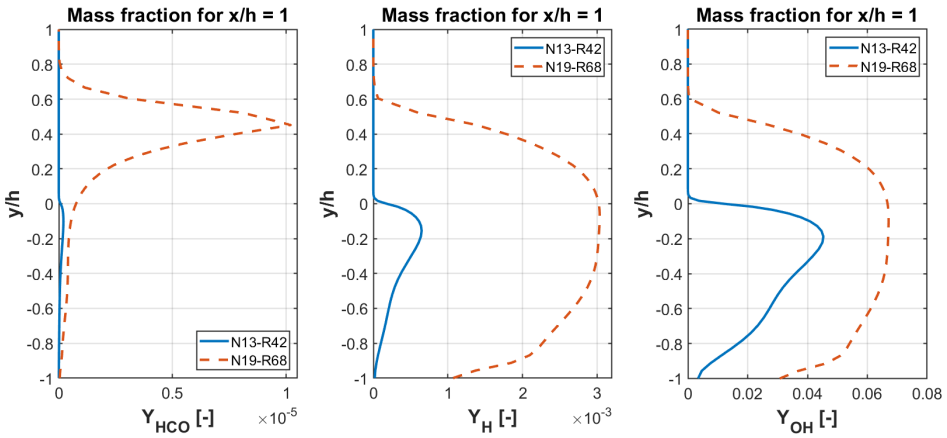

Figure 5.18: Comparison between different chemical kinetic mechanism for the axial mass fraction of HCO, H and OH respectively at x/h = 1 with $\Phi = 0.75$.

As discussed in previous paragraphs, considerable differences has been obtained including the prompt HCO dissociation in flame speed [46]. According to the results in Figure 5.18, it can be observed that the HCO production has been increased by 100 and the generation of reactive H-atoms by 10 for the `N19-R68` mechanism with respect to the `N13-R42` mechanism. In turn, the mass fraction of OH has been increased as well. Therefore, it can be concluded that the amount of HCO, H and OH obtained with the `N19-R68` mechanism is greater than `N13-R42` mechanism, which implies a substantial increase in the heat release by the prompt source of reactive H-atoms that increases the flame speed, in turn, encourages the chain branching through H + O2 → O + OH and subsequent CO2 generation by the CO + OH → CO2 + H reaction.

Finally, probably the addition of CH_3O_2 and CH_3O help to generate more CH_2O and hence HCO, which will lead to a higher flame speed which results in Figure 5.17 (b).

5.5 Sensitivity to operating conditions

As it was presented in Section 3.4, flame speed may change due to other parameters, not only with the fuel composition, as it was observed in the previous section. Initial pressure or preheat temperature directly impact into the flame speed, and hence, in boundary wall flashback. According to [16], a rising of the operating pressure or preheat temperature, involves an increase of the flashback propensity.

As the initial thermodynamics considerations have influence over the boundary wall flashback, it will be interesting to observe whether the way in which the flame is ignited could have a great influence at the final location of the boundary wall flashback, as a consequence of the initial configuration.

Throughout the work, the combustion of the flame was initiated by preheating the whole domain with an inert gas (N_2) at 1700 K, which allowed, through diffusion processes, to preheat the CH_4/O_2 mixture and initiate combustion. Nevertheless, there are other ways, such as using a hot point to serve as a combustion initiator. This point is called the ignition point. In Figure 5.19 is showed the location of the ignition point, which has been located near the step. Its position is x_{ig} = 3 mm and y_{ig} = - 3 mm, with a radius of r_{ig} = 2.5 mm, (subscript $_{ig}$ refers to parameters related with the ignition point). Hot point is placed from instant t_{i-ig} = 0 s and is removed after t_{f-ig} = 0.01 s, long enough time to allow the mixture to burn.

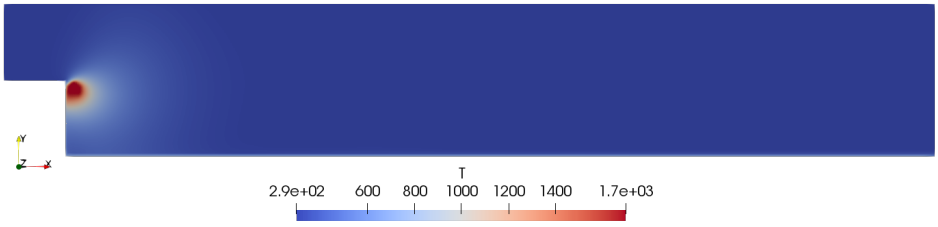

Figure 5.19: Position of the ignition point.

Next, by initialising with the same initial conditions presented in Table 5.1, except for the preheating temperature, both cases has been solved. In Figure 5.20 it has been illustrated the transient regime until the flashback is stable for the two different ignition conditions. On the left, the fresh mixture is burned by setting up a preheat temperature of 1700 K, while on the right, unburned mixture is ignited due to an ignition point, which is temporally located close to the step.

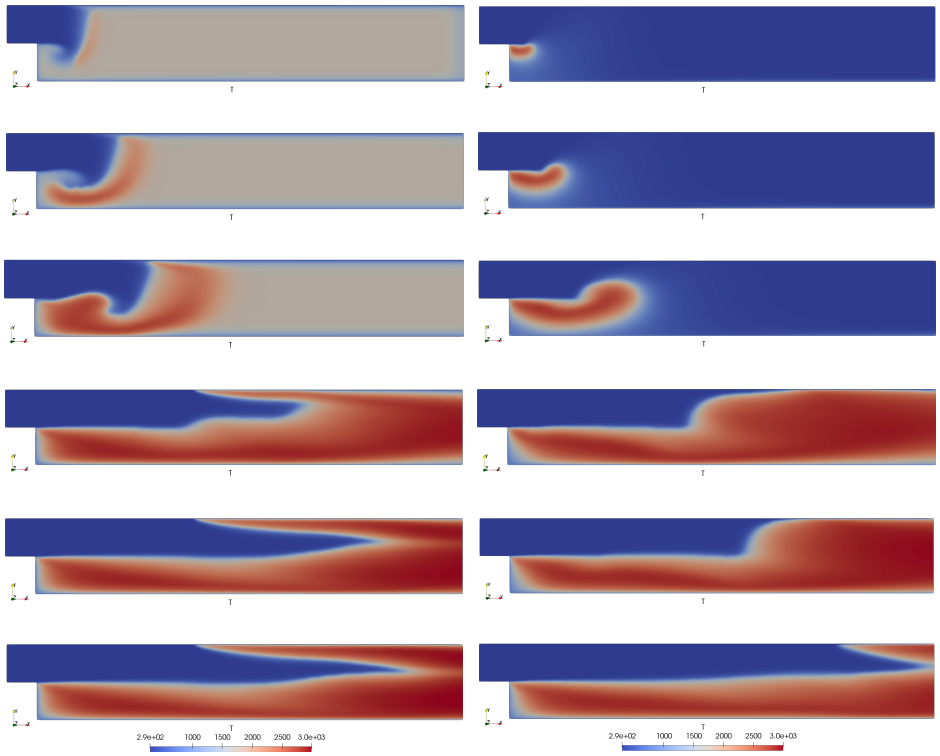

Figure 5.20: Transient regime during several time instants for both a initial temperature domain of 1700 K (left) and an ignition point of 1700 K near the step (right). Time instants: 0.01 s, 0.015 s, 0.02 s, 0.04 s, 0.06 s and 0.08 s.

On the one hand, in Figure 5.19 left, at the starting time, the whole domain is uniformly preheated at 1700 K. Then, as the premixed mixture enters to the domain, a large eddy is being generated, carry with it the combustion of the mixture, as it can be observed during the first frames. As the time passes, the large eddy has been able to initiate combustion near the upper wall, and being enough to collide with the top wall, resulting in a burning region close to the wall, the onset of the flashback. While, in the $t = 0.02$ s, by the appearance of a small temperature spike and the decrease of the flow velocity at the vicinity of the wall, flashback seems to be attached, however it is noticeable that is not until $t = 0.04$ s approximately, the flame propagates downstream as far as a new balancing condition between the local flow velocity and flame speed is reached. Finally, for the subsequent frames, it is checked that the position of the flashback is invariant, only the fresh mixture flow is seen to go downstream along the domain until it reaches the beginning of the steady state, $t = 0.08$ s approximately.

Whereas, on the other hand, Figure 5.19 right, laying on an ignition point close to the step generates an eddy that propagates downstream the flow. However, due to the step and the position of the ignition point, the burned mixture starts to burn through the recirculation zone and in turn, generates an eddy as can be seen during the first few frames. Nevertheless, as the unburned mixture is coming into the domain, the eddy with hot gases is transported downstream preventing it from reaching the upper wall at the same point where the flashback started for the left case. It will be rather in $t = 0.04$ s where the flame collides with the upper wall, the fresh mixture is continuously burning, however, the flashback takes place at a further point. Therefore, a new balancing condition between the local flow velocity and flame speed is reached at $t = 0.08$ s.

Emphasise the importance of the transient regime during the combustion process. It will be when the flame hits or gets close enough to the wall that its local flame velocity matches the velocity in the boundary of the upper wall.

Next, in Figure 5.21 shows the the streamlines and temperature field for the two different ignition conditions.

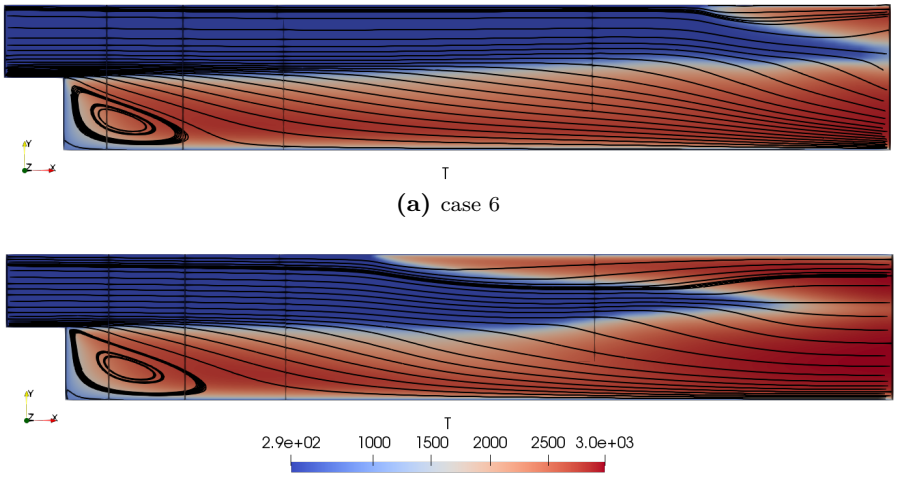

(a) case 6

(b) case 7

Figure 5.21: Representation of the streamlines and temperature [in K] for a combustion of a premixed mixture of CH_4/O_2, with $\Phi = 0.75$, after t = 0.3 s, for (a) with an ignition point, (b) without an ignition point (whole domain at 1700 K).

Finally, one would expect that, given the same conditions, the same equilibrium situation will be reached for both cases. However, the importance of the cone generated by the combustion after the step must be highlighted.

Whereas for the preheating situation its equilibrium state is reached by moving downstream the flashback from the colliding point, the beginning of the combustion near the wall, as it has been proved in previous subsections, for the case where an ignition point is used, the situation changes, as it can as seen in the new position of the flashback.

Paying attention to the upper situation in Figure 5.21, due to the cone generated by the combustion of the mixture after the step and its passage through the recirculation zone, it can be seen how the streamlines are more and more close together in the x axis, as if the flame front were a wall. This effect causes an increase in the axial velocity of the unburned mixture, as it can be seen in Figure 5.22, resulting, near the end of the domain, a new balancing condition, which has the similar conditions to those obtained in the lower case. Moreover, due to the fact that the leading edge is convex with respect to the incoming flow, a stretching of the flame can be appreciated in Figure 5.21, which in turn causes the flow velocity of the reactants to decrease as it approaches the flame front.

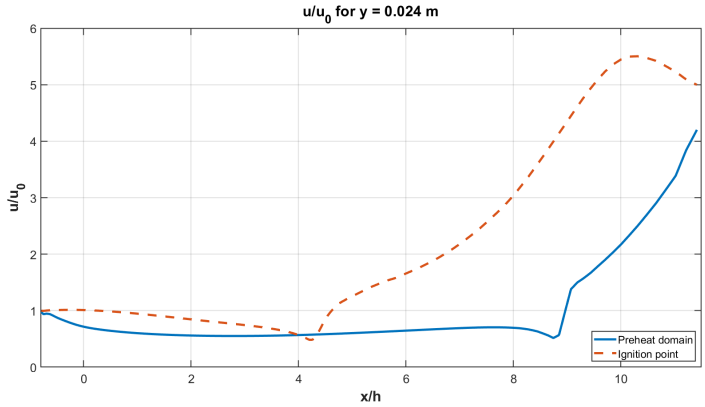

Figure 5.22: Axial velocity at y = 0.024 m for a combustion of a premixed mixture of CH_4/O_2, with $\Phi = 0.75$, after t = 0.3 s.

5.6 Sensitivity to wall temperature

Finally, the interaction between the flow and the flame close to the tip burner is strongly dependent on the wall material, and its respective temperature. Furthermore, in commercial burners, the cooling system plays a key role, managing the wall temperature inside the combustor. the heat transfer and quenching distance between the burner rim and flame front change because of the wall temperature. Thereby, the flashback propensity is affected.

In order to visualise the effect of the cooling system on the top wall, it has been considered more appropriate to use an ignition point as the way of burning the premixed mixture due to the flashback is located further away from the inlet, thereby, a change in the flashback position will be noticed more easily. So as to observe the propagation of the flame, it has been decided to simulate three cases with three different top wall temperatures, 293 K, 600 K and 900 K. Then, the cases to be studied are shown in the Table 5.5

	Φ	Y_{CH_4}	Y_{O_2}	T_{wall} [K]	p [Pa]	u_x [m/s]
case 8	0.5	0.1111	0.8889	293	$1{\cdot}10^5$	5.0
case 9	0.6	0.1304	0.8696	600	$1{\cdot}10^5$	5.0
case 10	0.75	0.1579	0.8421	900	$1{\cdot}10^5$	5.0

Table 5.5: Initial physical conditions for the wall temperature simulations with OpenFOAM.

In addition, Figure 5.23 shows the obtained results for the temperature fields and its respective streamlines.

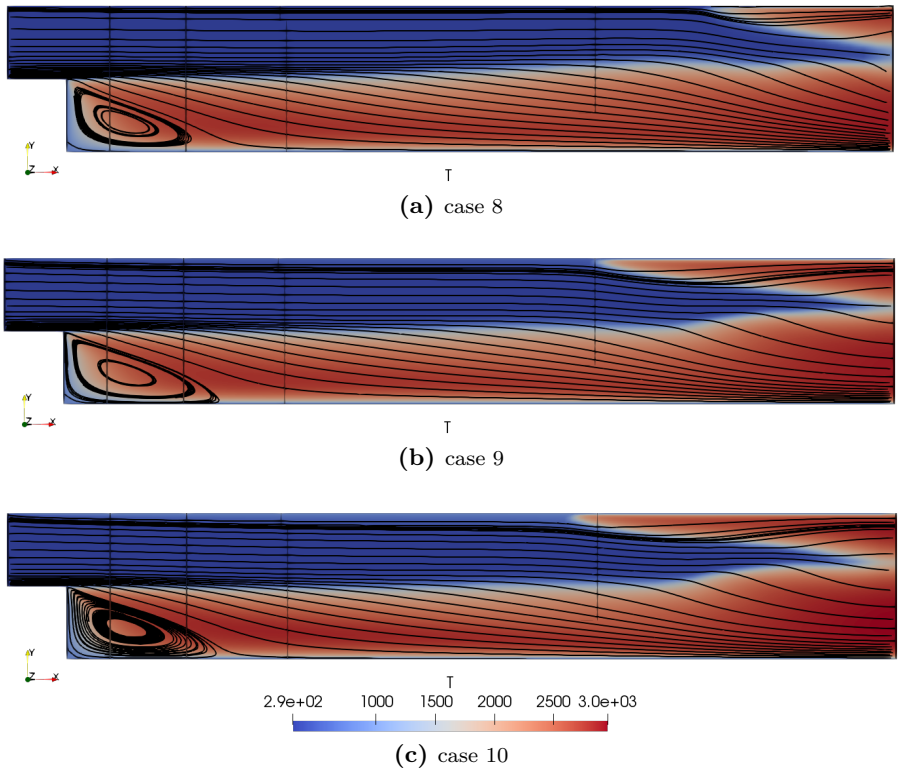

(a) case 8

(b) case 9

(c) case 10

Figure 5.23: Representation of the streamlines and temperature [in K] for a combustion of a premixed mixture of CH_4/O_2, with $\Phi = 0.75$, after t = 0.3 s, for different top wall temperatures (a) T = 293 K, (b) T = 600 K, (c) T = 900 K.

As can be seen in Figure 5.23, the effect of having a worse cooling system, i.e. a higher wall temperature, implies that the flashback moves upstream to find a new equilibrium situation. Despite the fact of the higher increase of the temperature in each case, its impact is evident less pronounced than the effect obtained in Section 5.3. In addition, the recirculation zone is slightly modified, as was the case with a change in the equivalence ratio, but on a smaller scale. Consequently, it can be concluded that flashback tendency is more noticeable for uncooled burners.

Chapter 6

Conclusions and future works

Along the project, a theoretical basis about the main characteristics and modelling of turbulent flows and combustion has been presented in order to understand their interaction. Furthermore, flashback and its mechanisms have been introduced, being one of the operability problems present in premixed combustion. All of this, will thus enable the modelling of a backward facing step, where if a methane/oxygen premixed combustion occurs, the flashback phenomenon is observed.

Afterwards, the obtained results have been presented and then, a sensitivity analysis has been carried out for several parameters that may have a direct impact on the flashback phenomenon.

This last chapter of the thesis compiles all the conclusions obtained throughout the project derived from the sensitivity analysis of the results mentioned in the previous paragraph. Furthermore, it will conclude by suggesting possible trends for future research so as to validate and improve the current results.

6.1 Conclusions

In Section 1.2, modelling a simulation of a premixed combustion LOX/CH_4 through a backward facing step and, carrying out a parametrical sensitivity study about the flashback were defined as the main objectives. In addition to these main objectives, there were also some secondary objectives, which have been achieved, as discussed below.

- Despite the fact of the limited literature about the flashback phenomenon experimentally and numerically, a solid theoretical basis has been identified that explains the theoretical mechanism by which boundary layer flashback

occurs. In addition, it has also been possible to learn about the different types of flashback known to date and the physical parameters on which they tend to depend.

- Based on the PitzDaily geometry, a backward facing step model has been designed which generates a recirculation zone that self-sustains the premixed combustion. In addition, an optimal number of cells has been selected to reduce the computational time, obtaining reliable results that in turn, fulfil with the y^+ reference values.

- Having the help of the `PyCSP` algorithm, it has been possible to obtain two reliable chemical kinetic mechanisms that fit with the designed model.

- Finally, the designed model has been developed to test these chemical kinetic mechanisms, which have to be in `CHEMKIN` format, in order to check their numerical performance.

Finally, according to the results obtained in Section 5, several conclusions could be drawn:

- It has been shown that using higher order solvers, such as the `Rosenbrock`, gives slightly more accurate results than lower order solvers such as the `seulex`. In addition, using extra algorithms that reduce the computational time by reducing or removing intermediate reactions, as is the case of `TDAC`, gives good results when obtaining velocity, temperature and some species fields. However, large differences are found for some intermediate species, such as OH, and hence, `TDAC` does not correctly predict the boundary flashback because they underestimate it.

- It has been proven that after removing the convergent part from the PitzDaily geometry, the simulation's result slightly changes, and in turn, a reduction in the computational time has been achieved. Thus, this new geometry has been used for the rest of the simulations.

- It has been found that both the equivalence ratio and the temperature of the upper wall has similar effects on the flashback position. As the parameter is increased, flashback position moves upstream until reaches a new balancing conditions, due to a rise in the burning mixture velocity.

- It was expected a movement in the flashback due to a change in the chemical kinetic mechanism, from `N13-R42` to `N19-R68`. However, results showed a flame front away from the recirculation zone, completely different from the one obtained with `N13-R42`. This effect is possibly due to the fact that the `N19-R68` mechanism generates a higher amount of HCO, which results in a higher amount of reactive H-atoms resulting in a noticeable increase of the flame speed.

- Lastly, the importance of the transient regime during a combustion of methane/oxygen has been proved due to the fact that the position of the flashback is completely different from initiating the combustion by preheating the domain with an inert gas than with an ignition point close to the step.

6.2 Future research

As it has been verified throughout the project, there are no experimental results available to verify the results obtained using numerical tools. Thereby, it would be interesting to carry out several experimental tests in order to corroborate the obtained results in this work. In addition, with these tests it would be possible to tune the simulation's parameters in order to adapt the numerical simulation.

Once the numerical results are similar to those obtained with reliable experimental data, could be achieved other kind of experiments. One of them is to evaluate more precisely the amount of intermediate species inside the recirculation zone for different chemical kinetic mechanism using the `PyCSP`.

The interaction between turbulent flows and combustion is still a field in full expansion and study. Getting simulations that are able to approximate the reality can facilitate the work for many researchers, reducing the expenses in the experiments.

Bibliography

[1] V S Arutyunov and G V Lisichkin. "Energy resources of the 21st century: problems and forecasts. Can renewable energy sources replace fossil fuels?" In: *Russian Chemical Reviews* 86 (8 2017), pp. 777–804. ISSN: 0036-021X. DOI: 10.1070/rcr4723.

[2] R. M. Dell and D. A.J. Rand. "Energy storage - A key technology for global energy sustainability". In: *Journal of Power Sources* 100 (1-2 2001), pp. 2–17. ISSN: 03787753. DOI: 10.1016/S0378-7753(01)00894-1.

[3] Hannah Hyunah Cho and Vladimir Strezov. "A Comparative Review on the Environmental Impacts of Combustion-Based Electricity Generation Technologies". In: *Energy and Fuels* 34 (9 2020), pp. 10486–10502. ISSN: 15205029. DOI: 10.1021/acs.energyfuels.0c02139.

[4] H. Ali et al. "Analysing CO2 emissions from Singapore's electricity generation sector: Strategies for 2020 and beyond". In: *Energy* 124 (2017 2017), pp. 553–564. ISSN: 03605442. DOI: 10.1016/j.energy.2017.01.112. URL: http://dx.doi.org/10.1016/j.energy.2017.01.112.

[5] Harry W Jones. "The Recent Large Reduction in Space Launch Cost". In: *48th International Conference on Environmental Systems* (July 2018 2018), p. 81. URL: https://ttu-ir.tdl.org/handle/2346/74082.

[6] A. Preuss et al. "LOX/Methane Technology Efforts for Future Liquid Rocket Engines". In: *5th International Spacecraft Propulsion Conference* (2008).

[7] D. Preclik et al. "LOX/hydrocarbon preparatory thrust chamber technology activities in germany". In: *41st AIAA/ASME/SAE/ASEE Joint Propulsion Conference and Exhibit* (2005). DOI: 10.2514/6.2005-4555.

[8] Victor P. Zhukov and Alan F. Kong. "A compact reaction mechanism of methane oxidation at high pressures". In: *Progress in Reaction Kinetics and Mechanism* 43 (1 2018), pp. 62–78. ISSN: 14686783. DOI: 10.3184/146867818X15066862094914.

[9] C.K. Law. *Combustion Physics*. Cambridge University Press, 2010. ISBN: 9781139459242.

[10] Tim Lieuwen et al. “Fuel Flexibility Influences on Premixed Combustor Blowout, Flashback, Autoignition and Instability”. In: *Turbo Expo: Power for Land, Sea, and Air* 42363 (2006), pp. 601–615.

[11] Stephen B Pope and Stephen B Pope. *Turbulent flows*. Cambridge university press, 2000.

[12] Rihab Mahmoud. *Development and Application of an Eulerian Density Function Methodology coupled to Flamelet Progress Variable Approach for the Simulation of Oxyfuel Combustion*. 2020.

[13] Stephen B Pope. “Computationally efficient implementation of combustion chemistry using in situ adaptive tabulation”. In: (1997).

[14] Eric Furbo. *Evaluation of RANS turbulence models for flow problems with signigicant impact of boundary layers*. 2010.

[15] Joel Guerrero. *Introduction to Computational Fluid Dynamics: Governing Equations, Turbulence Modeling Introduction and Finite Volume Discretization Basics*. 2015. URL: https://www.researchgate.net/publication/280385280.

[16] A.H. Lefebvre and D.R. Ballal. *Gas Turbine Combustion: Alternative Fuels and Emissions, Third Edition (3rd ed.)* 2010. ISBN: 2013206534.

[17] Benoît Fiorina, Denis Veynante, and Sébastien Candel. “Modeling combustion chemistry in large eddy simulation of turbulent flames”. In: *Flow, Turbulence and Combustion* 94.1 (2015), pp. 3–42. ISSN: 15731987. DOI: 10.1007/s10494-014-9579-8.

[18] R. Hilbert et al. “Impact of detailed chemistry and transport models on turbulent combustion simulations”. In: *Progress in Energy and Combustion Science* 30.1 (2004), pp. 61–117. ISSN: 03601285. DOI: 10.1016/j.pecs.2003.10.001.

[19] *Smith, G.P.; Golden, D.M.; Frenklach, F.; Moriarty, N.W.; Eiteneer, B.; Goldenberg, M.; Bowman, C.T.; Hanson, R.K.; Song, S.; Gardiner, W.C.; et al. GRI-Mech 3.0.* URL: http://combustion.berkeley.edu/gri-mech/version30/text30.html (visited on 04/27/2022).

[20] *Chemical-Kinetic Mechanisms for Combustion Applications.* URL: http://combustion.ucsd.edu (visited on 04/27/2022).

[21] *M. Frenklach, H. Wang, C.-L. Yu, M. Goldenberg, C.T. Bowman, R.K. Hanson, D.F. Davidson, E.J. Chang, G.P. Smith, D.M. Golden, W.C. Gardiner and V. Lissianski GRI-Mech 1.2.* URL: http://www.me.berkeley.edu/gri_mech/ (visited on 04/27/2022).

[22] Hai Wang and Michael Frenklach. “Detailed reduction of reaction mechanisms for flame modeling”. In: *Combustion and Flame* 87.3 (1991), pp. 365–370. ISSN: 0010-2180. DOI: https://doi.org/10.1016/0010-2180(91)90120-Z. URL: https://www.sciencedirect.com/science/article/pii/001021809190120Z.

[23] Andrei Kazakov and Michael Frenklach. *Reduced Reaction Sets based on GRI-Mech 1.2*. URL: `http://www.combustion.berkeley.edu/drm/` (visited on 04/27/2022).

[24] Niklas Zettervall, Christer Fureby, and Elna J. K. Nilsson. "Evaluation of Chemical Kinetic Mechanisms for Methane Combustion: A Review from a CFD Perspective". In: *Fuels* 2.2 (2021), pp. 210–240. DOI: `10.3390/fuels2020013`.

[25] Tim Lieuwen et al. "Fuel Flexibility Influences on Premixed Combustor Blowout, Flashback, Autoignition and Instability". In: *Turbo Expo: Power for Land, Sea, and Air* 42363 (2006), pp. 601–615.

[26] Alireza Kalantari and Vincent McDonell. "Boundary layer flashback of non-swirling premixed flames: Mechanisms, fundamental research, and recent advances". In: *Progress in Energy and Combustion Science* 61 (2017), pp. 249–292.

[27] Christian Thomas Eichler. *Flame flashback in wall boundary layers of premixed combustion systems*. Verlag Dr. Hut München, Germany, 2011.

[28] Tim Lieuwen et al. "Burner development and operability issues associated with steady flowing syngas fired combustors". In: *Combustion Science and Technology* 180.6 (2008), pp. 1169–1192.

[29] Denis Thibaut and Sebastien Candel. "Numerical study of unsteady turbulent premixed combustion: Application to flashback simulation". In: *Combustion and Flame* 113.1-2 (1998), pp. 53–65.

[30] Ahmed F Ghoniem et al. "Mechanism of combustion dynamics in a backward-facing step stabilized premixed flame". In: *Proceedings of the Combustion Institute* 30.2 (2005), pp. 1783–1790.

[31] Robert W Pitz and John W Daily. "Combustion in a turbulent mixing layer formed at a rearward-facing step". In: *AIAA journal* 21.11 (1983), pp. 1565–1570.

[32] Francesco Contino et al. "Coupling of in situ adaptive tabulation and dynamic adaptive chemistry: An effective method for solving combustion in engine simulations". In: *Proceedings of the Combustion Institute* 33.2 (2011), pp. 3057–3064.

[33] Long Liang, John G Stevens, and John T Farrell. "A dynamic adaptive chemistry scheme for reactive flow computations". In: *Proceedings of the Combustion Institute* 32.1 (2009), pp. 527–534.

[34] Markus Bösenhofer et al. "The eddy dissipation Concept—Analysis of different fine structure treatments for classical combustion". In: *Energies* 11.7 (2018), p. 1902.

[35] Bjorn F Magnussen. "The eddy dissipation concept: A bridge between science and technology". In: *ECCOMAS thematic conference on computational combustion*. Vol. 21. Libson, Portugal. 2005, p. 24.

[36] Riccardo Malpica Galassi et al. “Chemical model reduction under uncertainty”. In: *Combustion and Flame* 179 (2017), pp. 242–252.

[37] Sau-Hai Lam and Dimitris A Goussis. “Understanding complex chemical kinetics with computational singular perturbation”. In: *Symposium (International) on Combustion*. Vol. 22. 1. Elsevier. 1989, pp. 931–941.

[38] Riccardo Malpica Galassi. “PyCSP: A Python package for the analysis and simplification of chemically reacting systems based on Computational Singular Perturbation”. In: *Computer Physics Communications* 276 (2022), p. 108364.

[39] “Bertsch, M.: Description of the reacting flow solver FGMFoam. In Proceedings of CFD with OpenSource Software, 2019, Edited by Nilsson. H.,” in: (). URL: http://dx.doi.org/10.17196/OS_CFD#YEAR_2019.

[40] Jure Oder et al. “Thermal fluctuations in low-Prandtl number fluid flows over a backward facing step”. In: *Nuclear Engineering and Design* 359 (2020), p. 110460.

[41] Medhat A Nemitallah et al. “Investigation of a turbulent premixed combustion flame in a backward-facing step combustor; effect of equivalence ratio”. In: *Energy* 95 (2016), pp. 211–222.

[42] F Dupoirieux et al. “Numerical simulation of a premixed CH4-air burner for comparison of RANS and LES methodologies”. In: *NEPCAP 2016*. 2016.

[43] Nam Seob Park and Sang Cheol Ko. “Large eddy simulation of turbulent premixed combustion flows over backward facing step”. In: *Journal of mechanical science and technology* 25.3 (2011), pp. 713–719.

[44] Umair Ahmed and Robert Prosser. “Modelling flame turbulence interaction in RANS simulation of premixed turbulent combustion”. In: *Combustion Theory and Modelling* 20.1 (2016), pp. 34–57.

[45] Victor P Zhukov, Alan F Kong, et al. “Skeletal Kinetic Mechanism of Methane Oxidation for High Pressures and Temperatures”. In: *Proceedings of 7th European Conference for Aeronautics and Space Sciences (EUCASS)*. 2015.

[46] Nicole J Labbe et al. “Ramifications of including non-equilibrium effects for HCO in flame chemistry”. In: *Proceedings of the Combustion Institute* 36.1 (2017), pp. 525–532.

Appendix

A. Reaction Mechanisms

N13-R42

Skeletal mechanism composed by 13 species and 42 reactions used during the project:

```
Chemkin file converted from solution object:
skeletal_N13_R46
ELEMENTS
O  C  H  N
END
SPECIES
O2  CO  CO2  CH3  O
HO2  H2  H2O  H  OH
HCO  CH4  CH2O
END
REACTIONS
2 O + M <=> O2 + M                    1.2000e+17  -1.000   0.00
CH4/2.0/  CO/1.75/  CO2/3.6/  H2/2.4/  H2O/15.4/
H + O + M <=> OH + M                  5.0000e+17  -1.000   0.00
CH4/2.0/  CO/1.5/  CO2/2.0/  H2/2.0/  H2O/6.0/
H2 + O <=> H + OH                     5.0000e+04   2.670   6290.00
HO2 + O <=> O2 + OH                   2.0000e+13   0.000   0.00
CH3 + O <=> CH2O + H                  8.4300e+13   0.000   0.00
CH4 + O <=> CH3 + OH                  1.0200e+09   1.500   8600.00
CO + O + M <=> CO2 + M                6.0200e+14   0.000   3000.00
CH4/2.0/  CO/1.5/  CO2/3.5/  H2/2.0/  H2O/6.0/  O2/6.0/
HCO + O <=> CO + OH                   3.0000e+13   0.000   0.00
HCO + O <=> CO2 + H                   3.0000e+13   0.000   0.00
CH2O + O <=> HCO + OH                 3.9000e+13   0.000   3540.00
CO + O2 <=> CO2 + O                   2.5000e+12   0.000   47800.00
CH2O + O2 <=> HCO + HO2               1.0000e+14   0.000   40000.00
H + O2 + M <=> HO2 + M                2.8000e+18  -0.860   0.00
CO/0.75/  CO2/1.5/  H2O/0.0/  O2/0.0/
H + 2 O2 <=> HO2 + O2                 3.0000e+20  -1.720   0.00
H + H2O + O2 <=> H2O + HO2            9.3800e+18  -0.760   0.00
H + O2 <=> O + OH                     8.3000e+13   0.000   14413.00
2 H + M <=> H2 + M                    1.0000e+18  -1.000   0.00
CH4/2.0/  CO2/0.0/  H2/0.0/  H2O/0.0/
2 H + H2 <=> 2 H2                     9.0000e+16  -0.600   0.00
2 H + H2O <=> H2 + H2O                6.0000e+19  -1.250   0.00
CO2 + 2 H <=> CO2 + H2                5.5000e+20  -2.000   0.00
H + OH + M <=> H2O + M                2.2000e+22  -2.000   0.00
CH4/2.0/  H2/0.73/  H2O/3.65/
H + HO2 <=> H2O + O                   3.9700e+12   0.000   671.00
H + HO2 <=> H2 + O2                   2.8000e+13   0.000   1068.00
```

```
H + HO2 <=> 2 OH                          1.3400e+14   0.000   635.00
CH3 + H (+M) <=> CH4 (+M)                 1.2700e+16   -0.630  3.830e+02
CH4/2.0/  CO/1.5/  CO2/2.0/  H2/2.0/  H2O/6.0/
LOW / 1.2700e+19  -0.630  3.830e+02 /
TROE / 0.783  74.0  2941.0  6964.0 /
CH4 + H <=> CH3 + H2                      6.6000e+08   1.620   10840.00
H + HCO (+M) <=> CH2O (+M)                1.0900e+12   0.480   -2.600e+02
CH4/2.0/  CO/1.5/  CO2/2.0/  H2/2.0/  H2O/6.0/
LOW / 1.0900e+15  0.480  -2.600e+02 /
TROE / 0.7824  271.0  2755.0  6570.0 /
H + HCO <=> CO + H2                       7.3400e+13   0.000   0.00
CH2O + H <=> H2 + HCO                     2.3000e+10   1.050   3275.00
CO + H2 (+M) <=> CH2O (+M)                4.3000e+07   1.500   7.960e+04
CH4/2.0/  CO/1.5/  CO2/2.0/  H2/2.0/  H2O/6.0/
LOW / 4.3000e+10  1.500  7.960e+04 /
TROE / 0.932  197.00000000000003  1540.0  10300.0 /
H2 + OH <=> H + H2O                       2.1600e+08   1.510   3430.00
2 OH <=> H2O + O                          3.5700e+04   2.400   -2110.00
HO2 + OH <=> H2O + O2                     2.9000e+13   0.000   -500.00
CH4 + OH <=> CH3 + H2O                    1.0000e+08   1.600   3120.00
CO + OH <=> CO2 + H                       4.7600e+07   1.228   70.00
HCO + OH <=> CO + H2O                     5.0000e+13   0.000   0.00
CH2O + OH <=> H2O + HCO                   3.4300e+09   1.180   -447.00
CH3 + HO2 <=> CH4 + O2                    1.0000e+12   0.000   0.00
CO + HO2 <=> CO2 + OH                     1.5000e+14   0.000   23600.00
CH3 + O2 <=> CH2O + OH                    3.6000e+10   0.000   8940.00
CH3 + HCO <=> CH4 + CO                    2.6480e+13   0.000   0.00
CH2O + CH3 <=> CH4 + HCO                  3.3200e+03   2.810   5860.00
H2O + HCO <=> CO + H + H2O                2.2440e+18   -1.000  17000.00
HCO + M <=> CO + H + M                    1.8700e+17   -1.000  17000.00
CH4/2.0/  CO/1.5/  CO2/2.0/  H2/2.0/  H2O/0.0/
```

N19-R68

Skeletal mechanism composed by 19 species and 68 reactions used during the project:

```
Chemkin file converted from solution object:
skeletal_N19_R68
ELEMENTS
O  C  H  N
END
SPECIES
CH2O  CH3O  C3H3  O2  CO
H  CH2  CH2(S)  OH  CH4
C2H  O  CH3O2  H2  CH3
HCO  C2H6  H2O  CO2
END
REACTIONS
2 O + M <=> O2 + M                      1.2000e+17  -1.000  0.00
C2H6/3.0/  CH4/2.0/  CO/1.75/  CO2/3.6/  H2/2.4/  H2O/15.4/
H + O + M <=> OH + M                    5.0000e+17  -1.000  0.00
C2H6/3.0/  CH4/2.0/  CO/1.5/  CO2/2.0/  H2/2.0/  H2O/6.0/
H2 + O <=> H + OH                       5.0000e+04  2.670  6290.00
CH2 + O <=> H + HCO                     8.0000e+13  0.000  0.00
CH2(S) + O <=> CO + H2                  1.5000e+13  0.000  0.00
CH2(S) + O <=> H + HCO                  1.5000e+13  0.000  0.00
CH3 + O <=> CH2O + H                    8.4300e+13  0.000  0.00
CH4 + O <=> CH3 + OH                    1.0200e+09  1.500  8600.00
CO + O + M <=> CO2 + M                  6.0200e+14  0.000  3000.00
C2H6/3.0/  CH4/2.0/  CO/1.5/  CO2/3.5/
H2/2.0/  H2O/6.0/  O2/6.0/
HCO + O <=> CO + OH                     3.0000e+13  0.000  0.00
HCO + O <=> CO2 + H                     3.0000e+13  0.000  0.00
CH2O + O <=> HCO + OH                   3.9000e+13  0.000  3540.00
CH3O + O <=> CH2O + OH                  1.0000e+13  0.000  0.00
CO + O2 <=> CO2 + O                     2.5000e+12  0.000  47800.00
H + O2 <=> O + OH                       8.3000e+13  0.000  14413.00
2 H + M <=> H2 + M                      1.0000e+18  -1.000  0.00
C2H6/3.0/  CH4/2.0/  CO2/0.0/  H2/0.0/  H2O/0.0/
2 H + H2 <=> 2 H2                       9.0000e+16  -0.600  0.00
2 H + H2O <=> H2 + H2O                  6.0000e+19  -1.250  0.00
CO2 + 2 H <=> CO2 + H2                  5.5000e+20  -2.000  0.00
H + OH + M <=> H2O + M                  2.2000e+22  -2.000  0.00
C2H6/3.0/  CH4/2.0/  H2/0.73/  H2O/3.65/
CH2 + H (+M) <=> CH3 (+M)               2.5000e+16  -0.800  0.000e+00
C2H6/3.0/  CH4/2.0/  CO/1.5/  CO2/2.0/  H2/2.0/  H2O/6.0/
LOW / 2.5000e+19  -0.800  0.000e+00 /
TROE / 0.68  78.0  1995.0  5590.0 /
CH3 + H (+M) <=> CH4 (+M)               1.2700e+16  -0.630  3.830e+02
```

```
C2H6/3.0/  CH4/2.0/  CO/1.5/  CO2/2.0/  H2/2.0/  H2O/6.0/
LOW / 1.2700e+19  -0.630  3.830e+02 /
TROE / 0.783  74.0  2941.0  6964.0 /
CH4 + H <=> CH3 + H2                    6.6000e+08  1.620  10840.00
H + HCO (+M) <=> CH2O (+M)              1.0900e+12  0.480  -2.600e+02
C2H6/3.0/  CH4/2.0/  CO/1.5/  CO2/2.0/  H2/2.0/  H2O/6.0/
LOW / 1.0900e+15  0.480  -2.600e+02 /
TROE / 0.7824  271.0  2755.0  6570.0 /
H + HCO <=> CO + H2                     7.3400e+13  0.000  0.00
CH2O + H (+M) <=> CH3O (+M)             5.4000e+11  0.454  2.600e+03
C2H6/3.0/  CH4/2.0/  CO/1.5/  CO2/2.0/  H2/2.0/  H2O/6.0/
LOW / 5.4000e+14  0.454  2.600e+03 /
TROE / 0.758  94.0  1555.0  4200.0 /
CH2O + H <=> H2 + HCO                   2.3000e+10  1.050  3275.00
CH3O + H <=> CH2O + H2                  2.0000e+13  0.000  0.00
CH3O + H <=> CH3 + OH                   3.2000e+13  0.000  0.00
CH3O + H <=> CH2(S) + H2O               1.6000e+13  0.000  0.00
CO + H2 (+M) <=> CH2O (+M)              4.3000e+07  1.500  7.960e+04
C2H6/3.0/  CH4/2.0/  CO/1.5/  CO2/2.0/  H2/2.0/  H2O/6.0/
LOW / 4.3000e+10  1.500  7.960e+04 /
TROE / 0.932  197.00000000000003  1540.0  10300.0 /
H2 + OH <=> H + H2O                     2.1600e+08  1.510  3430.00
2 OH <=> H2O + O                        3.5700e+04  2.400  -2110.00
CH2 + OH <=> CH2O + H                   2.0000e+13  0.000  0.00
CH2(S) + OH <=> CH2O + H                3.0000e+13  0.000  0.00
CH3 + OH <=> CH2 + H2O                  5.6000e+07  1.600  5420.00
CH3 + OH <=> CH2(S) + H2O               2.5010e+13  0.000  0.00
CH4 + OH <=> CH3 + H2O                  1.0000e+08  1.600  3120.00
CO + OH <=> CO2 + H                     4.7600e+07  1.228  70.00
HCO + OH <=> CO + H2O                   5.0000e+13  0.000  0.00
CH2O + OH <=> H2O + HCO                 3.4300e+09  1.180  -447.00
CH3O + OH <=> CH2O + H2O                5.0000e+12  0.000  0.00
CH2 + O2 <=> HCO + OH                   1.3200e+13  0.000  1500.00
CH2 + H2 <=> CH3 + H                    5.0000e+05  2.000  7230.00
CH2 + CH4 <=> 2 CH3                     2.4600e+06  2.000  8270.00
CH2(S) + O2 <=> CO + H + OH             2.8000e+13  0.000  0.00
CH2(S) + O2 <=> CO + H2O                1.2000e+13  0.000  0.00
CH2(S) + H2 <=> CH3 + H                 7.0000e+13  0.000  0.00
CH2(S) + H2O <=> CH2 + H2O              3.0000e+13  0.000  0.00
CH2(S) + CH4 <=> 2 CH3                  1.6000e+13  0.000  -570.00
CH2(S) + CO <=> CH2 + CO                9.0000e+12  0.000  0.00
CH2(S) + CO2 <=> CH2 + CO2              7.0000e+12  0.000  0.00
CH2(S) + CO2 <=> CH2O + CO              1.4000e+13  0.000  0.00
CH3 + O2 <=> CH3O + O                   2.6750e+13  0.000  28800.00
CH3 + O2 <=> CH2O + OH                  3.6000e+10  0.000  8940.00
2 CH3 (+M) <=> C2H6 (+M)                2.1200e+16  -0.970  6.200e+02
C2H6/3.0/  CH4/2.0/  CO/1.5/  CO2/2.0/  H2/2.0/  H2O/6.0/
LOW / 2.1200e+19  -0.970  6.200e+02 /
```

```
TROE / 0.5325  151.0  1038.0  4970.0 /
CH3 + HCO <=> CH4 + CO                    2.6480e+13  0.000  0.00
CH2O + CH3 <=> CH4 + HCO                  3.3200e+03  2.810  5860.00
H2O + HCO <=> CO + H + H2O                2.2440e+18  -1.000  17000.00
HCO + M <=> CO + H + M                    1.8700e+17  -1.000  17000.00
C2H6/3.0/  CH4/2.0/  CO/1.5/  CO2/2.0/  H2/2.0/  H2O/0.0/
C2H + O2 <=> CO + HCO                     5.0000e+13  0.000  1500.00
CH3 + OH <=> CH2O + H2                    8.0000e+12  0.000  0.00
CH3 + O2 <=> CH3O2                        1.7000e+60  -15.100  18785.00
CH3 + CH3O <=> CH2O + CH4                 2.4100e+13  0.000  0.00
CH3 + CH3O2 <=> 2 CH3O                    3.0000e+13  0.000  -1200.00
2 CH3O2 => 2 CH3O + O2                    3.7000e+11  0.000  2200.00
C3H3 + O => C2H + CH2O                    1.0000e+13  0.000  0.00
C2H + CH2O => C3H3 + O                    5.4460e+14  0.000  31610.00
```

Part II

PLIEGO DE CONDICIONES

Chapter 1

General conditions

1.1 General

The scope statement is a fundamental part of every project, since it includes the right guidelines to be followed so as to attain optimal and reliable results. Along this part, all the compulsory technical and security conditions that must be achieved will be detailed, in order to reduce all the possible personal and facilities risks.

As the project has been mainly based on the use of a *software* tool, and in the absence of experimental results due to their considerable difficulty, it will only discuss about the aspects that must be taken into account for the proper execution of the experimental part.

Reliability

At the time of carrying out the tests, it is necessary to check the proper operation of the facilities, which means, checking the quality of the materials and the correct assembly of all the elements. Otherwise, uncertainties and errors in the measurements could appear, which may distort the data obtained.

Accuracy

It is important to use calibrated tools in order to obtain accurate results during the performed tests. Consequently, it is necessary to be rigorous in the choice of the appropriate instrumentation.

Security

Before any test, it is necessary to follow safety standards according to current regulations, in order to minimise any possible accident, and hence, any damage to the present personal.

Repeatability and controllability

Automating and following the appropriate procedures is essential to obtain reliable results, as well as to keep a correct control of all the studied parameters. At the same time, the repetition of the tests removes the potential uncertainty in the measurements, even ruling out possible erroneous tests.

Maintenance

Finally, maintenance work on installations and tools helps to reduce deterioration or even the break the material. At the same time, a good knowledge of the tool conditions helps to avoid false measurements during the test.

Chapter 2

Technical conditions

As been showed in the previous chapter, this project is based on the use of an computational tool called OpenFOAM, hence, it is not required huge installations or expensive equipment. Rather, it is necessary tools such as: an appropriate *hardware*; a *software* (together with its documentation, manuals and licences); internet connection, previous knowledge of fluid dynamics and numerical methods; adequate and reliable bibliography and qualified personal for proper supervision.

2.1 Material and equipment specifications

Hardware

Over the years, computational tools have become more sophisticated and complex, leading to a notable increase in computational requirements, specially for storing and running the programs. Therefore, an appropriate *hardware* is required to simulate all the required test during the whole project with the highest possible precision and velocity.

Subsequently, a suitable laptop with 6 processors and 8 GB RAM is used, capable to simulate all the cases in an affordable time.

Software

Carrying out this project, several programs have been used to simulate, analyse and represent the obtained results. Next, the *software* used is shown below:

- OpenFOAM
- Oracle VM VirtualBox
- Matlab
- PDF reader
- Office 365

Internet connection

Nowadays, much of the necessary information for the realisation of any project can be acquired through the internet, such as books or articles. In addition, good communication and transfer of information from any place (files, archives, etc.) between all the personal involved in the project implies a substantial improvement in the development of the project. That is why a stable and powerful connection is essential for the realisation of the project.

A priori knowledge

In order to develop the project is required previous insights about engineering, paying special attention to subjects related with fluid dynamics, turbulence, combustion, numerical methods, etc. In addition, in recommendable to be familiar with the *software* tools to be used, in order to get the right information in a prompt and efficient way.

Additional material

Making use of reliable technical documentation, such as books used during the degree or master's course, or articles from well-regarded scientific journals can be fundamental to complement the project, as well as to be able to contrast the obtained results with those shown in the trustworthy references.

Supervision

A proper supervision of the project allows for the resolution of any doubts that the student may have throughout the project. Therefore, an experienced supervisor on the subject to be dealt with in the project is required in order to supervise the work done by the student.

2.2 Quality conditions

Above all, it is essential that the company or institution in charge of the project guarantees the quality of the final product. In the case of a Spanish company, it would be necessary to check that it has the ISO-9001 quality certificate. That is why the company is responsible for carrying out all the relevant tests in accordance with the regulations to ensure the appropriate quality.

In addition, each and every test carried out by the company must be properly documented, including all pertinent information about the test, such as: title, description, room environment, date of realisation, results, assessments and comments.

2.3 Guarantee and maintenance conditions

In the case of a product being offered for sale, the company in charge of the project must give warranty of the final product for a period of two years. Thus, it must be in charge of solving any doubts and problems that may arise about the product. This warranty period starts from the moment the buyer receives the product.

Proper use of it should ensure its quality and proper functioning. However, the warranty will be invalidated if the guidelines/instructions for use of the product have not been correctly followed.

2.4 Complaints

In the case of a complaint, it will be necessary to submit a formal letter to the company within fifteen working days after the delivery of the product. This period can be extended up to one month if the delivery is outside Spain.

Furthermore, the seller commits to deliver the product in proper conditions. In the event of a defective product or lack of material, the seller shall replace it or supply the necessary pieces in accordance with the established conditions

2.5 Legal and contractual conditions

In the event of, during the execution of the project, the buyer wishes to extend the contract to other products, it will be necessary to establish a new budget to take them into account.

In the event of changes, modifications or other causes that may disrupt the delivery of the product, an equivalent extension of the contractual term may be requested, on condition that it submits such an request before the term has expired.

2.6 Review of prices

The prices detailed in the project budget are fixed and immovable, regardless of variations in the any materials or labour costs.

2.7 Deposit

The contractor is committed to guarantee a 10% of the total value of the price stated in the budget as a deposit by means of a bank guarantee in favour of the purchaser. This guarantee must be maintained from the start of the project until the end of the guarantee period. This deposit will be returned once the purchaser signs for the correct reception of the product.

2.8 Acceptance

Acceptance of the above points will be fulfilled through the use of programmes established by the seller. When the installation obligation lies with the seller, acceptance shall take place at the place of installation once the seller has proven the proper performance of all procedures.

If the installation is delayed by the buyer for more than thirty days from the delivery date, the seller will consider that the products have been accepted on the thirty-first day from this delivery.

Chapter 3

Health and safety conditions

3.1 Introduction

Finally, in this last section, it will be introduced the Spanish regulation related to the health and safety at work. Due to the nature of the project, special attention will be paid to the risks due to long periods of time spent in front of a computer screen. These risks can lead to vision and posture issues or continuous back pain.

The *Real Decreto 488/1997, del 14 de abril* defines the minimal regulations according to the security and health when it comes to use equipment that includes display screens, in which, the *disposiciones de la Ley 31/1995, del 8 de noviembre, de Prevención de Riesgos Laborales* are applied. Subsequently, the following aspects should be taken into account:

- Time spent in front of the screen.
- Degree of demand and complexity of the task.
- Necessity to obtain information quickly and accurately.

These aspects can be prevented by following a proper safety, hygiene and posture practices.

3.2 Real Decreto 488/1997 del 14 de abril

Artículo 1. Objeto

1. El presente Real Decreto establece las disposiciones mínimas de seguridad y de salud para la utilización por los trabajadores de equipos que incluyan pantallas de visualización.

2. Las disposiciones de la Ley 31/1995, de 8 de noviembre, de Prevención de Riesgos Laborales, se aplicarán plenamente al conjunto del ámbito contemplado en el apartado anterior.

3. Quedan excluidos del ámbito de aplicación de este Real Decreto:

   (a) Los puestos de conducción de vehículos o máquinas.

   (b) Los sistemas informáticos embarcados en un medio de transporte.

   (c) Los sistemas informáticos destinados prioritariamente a ser utilizados por el público.

   (d) Los sistemas llamados portátiles, siempre y cuando no se utilicen de modo continuado en un puesto de trabajo.

   (e) Las calculadores, cajas registradoras y todos aquellos equipos que tengan un pequeño dispositivo de visualización de datos o medidas necesario para la utilización directa de dichos equipos.

   (f) Las máquinas de escribir de diseño clásico, conocidas como máquinas de ventanilla.

Artículo 2. Definiciones

A efectos de este Real Decreto se atenderá por:

1. Pantalla de visualización: una pantalla alfanumérica o gráfica, independiente del método de representación visual utilizado.

2. Puesto de trabajo: el constituido por un equipo con pantalla de visualización provisto, en su caso, de un teclado o dispositivo de adquisición de datos, de un programa para la interconexión persona/máquina, de accesorios ofimáticos y de un asiento y mesa o superficie de trabajo, así como el entorno laboral inmediato.

3. Trabajador: cualquier trabajador que habitualmente y durante una parte relevante de su trabajo normal utilice un equipo con pantalla de visualización.

Artículo 3. Obligaciones generales del empresario

1. El empresario adoptará las medidas necesarias para que la utilización por los trabajadores de equipos con pantallas de visualización no suponga riesgos para su seguridad o salud o, si ello no fuera posible, para que tales riesgos se reduzcan al mínimo. En cualquier caso, los puestos de trabajo a que se refiere el presente Real Decreto deberán cumplir las disposiciones mínimas establecidas en el anexo del mismo.

2. A efectos de lo dispuesto en el primer párrafo del apartado anterior, el empresario deberá evaluar los riesgos para la seguridad y salud de los trabajadores, teniendo en cuenta en particular los posibles riesgos para la vista y los problemas físicos y de carga mental, así como el posible efecto añadido o combinado de los mismos. La evaluación se realizará tomando en consideración las características propias del puesto de trabajo y las exigencias de la tarea y entre estas, especialmente, las siguientes:

   (a) El tiempo promedio de utilización diaria del equipo.

   (b) El tiempo máximo de atención continua a la pantalla requerido por la tarea habitual.

   (c) El grado de atención que requiera dicha tarea.

3. Si la evaluación pone de manifiesto que la utilización por los trabajadores de equipos con pantallas de visualización supone o puede suponer un riesgo para su seguridad o salud, el empresario adoptará las medidas técnicas u organizativas necesarias para eliminar o reducir el riesgo al mínimo posible. En particular, deberá reducir la duración máxima del trabajo continuado en pantalla, organizando la actividad diaria de forma que esta tarea se alterne con otras o estableciendo pausas necesarias cuando la alternancia de las tareas no sea posible o no baste para disminuir el riesgo suficiente.

4. En los convenios colectivos podrá acordarse la periodicidad, duración y condiciones de organización de los cambios de actividad y pausas a que se refiere el apartado anterior.

Artículo 4. Vigilancia de la salud

1. El empresario garantizará el derecho de los trabajadores a una vigilancia adecuada de sus salud, teniendo en cuenta en particular los riesgos para la vista y los problemas físicos y de carga mental, el posible efecto añadido o combinado de los mismos, y la eventual patología acompañante. Tal vigilancia será realizada por personal sanitario competente y según determinen las autoridades sanitarias en las pautas y protocolos que se elaboren, de conformidad con lo dispuesto en el apartado 3 del artículo 37 del Real Decreto 39/1997, del 17 de enero, por el que se aprueba el Reglamento de los Servicios de Prevención. Dicha vigilancia deberá ofrecerse a los trabajadores en las siguientes ocasiones:

   (a) Antes de comenzar a trabajar con una pantalla de visualización.

   (b) Posteriormente, con una periodicidad ajustada al nivel de riesgo a juicio del médico responsable.

   (c) Cuando aparezcan trastornos que pudieran deberse a este tipo de trabajo.

2. Cuando los resultados de la vigilancia de la salud a que se refiere el apartado 1 lo hiciese necesario, los trabajadores tendrán derecho a un reconocimiento oftalmológico.

3. El empresario proporcionará gratuitamente a los trabajadores dispositivos correctores especiales para la protección de la vista adecuados al trabajo con el equipo del que se trate, si los resultados de la vigilancia de la salud a los que se refieren los apartados anteriores demuestran su necesidad y no pueden utilizarse dispositivos correctores normales.

Artículo 5. Obligaciones en materia de información y formación

1. De conformidad con los artículos 18 y 19 de la Ley de Prevención de Riesgos Laborales, el empresario deberá garantizar que los trabajadores y los representantes de los trabajadores reciban una formación e información adecuadas sobre los riesgos derivados de la utilización de los equipos que incluyan pantallas de visualización, así como sobre las medidas de prevención y protección que hayan de adoptarse en aplicaciones del presente Real Decreto.

2. El empresario deberá informar a los trabajadores sobre todos los aspectos relacionados con la seguridad y la salud en su puesto de trabajo y sobre las medidas llevadas a cabo de conformidad con lo dispuesto en los artículos 3 y 4 de este Real Decreto.

3. El empresario deberá garantizar que cada trabajador reciba una formación adecuada sobre las modalidades de uso de los equipos con pantallas de visualización, antes de comenzar este tipo de trabajo y cada vez que la organización del puesto de trabajo se modifique de manera apreciable.

Artículo 6. Consulta y participación de los trabajadores

La consulta y participación de los trabajadores o sus representantes sobre las cuestiones a que se refiere este Real Decreto se realizarán de conformidad con lo dispuesto en el apartado 2 del artículo 18 de la Ley de Prevención de Riesgos Laborales.

Anexo

Por todo lo dispuesto anteriormente, se va a definir el puesto de trabajo específico para la prevención de riesgos laborales y seguridad.

1. Equipo.

   (a) Observación general. La utilización en sí misma del equipo no debe ser una fuente de riesgo para los trabajadores.

   (b) Pantalla. Los caracteres de la pantalla deberán estar bien definidos y configurados de forma clara, y tener una dimensión suficiente, disponiendo de un espacio adecuado entre los caracteres y los renglones. La imagen de la pantalla deberá ser estable, sin fenómenos de destellos, centelleos y otras formas de inestabilidad. El usuario de terminales con pantalla deberá poder ajustar fácilmente la luminosidad y el contraste entre los caracteres y el fondo de la pantalla, y adaptarlos fácilmente a las condiciones del entorno. La pantalla deberá ser orientable e inclinable a voluntad, con facilidad para adaptarse a las necesidades del usuario. Podrá utilizarse un pedestal independiente o una mesa regulable para la pantalla. La pantalla no deberá tener reflejos ni reverberaciones que puedan molestar al usuario.

   (c) Teclado. El teclado deberá ser inclinable e independiente de la pantalla para permitir que el trabajador adopte una postura cómoda qu no provoque cansancio en los brazos o las manos. Tendrá que haber espacio suficiente delante del teclado para que el usuario pueda apoyar los brazos y las manos. La superficie del teclado deberá ser mate para evitar reflejos. La disposición del teclado y las características de las teclas deberán tender a facilitar su utilización. Los símbolos de las

teclas deberán resaltar suficientemente y ser legibles desde la posición normal de trabajo.

(d) Mesa o superficie de trabajo. La mesa o superficie de trabajo deberá ser poco reflectante, tener dimensiones suficientes y permitir una colocación flexible de la pantalla, del teclado, de los documentos y del material accesorios. El soporte de los documentos deberá ser estable y regulable y estará colocado de tal modo que se reduzcan al mínimo los movimientos para permitir a los trabajadores una posición óptima.

(e) Asiento de trabajo. El asiento de trabajo deberá ser estable, proporcionando al usuario libertad de movimiento y procurándole una postura confortable. La altura del mismo deberá ser regulable. El respaldo deberá ser reclinable y su altura ajustable. Se pondrá un reposapiés a disposición de quienes lo deseen.

2. Entorno.

(a) Espacio. El puesto de trabajo deberá tener una dimensión suficiente y estar acondicionado de tal manera que haya espacio para permitir los cambios de postura y movimientos del trabajo.

(b) Iluminación. La iluminación general y la iluminación especial (lámparas de trabajo), cuando sea necesaria, deberán garantizar unos niveles adecuados de iluminación y unas relaciones adecuadas de luminancias entre la pantalla y su entorno, habida en cuenta del carácter del trabajo, de las necesidades visuales del usuario y del tipo de pantalla utilizado. El acondicionamiento del lugar de trabajo y del puesto de trabajo, así como la situación y las características técnicas de las fuentes de luz artificial, deberán coordinarse de tal manera que se eviten los deslumbramientos y los reflejos molestos en la pantalla u otras partes del equipo.

(c) Reflejos y deslumbramientos. Los puestos de trabajo deberán instalarse de tal forma que las fuentes de luz, tales como ventanas y otras aberturas, los tabiques transparentes o traslúcidos y los equipos o tabiques de color claro no provoquen deslumbramiento directo ni produzcan reflejos molestos en la pantalla. Las ventanas deberán ir equipadas con un dispositivo de cobertura adecuado y regulable para atenuar la luz del día que ilumine el puesto de trabajo.

(d) Ruido. El ruido producido por los equipos instalados en el puesto de trabajo deberá tenerse en cuenta al diseñar el mismo, en especial para que no se perturbe la atención ni la palabra.

(e) Calor. Los equipos instalados en el puesto de trabajo no deberán producir un claor adicional que pueda ocasionar molestias a los trabajadores.

(f) Emisiones. Toda la radiación, excepto la parte visible del espectro electromagnético, deberá reducirse a niveles insignificantes desde el punto de vista de la protección de la seguridad y de la salud de los trabajadores.

(g) Humedad. Deberá crearse y mantenerse una humedad aceptable.

3. Interconexión ordenador/persona Para la elaboración, la elección, la compra y la modificación de programas, así como para la definición de las tareas que requieran pantallas de visualización el empresario tendrá en cuenta los siguientes fatores:

   (a) El programa deberá estar adaptado a la tarea que deba realizarse.

   (b) El Programa deberá de ser fácil de utilizar además de, en su caso, poder adaptarse al nivel de conocimientos y de experiencia del usuario; no deberá utilizarse ningún dispositivo cuantitativo o cualitativo de control sin que los trabajadores hayan sido informados y previa consulta con sus representantes.

   (c) Los sistemas deberán proporcionar a los trabajadores indicaciones sobre su desarrollo.

   (d) Los sistemas deberán mostrar la información en un formato y a un ritmo adaptado a los operadores.

   (e) Los principios de ergonomía deberán aplicarse en particular al tratamiento de la información por parte de la persona.

Part III

BUDGET

Chapter 1

Budget

Information about the project budget

In this last chapter a rough budget for the project will be presented. Emphasise the importance of the project budget for decision making during the project. In addition, allows to have a and knowledge about the cost of each part of the project.

The budget to be developed is for a research project, for that reason, it has been decided to divide it into items, which refers to each of the steps followed during this work. Thereby, the budget has been divided in the following items:

- Item 1: Bibliography study and documentation
- Item 2: Modelling and computational time
- Item 3: Report writing

About the the used equipment during the project, so as not to count the total price, it has been decided to assume that can be amortised in 1 year (usually, the the amortisation period come upon 8-10 years, however, the price per day would be negligible). As a consequence, in Table 1.1 have been shown the price per day for each equipment, for it, it has been assumed that each year has 12 months and each month 30 days.

Equipment	Purchase price	Price per day
LENOVO IdeaPad Gaming 3 15ARH05, 8GB, 512GB	834.00 €/ud	2.32 €/day
Matlab Educational subscription	250 €/year	0.69 €/day
OpenFOAM subscription	0 €/year	0 €/day

Table 1.1: Price per day for the used equipment during the project.

Furthermore, it has been searched for the annual salary of a project engineer in Rome. Then, assuming 8 hours per day as a workday, the price per hour has been calculated in Table 1.2

Professional	Annual salary	Price per hour
Project engineer (Rome)	42366.00 €/year	14.71 €/h

Table 1.2: Price per hour for the professionals. Source: www.glassdoor.it

Finally, it has been assumed that the working average hours by the engineer is 525 hours during the whole project. Highlight that part of this time has been spent learning how to use OpenFOAM from scratch.

Project budget

Date of issuance: 28/06/2022

Item 1:

Unity	Description of work units	Yield	Price	Cost
	Bibliography study and documentation Information research in books, articles, reports, etc			
h	Project engineer	80.00	14.71 €/h	1176.80 €
	Direct costs		1176.80 €	
%	Direct complementary costs (3%)	0.03	1176.80 €	35.30 €
	Total item cost		1212.10 €	

Project budget

Date of issuance: 28/06/2022

Item 2:

Unity	Description of the work units	Yield	Price	Cost
	Modelling and computational time Modelling of the PitzDaily and its subsequent simulations carried out during the project			
h	Project ingeneer	285.00	14.71 €/h	4192.35 €
day	OpenFOAM subscription	11.86	0 €/day	0 €
day	Matlab Educational subscription	11.86	0.69 €/day	8.18 €
day	LENOVO IdeaPad Gaming 3 15ARH05, 8GB, 512GB	11.86	2.32 €/day	27.52 €
	Direct costs		4228.05 €	
%	Direct complementary costs (3%)	0.03	4228.05 €	126.84 €
	Total item cost		4354.89 €	

Project budget

Date of issuance: 28/06/2022

Item 3:

Unity	Description of work units	Yield	Price	Cost
	Report writing Writing of the report (theory, methodology, results...) for its subsequent presentation			
h	Project engineer	160.00	14.71 €/h	2353.60 €
	Direct costs		2353.60 €	
%	Direct complementary costs (3%)	0.03	2353.60 €	70.61 €
	Total item cost		2424.21 €	

Project budget

Date of issuance: 28/06/2022

Total:

Description		Cost
Item 1:	Bibliography study and documentation	1212.10 €
Item 2:	Modelling and computational time	4354.89 €
Item 3:	Report writing	2424.21 €
Material Execution Budget		7991.20 €
General costs (16%)		1278.59 €
Contract Execution Budget		9269.79 €
I.V.A (21%)		1946.66 €
Tender Base Budget		**11216.44 €**

The present budget comes to the said amount of:
ELEVEN THOUSAND TWO HUNDRED AND SIXTEEN EUROS
AND FORTY-FOUR CENTS